AD-A052 042 AVCO LYCOMING DIV STRATFORD CONN F/G 21/5
TURBINE TIP-CLEARANCE MEASUREMENT.(U)
DEC 77 S D WHITE
UNCLASSIFIED LYC-77-46 USARTL-TR-77-47 DAAJ02-75-C-0051 NL

1 OF 2
AD A052 042

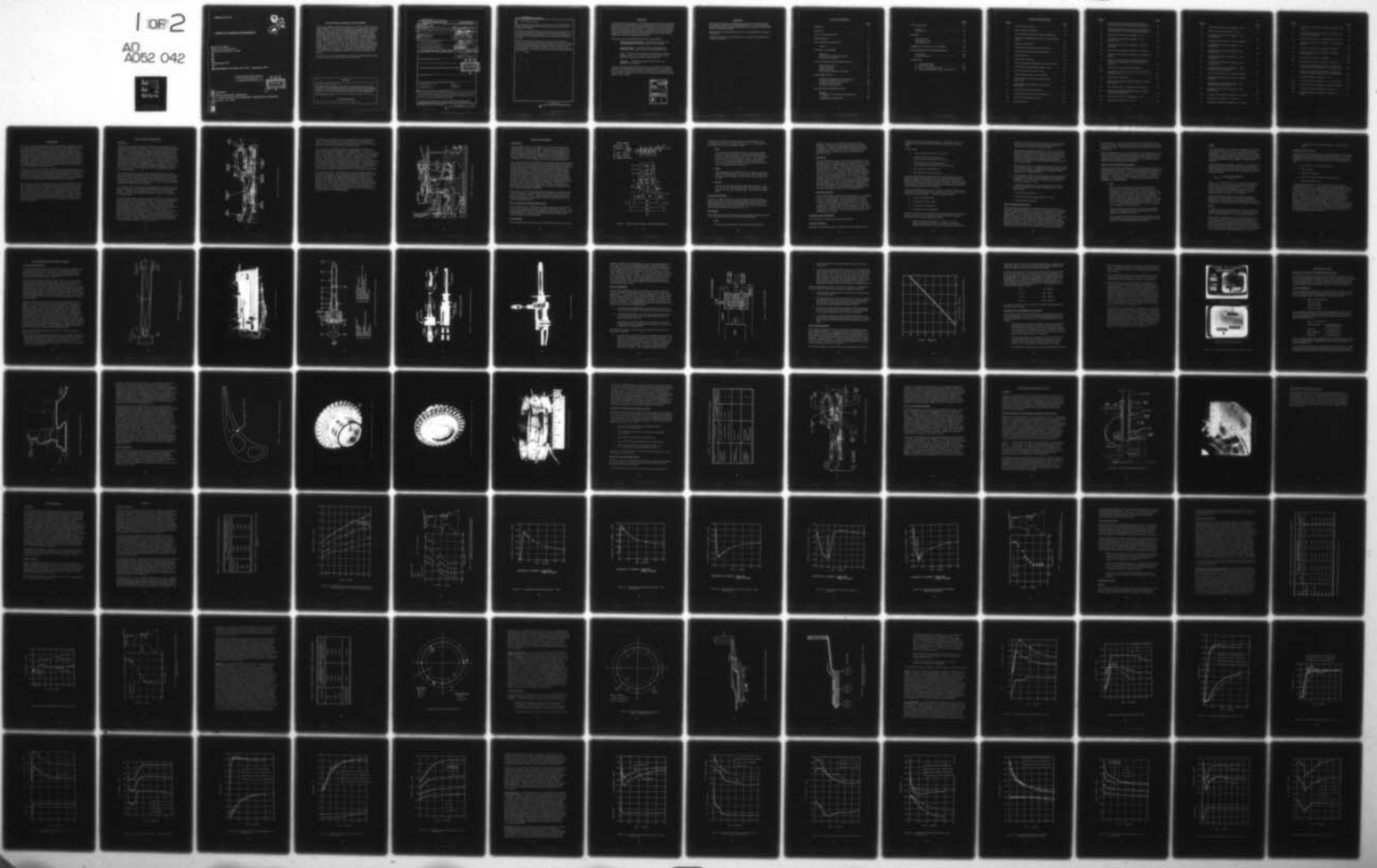

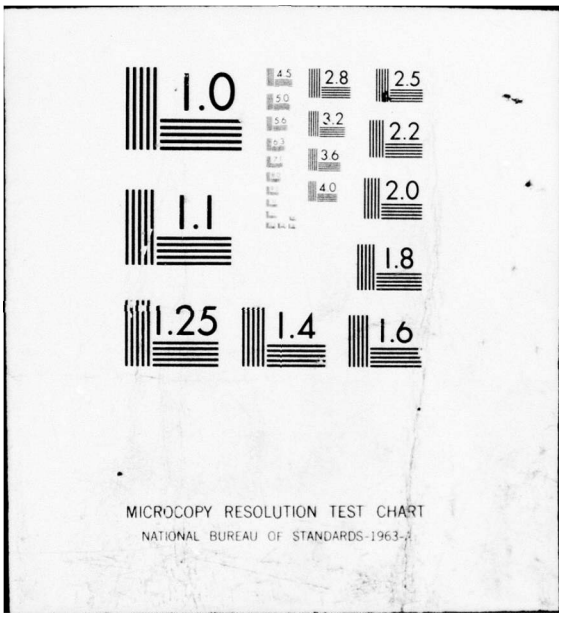
1.0
1.1
1.25
1.4
1.6
1.8
2.0
2.2
2.5
2.8
3.2
3.6
4.0
4.5
5.0
5.6
6.3
MICROCOPY RESOLUTION TEST CHART
NATIONAL BUREAU OF STANDARDS-1963-A

USARTL-TR-77-47

TURBINE TIP-CLEARANCE MEASUREMENT

Steven D. White
Avco Lycoming Division
Stratford, Connecticut 06497

December 1977

Final Report for Period July 1975 - September 1977

Approved for public release;
distribution unlimited.

Prepared for
APPLIED TECHNOLOGY LABORATORY
U. S. ARMY RESEARCH AND TECHNOLOGY LABORATORIES (AVRADCOM)
Fort Eustis, Va. 23604

APPLIED TECHNOLOGY LABORATORY POSITION STATEMENT

This report provides considerable insight into several research and development problems that have been and continue to be experienced in Army gas turbine engines. The problem of minimizing performance losses caused by turbine tip leakage has been previously approached analytically since measurement techniques have not provided suitable data. This program has provided realistic data and an assessment of the adequacy of analytical techniques. This program has also provided a valuable indication of the magnitude of the thermal distortion which occurs in small engine shrouds and the relative impact of this distortion on tip clearance losses. In reviewing this report, the reader is cautioned that the data presented is truly valid for only this test vehicle, and the conclusions reached may be valid only for this type of shroud configuration (a cantilevered shroud). The results of this contract have been incorporated in the improvement of analytical techniques and will be integrated into other research and development programs at the Applied Technology Laboratory.

Mr. Jan M. Lane of the Propulsion Technical Area, Technology Applications Division, served as Project Engineer for this effort.

Unclassified

SECURITY CLASSIFICATION OF THIS PAGE *(When Data Entered)*

REPORT DOCUMENTATION PAGE

READ INSTRUCTIONS BEFORE COMPLETING FORM

1. REPORT NUMBER: USARTL-TR-77-47
2. GOVT ACCESSION NO.
3. RECIPIENT'S CATALOG NUMBER
4. TITLE *(and Subtitle)*: TURBINE TIP-CLEARANCE MEASUREMENT
5. TYPE OF REPORT & PERIOD COVERED: Final Report, Jul 75 - Sep 77
6. PERFORMING ORG. REPORT NUMBER: LYC-77-46
7. AUTHOR(s): Steven D. White
8. CONTRACT OR GRANT NUMBER(s): DAAJ02-75-C-0051
9. PERFORMING ORGANIZATION NAME AND ADDRESS: Avco Lycoming Division, Stratford, Connecticut 06497
10. PROGRAM ELEMENT, PROJECT, TASK AREA & WORK UNIT NUMBERS: 62209A 1F262209AH76 00 082 EK
11. CONTROLLING OFFICE NAME AND ADDRESS: Applied Technology Laboratory, U. S. Army Research and Technology Laboratories (AVRADCOM), Fort Eustis, Virginia 23604
12. REPORT DATE: December 1977
13. NUMBER OF PAGES: 126
14. MONITORING AGENCY NAME & ADDRESS *(if different from Controlling Office)*
15. SECURITY CLASS. *(of this report)*: Unclassified
15a. DECLASSIFICATION/DOWNGRADING SCHEDULE: N/A
16. DISTRIBUTION STATEMENT *(of this Report)*: Approved for public release; distribution unlimited.
17. DISTRIBUTION STATEMENT *(of the abstract entered in Block 20, if different from Report)*
18. SUPPLEMENTARY NOTES
19. KEY WORDS *(Continue on reverse side if necessary and identify by block number)*: Clearance Measurement; Gas Turbines; Optical Instruments; Lasers; Tip Clearance; Turbines
20. ABSTRACT *(Continue on reverse side if necessary and identify by block number)*

This report describes the analysis and measurement of turbine tip clearance over the full range of operation of an advanced gas turbine engine. The first-stage turbine of the Lycoming advanced gas generator was used as the test vehicle for analytic and experimental evaluation.

Tip-clearance response of the stage was analyzed for steady-state and transient operating conditions through the use of a one-dimensional tip-

DD FORM 1 JAN 73 1473 EDITION OF 1 NOV 65 IS OBSOLETE

Unclassified

SECURITY CLASSIFICATION OF THIS PAGE *(When Data Entered)*

213 150 JOB

20. ABSTRACT (Continued)

clearance calculation technique. Measurement was accomplished with three laser tip-clearance measurement probes that operate on an optical beam triangulation principle.

Comparison of analytic and measured tip-clearance results showed measured clearance to be tighter than predicted over the entire power spectrum. This differential was attributed primarily to a two-dimensional thermal strain distribution in the shroud which had not been accounted for by the analytic technique.

Excellent correlation was obtained between the transient tip-clearance response characteristics resulting from analysis and measurement. Comparison of measured and predicted component temperatures under steady-state and transient operating conditions verified the accuracy of the thermal analysis procedure. Component distortion, as well as response to transient engine operation, was found to have significant impact on minimum operating tip clearance.

SUMMARY

The objective of this program was to apply accurate turbine tip-clearance measurement instrumentation to the full spectrum of actual gas generator operation and determine the tip-clearance response of an advanced high-pressure gas producer turbine stage. Comparison between the measurements and a one-dimensional analytical prediction of the tip-clearance response will provide a basis for optimization of turbine rotor/shroud designs for minimum operating tip clearance.

The program was accomplished through four basic phases:

- Definition of Test Program - Tip-clearance analysis was accomplished and the test procedures were defined.
- Instrumentation - Instrumentation was designed and procured, and the gas generator was prepared for test.
- Test - Tip-clearance response and associated component temperatures were measured over the full range of gas generator steady-state and transient operation.
- Analysis - Comparison between measurement and analysis was completed.

The analytical and experimental program was successful in providing a reliable correlation between analysis and measurement, verifying the accuracy and usefulness of the laser tip-clearance measurement device, and providing a record of the tip-clearance response of the advanced gas generator test vehicle.

PREFACE

The turbine tip-clearance measurement program was authorized and directed by the Applied Technology Laboratory, U. S. Army Research and Technology Laboratories (AVRADCOM), Fort Eustis, Virginia, under Contract DAAJ02-75-C-0051.

The program was conducted by the Avco Lycoming Division, Stratford, Connecticut.

Technical direction was provided by Mr. J. Lane of the Applied Technology Laboratories.

TABLE OF CONTENTS

	Page
SUMMARY	3
PREFACE	4
LIST OF ILLUSTRATIONS	7
INTRODUCTION	11
TEST VEHICLE DESCRIPTION	12
General	12
ANALYTIC TECHNIQUE	16
Approach	16
Heat-Transfer Model Description	16
Calculation Technique	19
TIP-CLEARANCE MEASUREMENT DEVICE	25
General Description	25
Setup Technique	31
Initial Calibration	33
Clearance Measurement Procedure	35
INSTRUMENTATION	38
Component Temperature Instrumentation	38
Boundary Condition Instrumentation	45
Additional Instrumentation	45
Data System Description	48
GAS GENERATOR MODIFICATIONS	49
General	49
Installation of Tip-Clearance Measurement Device	49
Instrumentation Installation	52

	Page
TEST PROCEDURE.	53
General.	53
Calibrations.	53
RESULTS.	54
Initial Analysis	54
Initial Setup Test	64
Final Setup Test	64
ASSESSMENT OF ANALYTIC TECHNIQUE.	106
CONCLUSIONS AND RECOMMENDATIONS.	109
Conclusions	109
Recommendations	109
APPENDIXES	
A. Fluid Node Model	111
B. Metal Node Model	113
C. Heat Transfer Coefficients	115
D. Boundary Conditions - Final Test Results . . .	118

LIST OF ILLUSTRATIONS

Figure		Page
1	PLT-34 Gas Generator	13
2	Rotor Cooling Air Network	15
3	Tip-Clearance Analytic Technique Nodal Model.	17
4	Tip-Clearance Measurement Device - Basic Optical Path.	26
5	System Configuration	27
6	Tip-Clearance Measurement Probe Layout	28
7	Tip-Clearance Measurement Probe Parts	29
8	Probe Assembly	30
9	Input Optics Assembly	32
10	Initial Tip-Clearance Calibration, Probe Number 3	34
11	Tip-Clearance Measurement Output Format	37
12	Instrumented Turbine Rotor Layout	39
13	Thermocouple Location in Rotor Blade.	41
14	Instrumented Gas Producer Turbine Rotor - Front View	42
15	Instrumented Gas Producer Turbine Rotor - Rear View.	43
16	Shroud Thermocouple Installation	44
17	Gas Generator Instrumentation Summary	47
18	Laser Probe Installation Layout.	50
19	Diffuser Rework.	51

Figure		Page
20	Calculated Component Growth Characteristics - Initial Analysis, 0.5 Percent Shroud Cooling Air. . .	56
21	Calculated Component Temperature Distribution - Initial Analysis, 0.5 Percent Shroud Cooling Air. . .	57
22	Calculated Tip-Clearance Response - Start.	58
23	Calculated Tip-Clearance Response - Jam Acceleration.	59
24	Calculated Tip-Clearance Response - Snap Deceleration.	60
25	Calculated Tip-Clearance Response - Wave-off . . .	61
26	Calculated Tip-Clearance Response - Shutdown and Restart.	62
27	Effect of Convective Heat Transfer Coefficient at the Disc Bore on Calculated Temperature Distribution.	63
28	Steady-State Tip-Clearance Comparison.	67
29	Component Temperature Distribution Comparison - Maximum Power.	68
30	Shroud Distortion Pattern.	71
31	Measured Temperature Distortion Pattern - Maximum Power.	73
32	Shroud Design Point Temperature Distribution. . . .	74
33	Shroud Finite Element Analysis Result - Design Temperature Distribution.	75
34	Transient Tip-Clearance Response - Start.	77
35	Measured Tip Clearance - Start.	78

Figure		Page
36	Component Temperature Response - Start.	79
37	Blade Temperature Response - Start.	80
38	Transient Tip-Clearance Response - Jam Acceleration.	81
39	Measured Tip Clearance - Jam Acceleration. . . .	82
40	Component Temperature Response - Jam Acceleration.	83
41	Component Temperature Response - Jam Acceleration.	84
42	Component Growth Characteristics - Jam Acceleration.	85
43	Transient Tip-Clearance Response - Snap Deceleration.	87
44	Transient Tip-Clearance Response - Snap Deceleration (0-30 Seconds).	88
45	Measured Tip Clearance - Snap Deceleration.	89
46	Component Temperature Response - Snap Deceleration.	90
47	Component Temperature Response - Snap Deceleration (0-30 Seconds).	91
48	Component Growth Characteristics - Snap Decleration.	92
49	Transient Tip-Clearance Response - Wave-off. . . .	93
50	Measured Tip Clearance - Wave-off.	94
51	Component Temperature Response - Wave-off. . . .	95

Figure		Page
52	Transient Tip-Clearance Response - Shutdown and Restart.	97
53	Transient Tip-Clearance Response - Shutdown and Restart (0-70 Seconds).	98
54	Measured Tip Clearance - Shutdown and Restart. . .	99
55	Component Temperature Response - Shutdown and Restart.	100
56	Transient Tip-Clearance Response - Shutdown. . . .	102
57	Transient Tip-Clearance Response - Shutdown (0-30 Seconds).	103
58	Measured Tip Clearance - Shutdown.	104
59	Component Temperature Response - Shutdown. . . .	105
60	Transient Tip-Clearance Response Analysis With Simplified Boundary Conditions - Jam Acceleration .	107
61	Transient Tip-Clearance Response Analysis With Simplified Boundary Conditions - Snap Deceleration.	108
D-1	Transient Boundary Conditions - Start.	119
D-2	Transient Boundary Conditions - Jam Acceleration. .	120
D-3	Transient Boundary Conditions - Snap Deceleration. .	122
D-4	Transient Boundary Conditions - Wave-off.	124
D-5	Transient Boundary Conditions - Shutdown and Restart.	126

INTRODUCTION

Tip clearances in advanced, improved performance gas turbines must be held at a minimum to avoid unacceptably large aerodynamic performance losses. Small, highly loaded gas producer turbine stages operating at a tip clearance of approximately one percent of blade height typically lose two to three percent in efficiency for each percentage point of additional tip clearance. The conflicting requirement for adequate clearance to preclude tip rubs under steady-state and transient engine operating conditions necessitates a comprehensive knowledge of the dynamic growth behavior of the turbine system in its operational environment. Consequently, an accurate analytical modeling approach to the design of the rotor/shroud systems in these high-performance engines is necessary. Successful reduction of operating clearances in gas turbine engines requires the application of analytical and experimental techniques to predict and verify the performance of the turbine rotor/shroud system over the full range of gas turbine operation.

The problem of tip-clearance determination was addressed analytically through the use of a Lycoming-developed, one-dimensional tip-clearance calculation technique and experimentally through test of an advanced gas generator turbine developed under the Army STAGG (Small Turbine Advanced Gas Generator) Program and designated PLT-34. The gas generator was equipped with three laser tip-clearance measurement probes and extensive instrumentation to measure aerodynamic parameters and turbine component temperatures.

This program was successful in verifying the accuracy of the analytic technique in calculating transient response rates of tip clearance and component temperature over the full range of gas generator operations. Differentials between measured and calculated steady-state tip clearance were caused primarily by a two-dimensional thermal strain distribution in the shroud which was not accounted for in the one-dimensional analytic technique. The laser tip-clearance measurement system was demonstrated to be a useful and accurate technique when used under carefully controlled laboratory/test cell conditions. Analysis and measurement results from this program will be used to provide a baseline for the improvement of the tip-clearance control of the Lycoming advanced technology demonstrator engine (ATDE).

TEST VEHICLE DESCRIPTION

GENERAL

The PLT 34 gas generator (Figure 1) employs a two-stage axial and a single-stage centrifugal compressor, a reverse-flow annular combustor, and a two-stage axial turbine. Two basic modules comprise the gas generator: the axial compressor module and the compressor-turbine module. The axial compressor module includes the inlet housing, all components of the axial compressor section including the intermediate housing, and the accessory drive gear. The structural support for the forward bearing is through the intermediate housing, which is the forward section of the inter-compressor duct. The shaft interface with the high-pressure module is a self-piloting splined coupling. The compressor-turbine module includes the middle bearing support (which is the rear section of the interstage duct), the centrifugal bearing, and the seal assemblies.

The gas generator rotor system uses three ball bearings to control rotor clearance and to exclude rotor critical speeds within the operating range. Two basic elements comprise the rotor system: (1) the axial compressor rotor, which is supported by the forward ball bearing and the splined coupling; and (2) the high-pressure rotor, which is straddle-mounted on the middle and aft bearings.

The combustor liner, fabricated from Hastelloy sheet stock, is mounted on four radial pins from the machined nickel alloy combustor housing header. The liner has a slip joint at the outer first turbine nozzle interface, and the axially flexible diaphragm is bolted to the inboard first nozzle flange.

The first turbine nozzle assembly is fabricated from formed sheet stock and an integral vane and flow-path casting. The nozzle uses two-pass cooling through cored passages with cooling air discharge near the trailing edge through two eloxed slots. Both inner and outer nozzle interface flanges are axially remote from the nozzle vanes to minimize the radial depth of the section over the vane end shrouds and to accommodate thermal expansion gradients. The first rotor cooling-air preswirl nozzle, which is bolted to the first turbine nozzle inboard flange, incorporates the cylinder for the diffuser piston ring seals. The location of the first nozzle is established at the outer flanged interface with the combustor header, which also connects the first rotor shroud and second nozzle assembly to the outer structure.

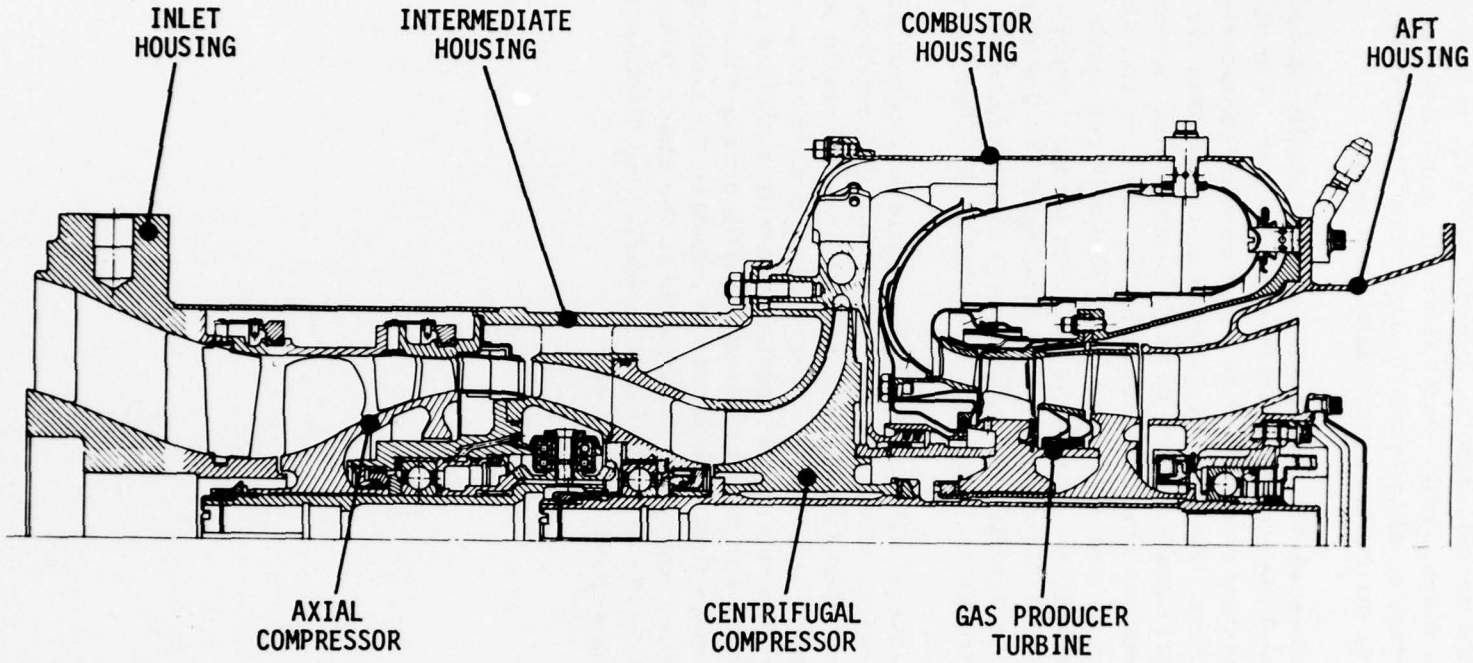

Figure 1. PLT-34 Gas Generator.

The second turbine nozzle, also an integral casting, is brazed to the inner sheet stock diaphragms, seal assembly, and machined outer flange. Pressurization air passes through holes in the outer flange and the cored vanes to the inboard rotor labyrinth seal.

The turbine rotor assembly comprises the individually bladed first rotor assembly and the integrally cast second rotor. The first rotor blade is an investment casting and is supplied with compressor discharge air for blade cooling. As shown in Figure 2, the cooling air is supplied through a preswirl nozzle, which imparts a tangential momentum to the coolant. This reduces static pressure in the rotor cavity, thereby minimizing labyrinth seal pressure drop, and reduces static temperature of the onboard cooling air as well as pumping losses. Individual holes are provided in the disc to transfer the cooling air to the blades where it flows through an integrally cast, three-pass cooling network. The coolant issues through an integrally cast slot at the blade's trailing edge.

The cooled first-stage turbine shroud is cantilever-supported from the combustor ID housing. The cooling air passage is formed between the shroud and a sheet-metal baffle attached to the first nozzle outer shroud. The shroud has stagger-spaced hexagonal knobs cast on the outer surface which are used to maintain a positive airflow passage between the cylinder and the sheet-metal baffle during engine operation. The knobs also act as flow turbulators to increase the cooling air heat-transfer rate. The cooling air is admitted to the space between the shroud and baffle at the aft end, flows forward, and discharges into the mainstream at the shroud leading edge.

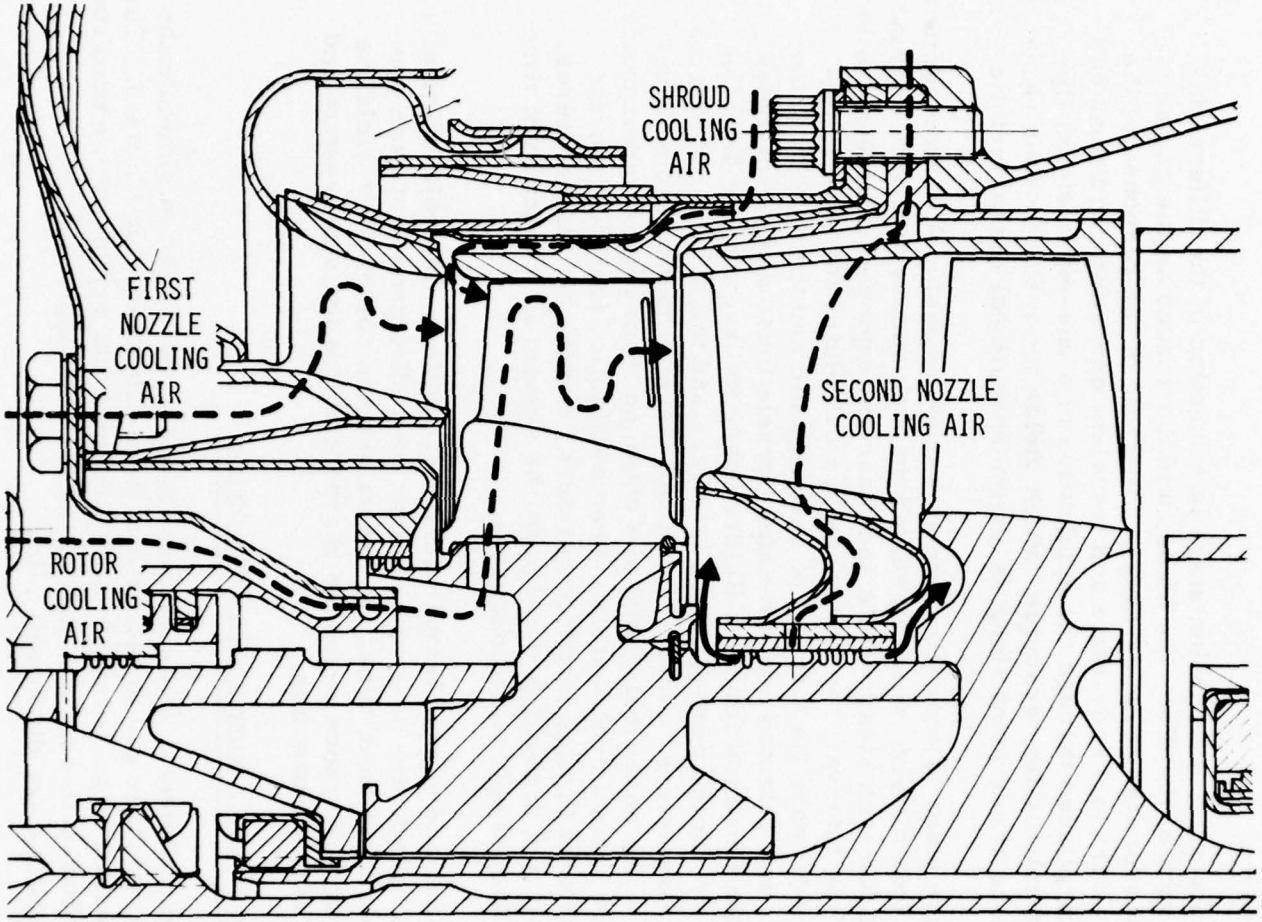

Figure 2. Rotor Cooling Air Network.

ANALYTIC TECHNIQUE

APPROACH

The tip clearance of a turbine stage is a function of the differential radial growth of the disc, the blade, and the shroud as the engine is exercised over its operating range. Analysis of the response of the turbine system to steady-state and transient operating conditions has been accomplished through the application of a one-dimensional tip-clearance calculation technique, which yields the instantaneous value of clearance at any point along an engine operational characteristic.

The turbine stage is characterized as a one-dimensional, finite-element, heat-transfer matrix, which is solved through successive time interval iterations for each steady-state and transient engine operating condition. At each time interval, temperatures are calculated for each finite-element nodal point as a result of aerodynamic and thermal boundary conditions and selected heat-transfer correlations to adjacent nodes. Correlation functions for each fluid/surface interaction are based on the geometry of the heat-transfer interface and the associated thermodynamic parameters. Aerodynamic and thermal boundary conditions for input to the analytical model are obtained from engine performance analysis or from actual test data when available. Included are the distributions of turbine inlet temperature, cooling air temperatures, flow rates, and pressures throughout the system as a function of time for the selected operating conditions.

Disc, blade, and shroud temperature distributions, in conjunction with rotational speed, are used to calculate the radial growth of each component as a function of time. These values are combined to yield the resulting tip-clearance response characteristics for steady-state and transient engine operation.

HEAT-TRANSFER MODEL DESCRIPTION

The one-dimensional, finite-element model constructed to simulate the PLT 34 first-stage gas producer turbine is illustrated in Figure 3. The model consists of an array of nodal elements that represent the material and fluid flow-path configuration of the turbine stage. These nodal representations are discussed below.

Material Nodes

Material nodes used to represent the turbine components were selected

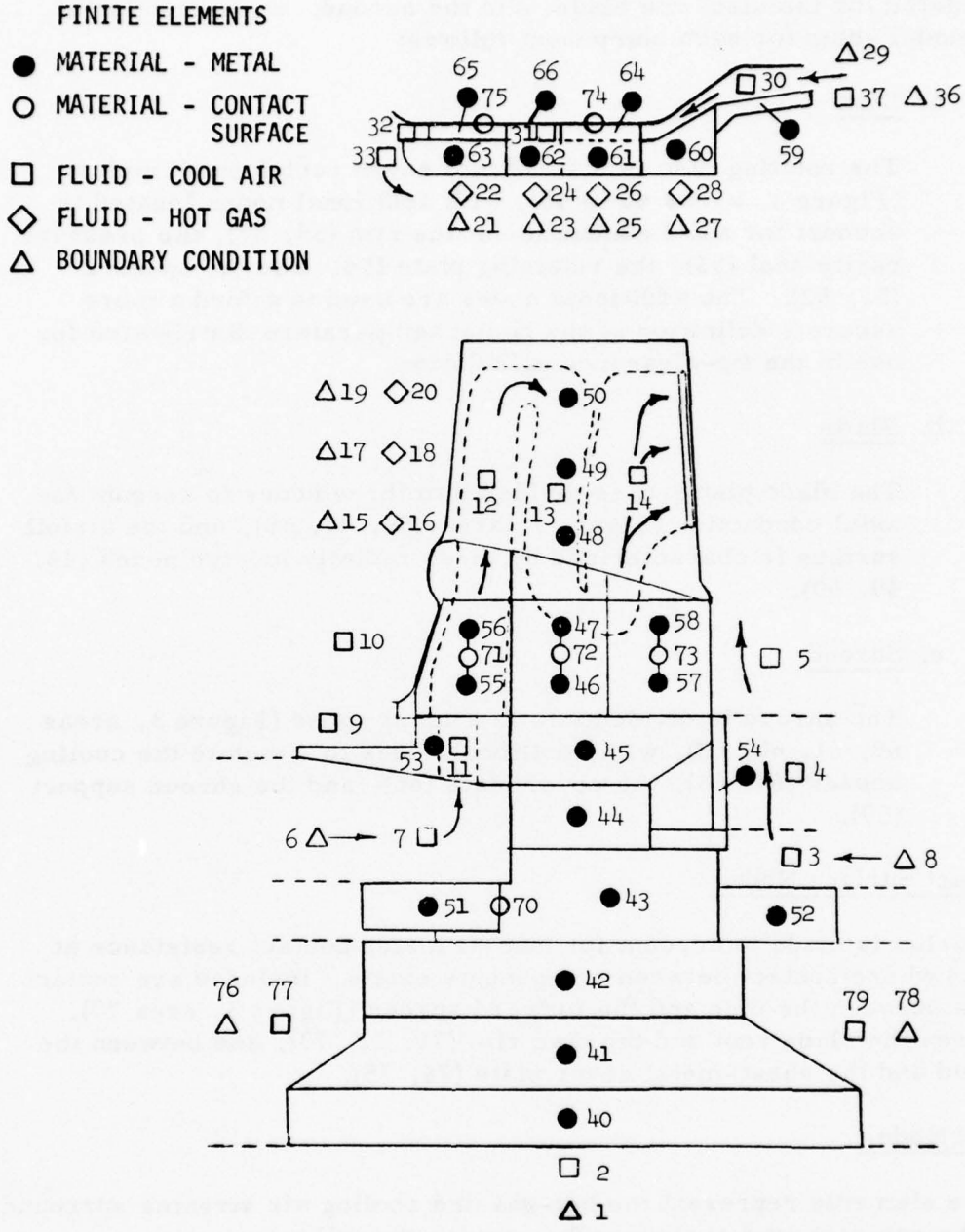

Figure 3. Tip-Clearance Analytic Technique Nodal Model.

to enable a one-dimensional radial temperature distribution to be calculated for the disc, the blade, and the shroud. A description of the model setup for each component follows:

a. Disc

The rotating disc is divided into seven radial metal nodes (Figure 3, areas 40 to 46), with additional nodes located to account for axial conduction at the rim (55, 57), the preswirl cavity seal (53), the retaining plate (54), and the spacers (51, 52). The additional nodes are used to afford a more accurate definition of the radial temperature distribution for use in the tip-clearance calculation.

b. Blade

The blade platform is divided into three nodes to account for axial conduction (Figure 3, areas 56, 47, 58), and the airfoil surface is characterized by three radially located nodes (48, 49, 50).

c. Shroud

The shroud is divided into four axial nodes (Figure 3, areas 60, 61, 62, 63), with additional nodes to simulate the cooling bosses (64, 65), the cover plate (66), and the shroud support (59).

Contact Surface Nodes

Provision is made to account for heat-transfer contact resistance at points where contact between components exists. Included are contact nodes between the disc and the forward spacer (Figure 3, area 70), between the blade root and the disc rim (71, 72, 73), and between the shroud and the sheet-metal cover plate (74, 75).

Fluid Nodes

These elements represent the hot-gas and cooling air streams surrounding the rotor/shroud system and comprise the following:

a. Gas

Inlet gas is represented by three radially located nodes

(Figure 3, areas 16, 18, 20) which are used to afford simulation of the turbine inlet radial temperature profile. In addition, the effect of temperature drop across the stage on distribution of shroud temperature is accounted for by assigning four gas temperature nodes along the shroud (22, 24, 26, 28).

b. Cooling air

Cycle cooling airflow rates are input as a percentage of main gas flow, and each coolant stream is represented by a series of nodal elements. Blade cooling air enters the system at the disc forward face (Figure 3, area 7) and flows through a transfer hole in the disc (11) and through the blade cooling network (12, 13, 14). Leakage through the forward disc labyrinth seal (9, 10) is also simulated. Disc aft face cooling air, which is supplied through the second nozzle vanes, is characterized by three fluid nodes (3, 4, 5). The stagnant air regions surrounding the disc in the hub area are also included as three nodes (77, 2, 79). Shroud cooling air flows between the shroud and the sheet-metal cover plate, exhausts at the shroud leading edge, and is simulated by four nodes (30, 31, 32, 33). The conduction link between the shroud support and its mounting flange is simulated by a fluid node (37).

c. Boundary conditions

Input values of gas and cooling air temperatures, as a function of time, are transferred to the analytic model through the boundary condition nodes. Gas inlet temperature is represented as three radially located nodes (Figure 3, areas 15, 17, 19) and four axially located nodes (21, 23, 25, 27); blade cooling air by node (6); disc aft face cooling by node (8); disc bore boundary temperatures by three nodes (76, 1, 78); shroud cooling air by node (29); and the shroud mounting flange conduction link by node (36).

CALCULATION TECHNIQUE

The calculation of tip clearance is discussed below.

Boundary Conditions

Boundary condition parameters are defined for each steady-state and

transient gas generator operating condition. Parameters that are related to turbine rotational speed only are supplied as a function of speed.

These include:

a. Turbine temperature drop - inlet to exit

b. Turbine relative inlet temperature - differential from inlet total temperature

c. Turbine cooling air inlet temperature - differential from compressor exit temperature

d. Disc upstream static pressure

e. Disc downstream static pressure

For the initial analysis, these parameters were defined from the gas generator design cycle analysis. For the analysis of actual engine operating conditions, the measured values for turbine cooling air temperature and disc upstream static pressure were used. Disc downstream static pressure was calculated from measured disc upstream pressure, assuming design pressure ratio variation.

Boundary condition parameters that change as a function of time during gas generator transient operation are defined for each transient and for steady-state operating points. These parameters include:

a. Turbine rotational speed

b. Gas generator inlet airflow

c. Turbine inlet temperature

d. Compressor exit temperature

At each time interval, the temperatures of the boundary condition nodal points of the heat-transfer model are calculated from the boundary condition parameters in the following manner:

a. Gas inlet temperature (Figure 3, areas 15, 17, 19) - Relative inlet temperature to the blade is calculated by applying the design combustor exit-temperature distribution

shape to the turbine inlet total temperature at the specified time and subtracting the total-to-relative temperature differential as a function of rotational speed.

b. Gas temperature along shroud (21, 23, 25, 27) - The value of inlet total temperature at the outer wall is determined by applying the combustor exit temperature distribution to the inlet total temperature. The axial variation of gas temperature along the shroud is determined by proportionally reducing the temperature corresponding to the work extracted in the turbine stage.

c. Blade cooling air (6) - The differential between turbine cooling air inlet temperature and compressor discharge temperature, as a function of speed, is applied to the compressor exit temperature at the specified time.

d. Shroud cooling air (29) - Shroud cooling air inlet temperature is calculated by adding to the compressor exit temperature a temperature-rise term which is prorated as a function of combustor temperature rise.

e. The following temperatures are prorated from the design values as a function of combustor temperature rise at the specified time:

- Disc aft face cooling (8)
- Disc bore boundary temperatures (76, 1, 78)
- Shroud support flange (36).

Heat-Transfer Matrix Solution

The calculation technique for the solution of the heat-transfer matrix employs a stepwise procedure over time intervals small enough to allow linear temperature averaging and evaluation of properties at constant temperature. Typical time intervals range from 0.2 second during rapid transients to 1.5 seconds as equilibrium is approached. The fluid-element temperatures are evaluated by assuming quasi-steady-state during each time interval to reflect the transient flow and temperature boundary conditions. Convective heat-transfer coefficient formulations, depending on the fluid flow path, are evaluated at each time interval to determine the heat-transfer rates between the fluid elements and the

material elements. During the calculation of fluid-element temperatures, the material nodes are held constant at the previously calculated temperature levels. The fluid node heat-balance formula is described in Appendix A.

Material temperatures are then reevaluated at each time interval. Their rate of temperature change is determined by a heat balance of the convective heat transfer from the fluid elements and the conductive heat transfer from the adjacent material elements. The metal node heat-balance formula is described in Appendix B.

Heat-Transfer Coefficient Determination

Convective heat-transfer coefficients at each fluid/metal interface are calculated at each time step as a function of geometry and the applicable thermodynamic parameters. The three basic correlations used are those for internal flow, flow adjacent to a rotating disc, and flow over a flat plate. A description of each correlation function is provided in Appendix C. A description of the correlation technique used for each component is presented below.

a. Disc

Heat-transfer coefficients for the purge flow forward (Figure 3, areas 9, 10) and aft (3, 4, 5) of the disc are determined by Kapinos' Method for small radial flows in the gap adjacent to rotating disc. Heat-transfer coefficients for the fluid nodes (77, 79) on the side of the disc below the spacers are held at a constant value ($h = 20$ Btu/hr $ft^2 \cdot F$) felt to reflect an induced enclosed air circulation. The fluid at the bore (2) is also held at a constant value ($h = 5.0$ Btu/hr $ft^2 \cdot F$) representing the conductivity through a stagnant air gap adjacent to the shafting (1).

Flow in the preswirl cavity (7) is treated using Colburn's equation for channel flow with the relative velocity of the preswirl air adjacent to the disc.

Contact between the disc and forward spacer (70) is treated as an effective convective heat-transfer coefficient of 1000 Btu/hr $ft^2 \cdot F$ acting over the area of contact.

b. Blade

The turbulent flow across a plate correlation is used for the gas side fluid (Figure 3, areas 16, 18, 20) heat-transfer coefficients. The heat-transfer coefficients for the interior cooling flow in both the platform and blade (11, 12, 13, 14) are calculated using Colburn's equation, with the appropriate factors corresponding to pins, pillars, and slots in the passages.

The average contact resistance, CR (71, 72, 73), between the blade and the disc at the ball root is determined by establishing the high-pressure load contact area (Ac), as well as the total ball root surface area (As), and performing an area weighted average:

$$\frac{1}{CR_{AVG}} = \frac{Hr\ (Ac) + (k/L)(Ac-As)}{As}$$

where Hr = 5000 Btu/hr ft^2 ° F is a typically large experimental value; L is the nominal gap between root and rim; and k is the thermal conductivity of air. This average contact resistance is then applied to the entire area of contact between the blade root and the disc. Effects of axial leakage along the ball root are ignored.

The heat-transfer coefficient for the hot gas along the platform (16) is determined by using the correlation for turbulent flow across a plate, where the flow length across the platform is approximated as the chord length of the blade.

c. Shroud

An experimentally determined factor is used in the Colburn equation to determine the heat-transfer coefficients for the interior cooling flow (30, 31, 32, 33) around the bosses.

Heat-transfer coefficients for the gas-side fluid (22, 24, 26, 28) are determined by using the flat-plate correlation for turbulent flow with a flow length equal to the helical spiral length from the nozzle trailing edge to the node, based on the exit swirl angle of the nozzle. It is believed that this length most accurately simulates the gas path in the forward portion of the shroud, without compromising accuracy in the aft

portion where the gas flow direction has been vectored to axial.

Tip-Clearance Calculation

Solution of the heat-transfer matrix results in definition of the component metal temperature distribution as a function of time. The nodal elements that represent the radial distribution of temperature in the components are used for tip-clearance calculation. These elements are:

a. Disc (Figure 3, areas 40 through 45)

b. Disc rim (46)

c. Blade (47 through 50)

d. Shroud - average of elements (60 through 63)

e. Shroud coverplate (66).

At selected time intervals, a strain calculation using the radial temperature distribution, in conjunction with rotational speed, determines the thermal and centrifugal growth of each component. The disc is approximated by a series of radially linked rings and the blade as a series of elements in a bar. The ball root transmits the blade centrifugal force to the disc. Thermal and centrifugal growth of the disc, the ball root, and the blade are added to determine blade tip growth. Shroud thermal growth is analyzed as a free ring or the resultant growth of two interfering rings. Thus, the restraint of a coverplate over the shroud can be evaluated. The difference of shroud growth minus blade tip growth determines the differential tip clearance. Turbine tip clearance at steady-state conditions, or at selected time intervals during a transient, is the sum of the assembly clearance and the calculated differential tip clearance.

TIP-CLEARANCE MEASUREMENT DEVICE

GENERAL DESCRIPTION

The tip-clearance measurement device used for these investigations is an optical system that uses a laser-beam triangulation technique to detect blade tip clearance. The basic system was developed under a previous program sponsored by the Eustis Directorate and is fully described in USAAMRDL Report TR-74-67.[1]

The principle of operation is illustrated in Figure 4, a diagram of the basic optical path within the probe system. Laser light transmitted through the input fiber optic bundle is focused by the lens onto the turbine blade. The prism at the probe tip deflects the beam at an angle to the blade surface, and the reflected beam is focused onto the coherent fiber optic output bundle. Tip-clearance readout is accomplished by a videcon optically coupled to the output fiber optic bundle. As illustrated, a change in blade position relative to the probe tip results in a change in the reflected spot location on the output fiber optic bundle and on the TV monitor readout.

Three tip-clearance measurement devices were installed in the gas generator. The optical system was rigidly mounted to a base plate as shown in Figure 5. Probes 1 and 2 were supplied by a 15-milliwatt helium-neon laser through a beam splitter and two input adjustment assemblies, while probe 3 used a 10-milliwatt laser as a light source. The three coherent fiber output bundles were mounted in close proximity and placed at the focal point of the TV camera. This allowed the simultaneous viewing and recording of all clearance measurements. Output was shown on a 19-inch monitor and recorded with a 1-inch video recorder. The signal from the gas generator tachometer speed pickup was recorded on the auxiliary audio track of the video recorder, insuring an accurate correlation between the measured tip clearance and the gas generator operating condition. During playback, a digital clock output was also included for transient clearance determination.

Details of the probe configuration are shown in Figures 6 through 8.

---

[1] M. J. Ford, J. R. Hildebrand, and J. C. Prosser, DESIGN, FABRICATION AND DEMONSTRATION OF A MINIATURIZED TIP CLEARANCE MEASURING DEVICE, Pratt & Whitney Aircraft Div., United Aircraft Corp., USAAMRDL-TR-74-67, Eustis Directorate, U.S. Army Mobility Research and Development Laboratory, Fort Eustis, Virginia, Sept. 1974, AD787318.

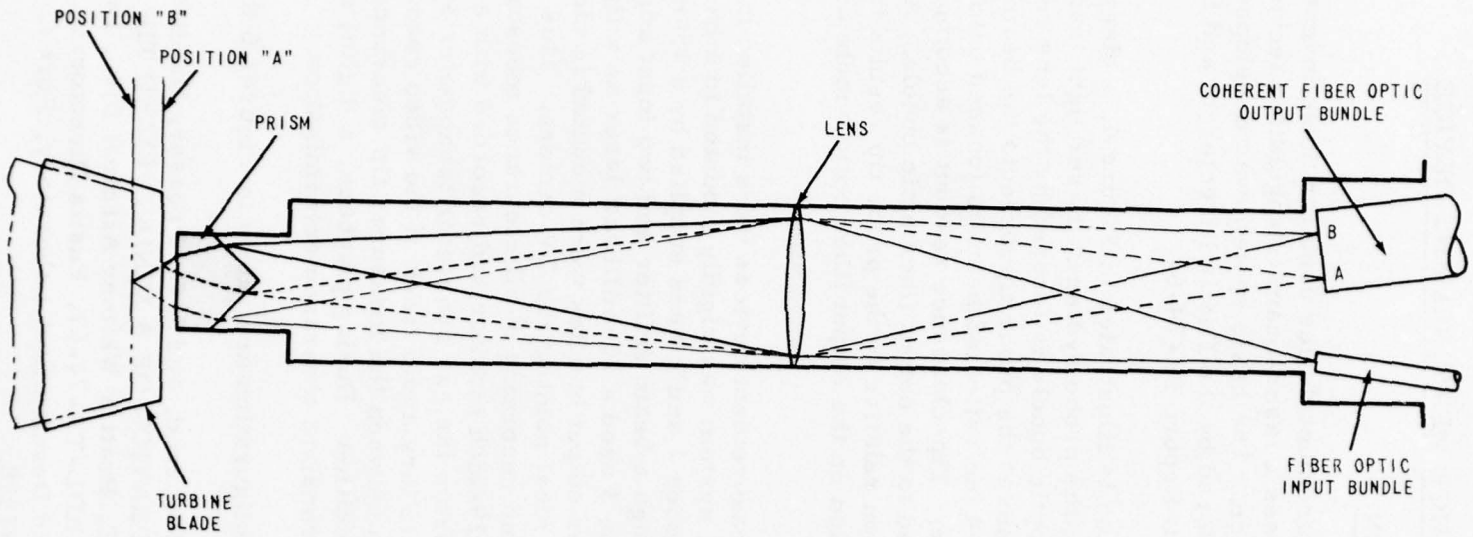

Figure 4. Tip-Clearance Measurement Device - Basic Optical Path.

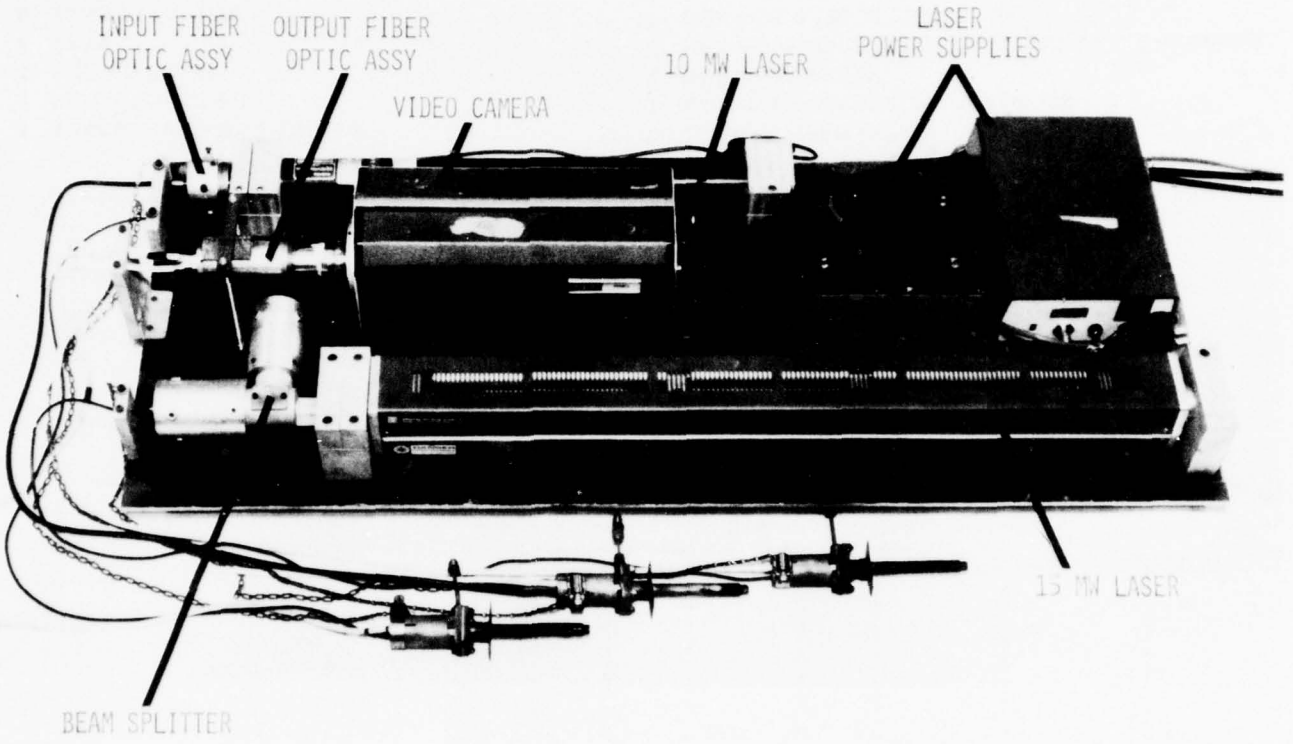

Figure 5. System Configuration.

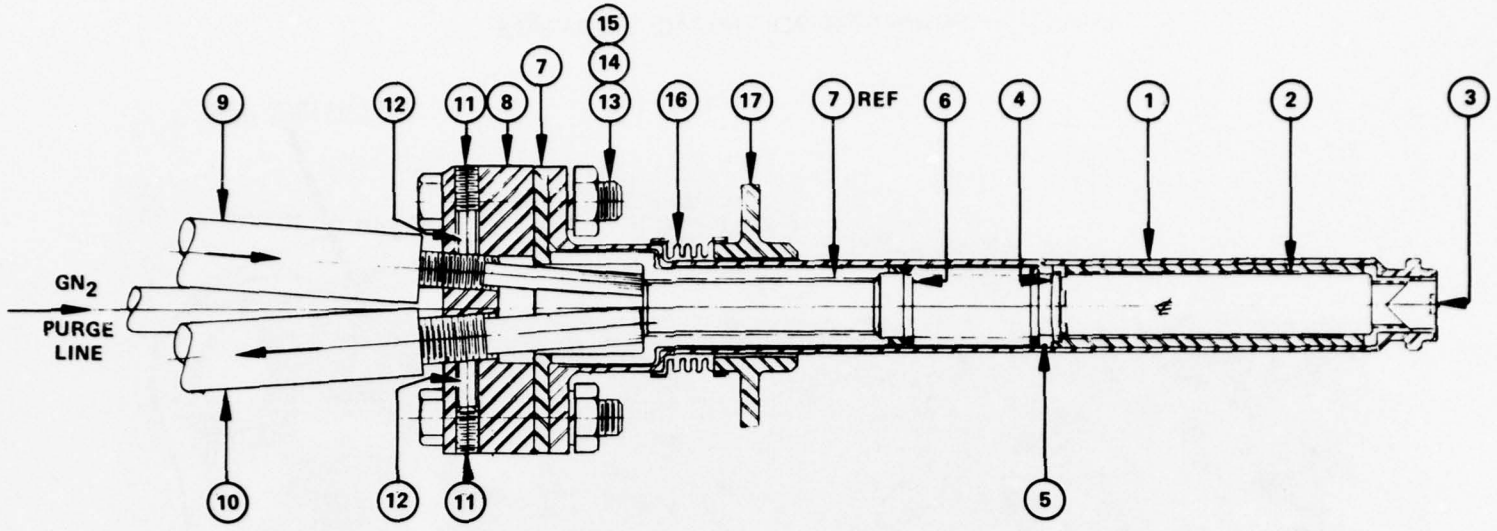

1 SUBASSY HOUSING AND TIP
2 PRISM RETAINER
3 3-SIDED PRISM
4 LENS
5 LENS RETAINER
6 COMPRESSION SPRING NO. 9655K22, S/S
7 SPACER
8 PROBE HEAD
9 INPUT FIBER OPTIC
10 OUTPUT FIBER OPTIC
11 NO. 5 HEX SOCKET SETSCREW S/S
12 ROD 0.100 in. DIA
13 HEX HD MACH BOLT, 0.190-32 UNF-3A x 1 in. LG S/S
14 HEX NUT 0.190-32 UNF-3B. S/S
15 LOCK WASHER FOR 0.190 in. BOLT, S/S
16 BELLOWS
17 PROBE FLANGE

Figure 6. Tip-Clearance Measurement Probe Layout.

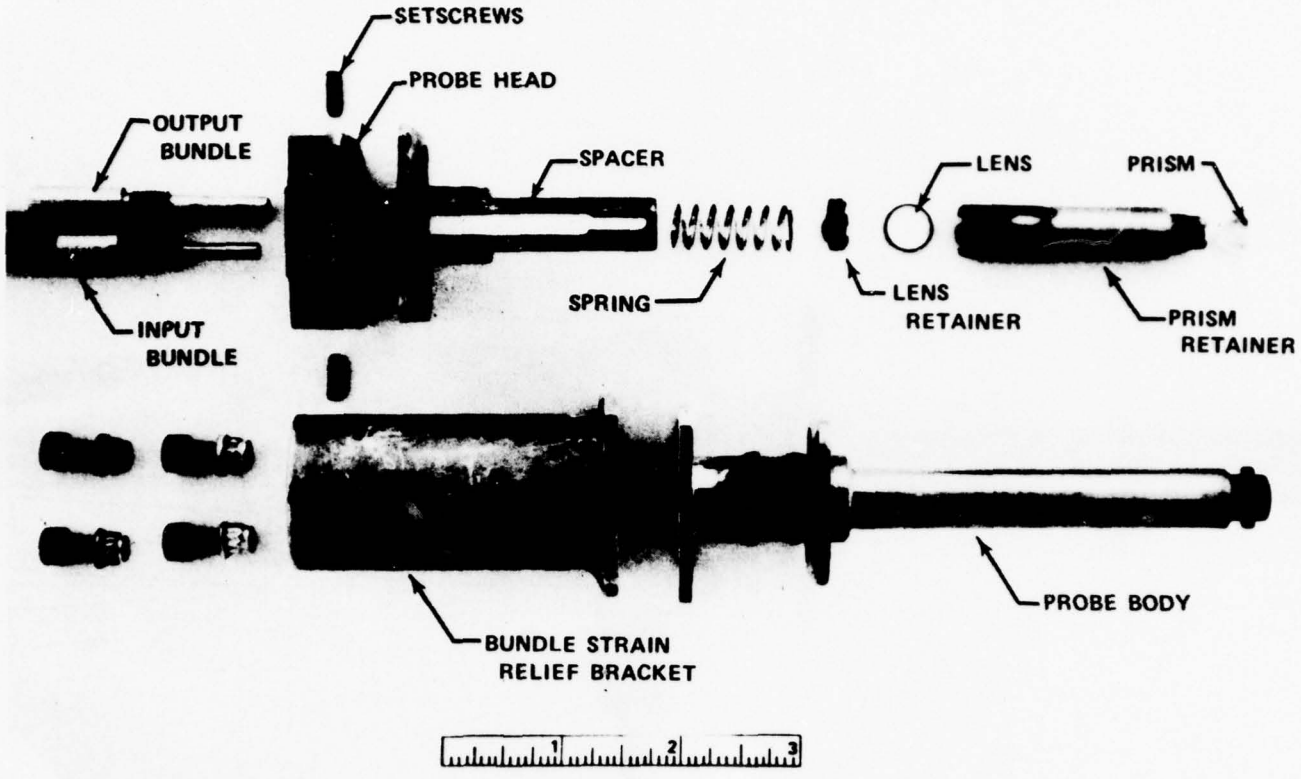

Figure 7. Tip-Clearance Measurement Probe Parts.

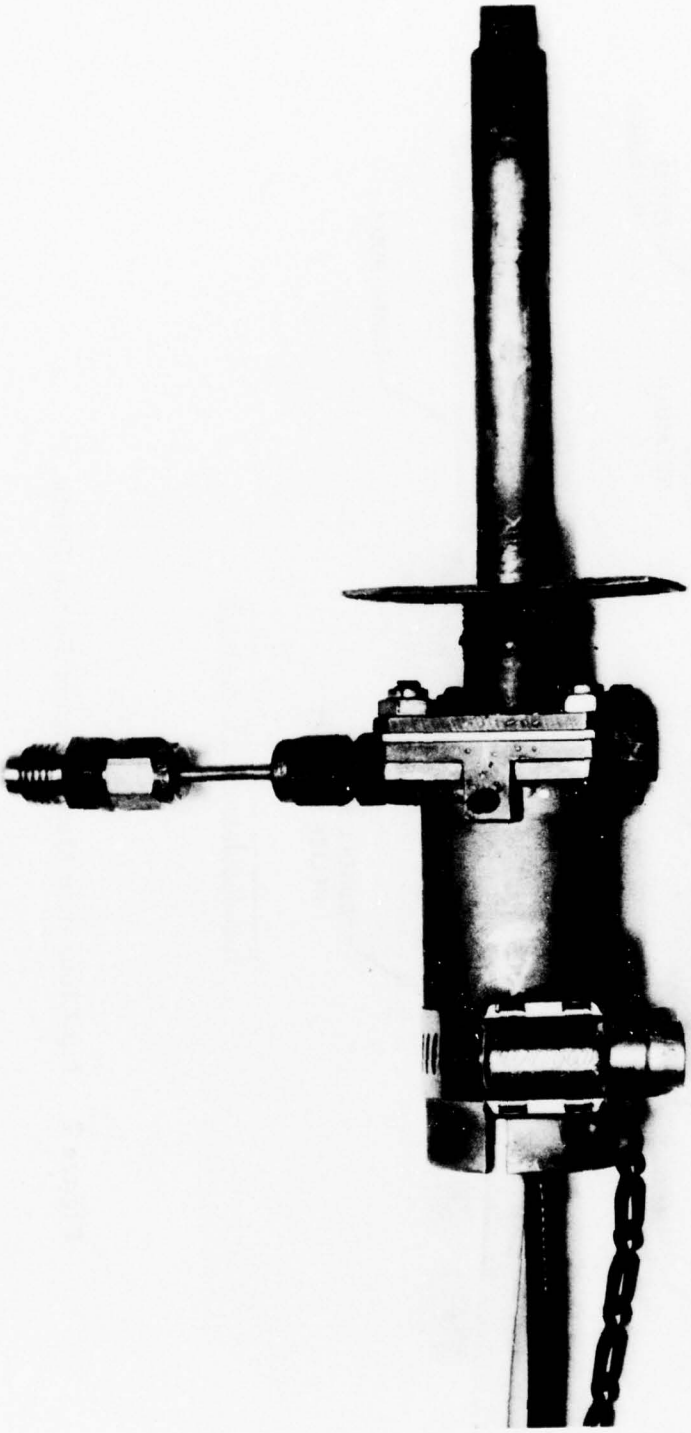

Figure 8. Probe Assembly.

Primary location is accomplished by the use of the bayonet lugs at the probe tip which lock into corresponding slots in the turbine shroud. The bellows at the outer mounting flange allow freedom of expansion so that the probe will follow the motion of the turbine shroud. The synthetic sapphire prism is located at the probe tip by the prism retainer, which is slotted to prevent rotation. The lens is positioned by the prism retainer and lens retainer, and the optical elements are held in place by a compression spring. Slots are provided in the retainers for the flow of the nitrogen coolant that is discharged through the probe tip. The input and output fiber optic bundles are located in the probe head and retained by set screws.

SETUP TECHNIQUE

Considerable development effort was necessary in order to make the laser tip-clearance measurement device a useful tool for engine test applications. The majority of the work was directed at the input optical system through which the laser beams were focused. The objective is to focus the laser beam on a single fiber of the input fiber optic bundle in order to present a close approximation to a point source input to the probe optical system. The following obstacles were encountered during the use of the initial input optical system:

a. The mechanical configuration of the system did not allow sufficiently fine adjustment of focal-length and focal-point position.

b. Crosstalk between fibers in the bundle caused multiple fibers to be illuminated at the output even when only one fiber was illuminated at the input end.

c. Readjustment of the input fiber optic assembly to maximize output light intensity required probe disassembly to insure that a single fiber was illuminated.

The following changes to the input optical system were made to overcome these problems:

a. The fiber optic support system was redesigned to allow precise adjustment of fiber position relative to the lens focal point. The system is illustrated in Figure 9. Adjustment screws are provided to move the fiber optic bundle fore and aft, to position it accurately at the focal point of the lens. Side-to-side adjustment is provided for by four screws which lock the entire assembly in position. This arrangement allows rapid and

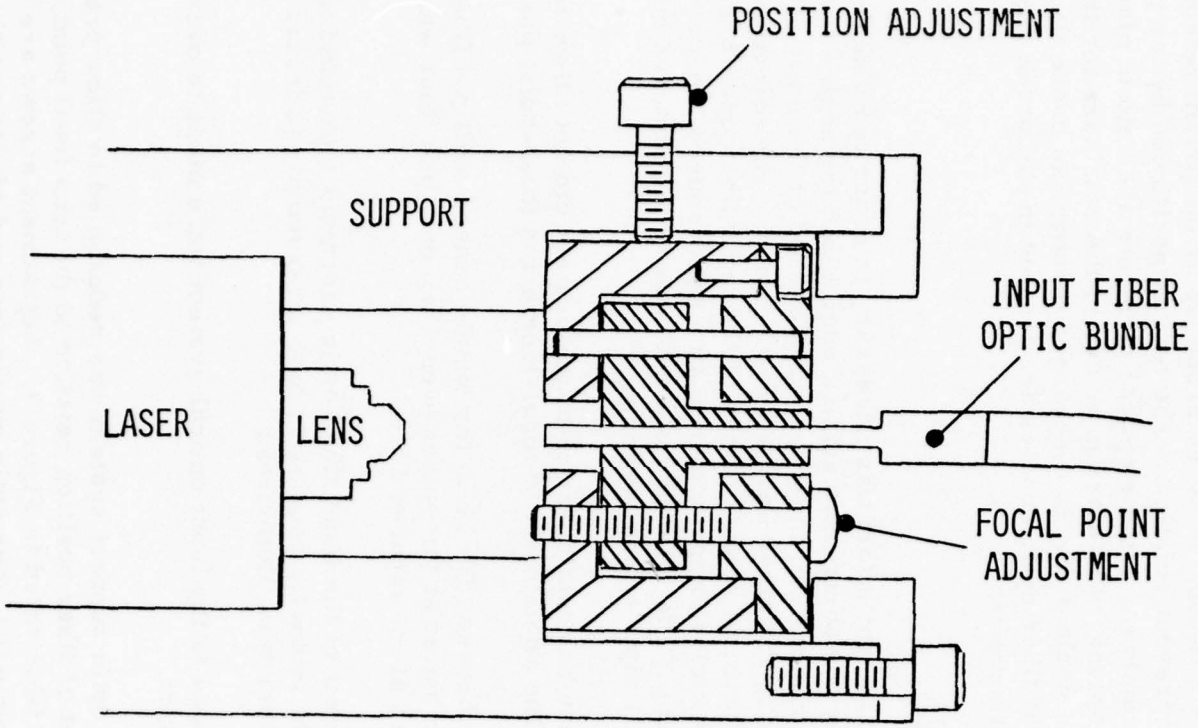

Figure 9. Input Optics Assembly.

accurate location of the single-fiber optic used as the light transmitter.

b. In order to guarantee that only a single fiber of the input fiber optic bundle was illuminated, all but one fiber was blocked off with nichrome tape at both the input and output end of the fiber optic bundle. Not only did this provide a minimum spot size, but it also allowed greater ease of adjustment for maximum light intensity. The fiber optic bundle position could be adjusted to give maximum output energy without the problem of illuminating multiple fibers and, thereby, increasing spot size.

Prior to calibration and after each major test phase, the probes were set up for optimum performance through the following technique:

a. The input optic assemblies were adjusted to provide maximum energy at the probe.

b. The positions of the output bundles at the TV camera interface were adjusted to be at the camera focal point by illuminating the fiber optic bundles with white light and focusing so that the individual fiber boundaries could be resolved.

c. The input fiber optic bundle was positioned in the probe head such that the output beam was focused on a target positioned at the average clearance distance from the probe tip.

d. The coherent output fiber optic bundle was positioned in the probe head to provide the smallest spot size on the TV monitor output consistent with sufficient range of clearance measurement.

INITIAL CALIBRATION

After initial assembly and setup, each probe was calibrated to determine range and accuracy. A depth micrometer was attached to a "V" block used to locate the probe perpendicularly to the micrometer face, and readings were taken at 0.002-inch intervals measured from the probe tip. Scales calibrated in inches were attached to the TV monitor screen for readout purposes. A typical calibration is shown in Figure 10; an accuracy of better than 0.001 inch and a sensitivity of less than 0.0005 inch were attained for each probe.

The dynamic response of the tip-clearance measurement system was

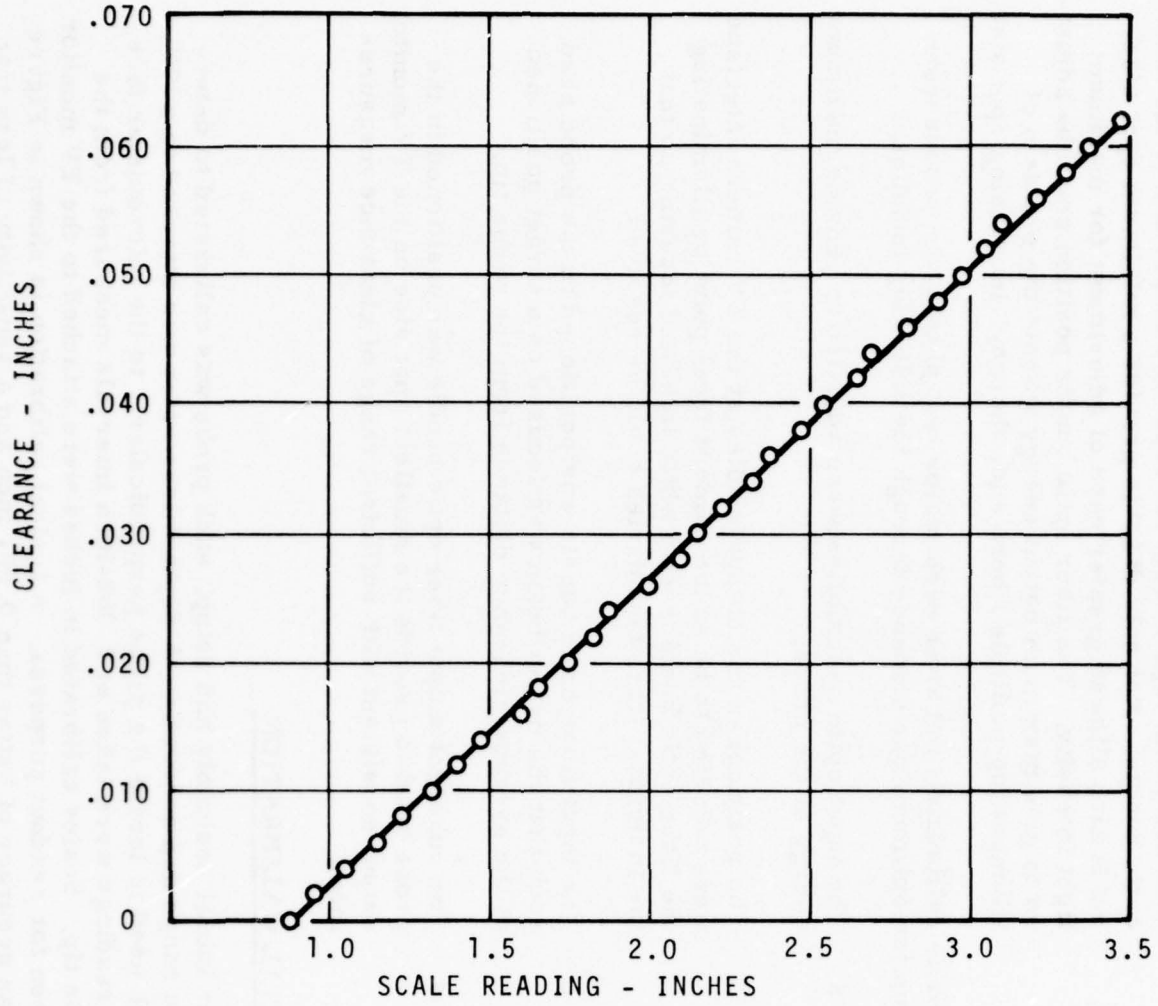

Figure 10. Initial Tip-Clearance Calibration, Probe Number 3.

verified through the use of a rotating calibration wheel. Observation of output spot position revealed no change in calibration during operation at up to 30,000 rpm with a 30-tooth calibration wheel.

A shaker table was used to determine the effects of vibration on probe operation and calibration. The probes were securely clamped in an aluminum block and vibrated in three planes: (1) along the probe axis, (2) perpendicular to the probe axis parallel to the prism axis, and (3) perpendicular to the probe axis perpendicular to the prism axis. A reflective plate attached to the mounting block allowed relative clearance readings to be recorded during the test. Two probes were vibrated over the following ranges:

±1G	:	40 - 250 Hz
±2.5 G	:	250 - 500 Hz
±10 G	:	500 - 1000 Hz
±20 G	:	1000 - 2500 Hz

No change in clearance measurement or calibration was detected during the vibration testing.

CLEARANCE MEASUREMENT PROCEDURE

The procedure used to record tip clearance during gas generator testing was developed to insure that the resulting measurements were as accurate as possible. On each test day, the following procedure was followed:

a. The probes were calibrated using the V block and micrometer setup previously described. Spot position was recorded on the video tape for each probe at 0.005-inch intervals measured from the probe tip. During gas generator assembly, the distance from the probe tip to the inner surface of the shroud had previously been measured for each probe.

b. After probe installation, the gas generator rotor was slowly rotated by hand and the tip-clearance measurement was recorded. This is termed the "in place calibration" and is a measure of the cold assembly clearance prior to testing.

c. Tip-clearance measurements were video recorded continuously

during all testing from initial cranking at startup through shutdown. Gas generator speed was simultaneously recorded to allow correlation of clearances data with gas generator operating condition.

d. At the completion of each test, the tip-clearance measurement probes were removed from the gas generator and the calibration procedure described in step a. was repeated.

e. Steady-state and transient tip-clearance results from the final test series were rerecorded for data analysis and presentation purposes. For these recordings, tip-clearance scales calibrated in inches of clearance between blade and shroud were made for each probe and positioned on the TV monitor screen consistent with the average probe calibration reading. Readouts of gas generator speed and elapsed time were superimposed on the TV monitor, and video recordings were made of all final steady-state and transient clearance results. Recordings were then replayed at a reduced frame rate, and tip-clearance values, as a function of engine operating condition and time, were extracted.

The output format is illustrated in Figure 11, an overall view showing the time and RPM outputs, as well as a closeup of the clearance measurement. The inherent problem in recording three outputs simultaneously is clearly shown by the probe-to-probe spot brightness variation. The spot produced by probe 1 was too bright to permit accurate reading, while the spot produced by probe 3 was barely visible. During readout of steady-state and transient clearances, the contrast and brightness settings of the readout monitor were adjusted to provide an optimum spot configuration for each probe in turn.

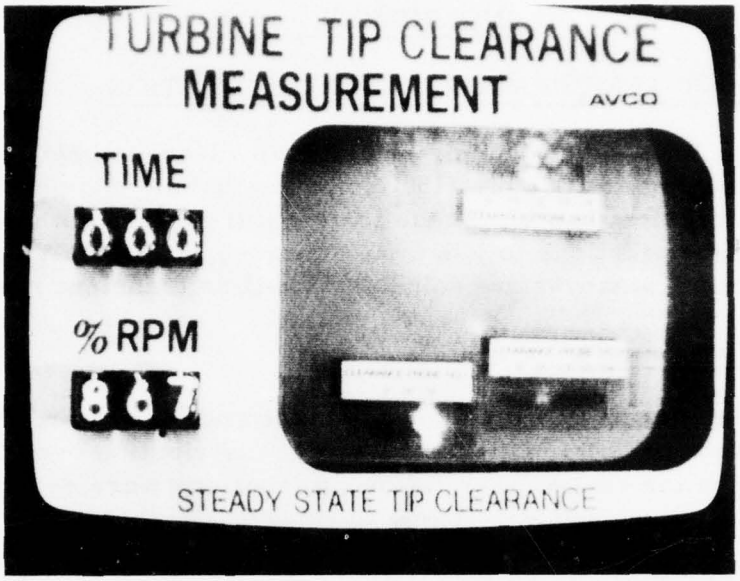

Overall Video Format

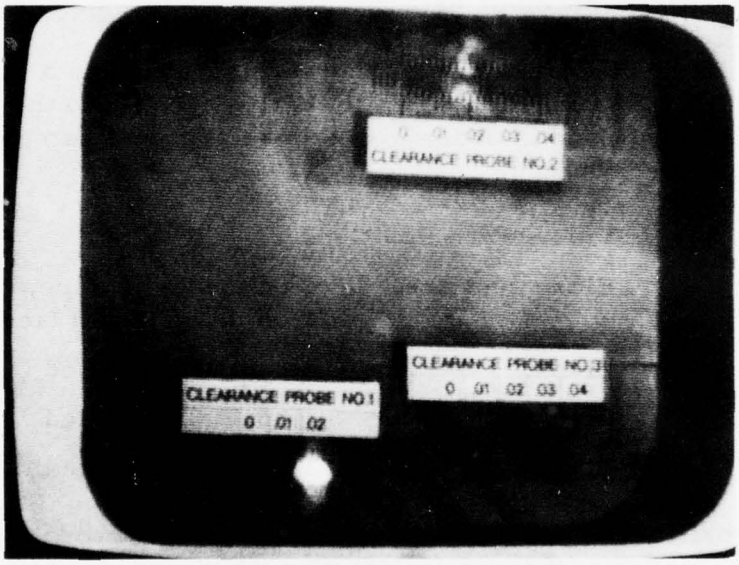

Close-up of Measurement Field

Figure 11. Tip-Clearance Measurement Output Format.

INSTRUMENTATION

COMPONENT TEMPERATURE INSTRUMENTATION

Correlation of calculated and measured tip clearance required measurement of the temperature distribution of the turbine components on a steady-state and transient basis. These temperatures were compared with the calculated distributions to judge the accuracy of the analytic technique in determining steady-state values, as well as transient response rates.

Rotating Components

Thermocouples were installed in the blade and disc to provide measurements of rotating component temperature distribution over the gas generator operating range. The following locations were selected:

Blade - Three Positions

25% blade height

50% blade height

70% blade height

The three blade measurements above were specified as a result of the relatively large contribution of blade thermal growth to the total rotating system growth and in order to obtain an adequate sample of blade temperature distribution.

Disc - Five Positions

Blade root area	-	1 on upstream face, 1 on downstream face
Disc web	-	1 centrally located
Disc midsection	-	1 centrally located
Disc bore	-	1 centrally located

The five positions above were selected to offer an optimal sample of disc radial and axial temperature distribution while retaining adequate disc low-cycle fatigue life.

A layout of the instrumented turbine wheel is shown in Figure 12. Blade temperature was sensed with chromel-alumel thermocouples encased in insulated 0.020-inch-diameter stainless steel sheaths and installed in

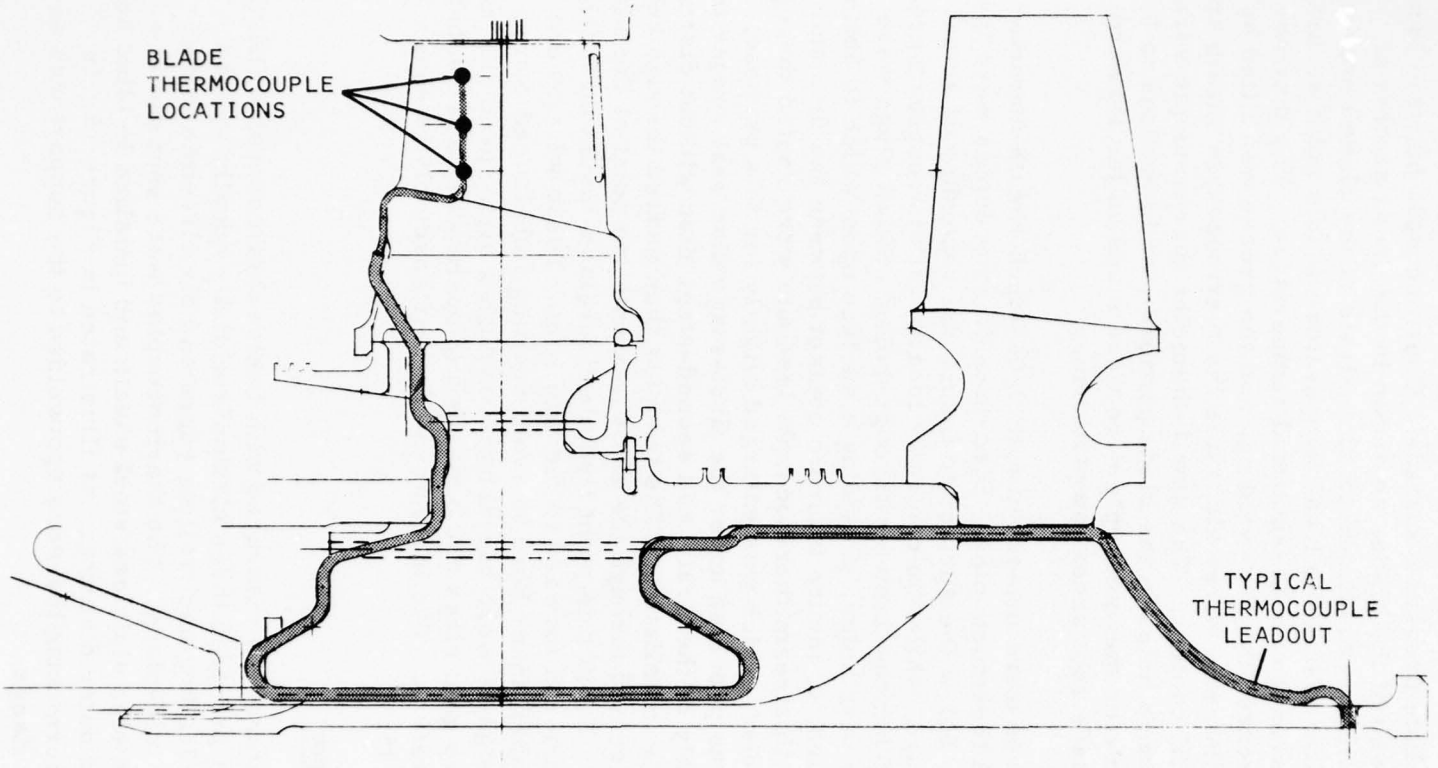

Figure 12. Instrumented Turbine Rotor Layout.

grooves in the blade pressure surface. Thermocouple junction location was in the web of the blade, as shown in the cross section of Figure 13. Previous two-dimensional analysis of the blade temperature distribution indicated that the local temperature at this point accurately represents the average cross-sectional temperature. The thermocouples were secured by tack-welding, and the groove was filled by tack-welding small-diameter wires alongside the thermocouple sheath and blending to airfoil contour. The small-diameter thermocouple wires were routed through holes in the blade platform, and junctions to 0.040-inch sheath diameter thermocouple wire were made on the forward portion of the blade root under the platform.

Disc temperatures were measured with 0.040-inch sheath diameter chromel-alumel thermocouples. Disc-face thermocouples were installed in shallow holes below the surface to insure the recording of actual metal temperature, while the centrally located thermocouples were installed in 0.050-inch-diameter through-holes. Small plugs were pressed into the disc holes, providing a surface upon which to bottom the thermocouples, to insure intimate contact between the disc and thermocouple. Upstream thermocouple leadouts were routed through the bore of the disc, which was enlarged slightly for this purpose. A junction point was provided under the first-stage disc seal runner to allow disassembly of the first- and second-stage disc without disrupting the thermocouple installation. The leadouts then passed through holes in the second disc and through the shaft to a junction point at the shaft inner diameter. From this point flexible fiberglass-insulated thermocouple wires were run forward to the slip ring. These wires were attached to the shaft inner bore to avoid rotating imbalanced components. Thermocouple signals were carried out through a high-speed slip ring that incorporates gold rings and brushes and operates in a freon bath at constant temperature. The instrumented rotor assembly is shown in Figures 14 and 15.

Shroud and Support

Shroud temperature was measured with twelve thermocouples installed in a pattern that provided three circumferentially equally spaced locations at the leading and trailing edges and six circumferential locations in the mid-plane. The thermocouples were encased in a 0.040-inch-diameter stainless steel sheath and installed in blind holes from the shroud outer diameter, as illustrated in Figure 16. In addition, two thermocouples were spotwelded to the support web and one to the mounting flange.

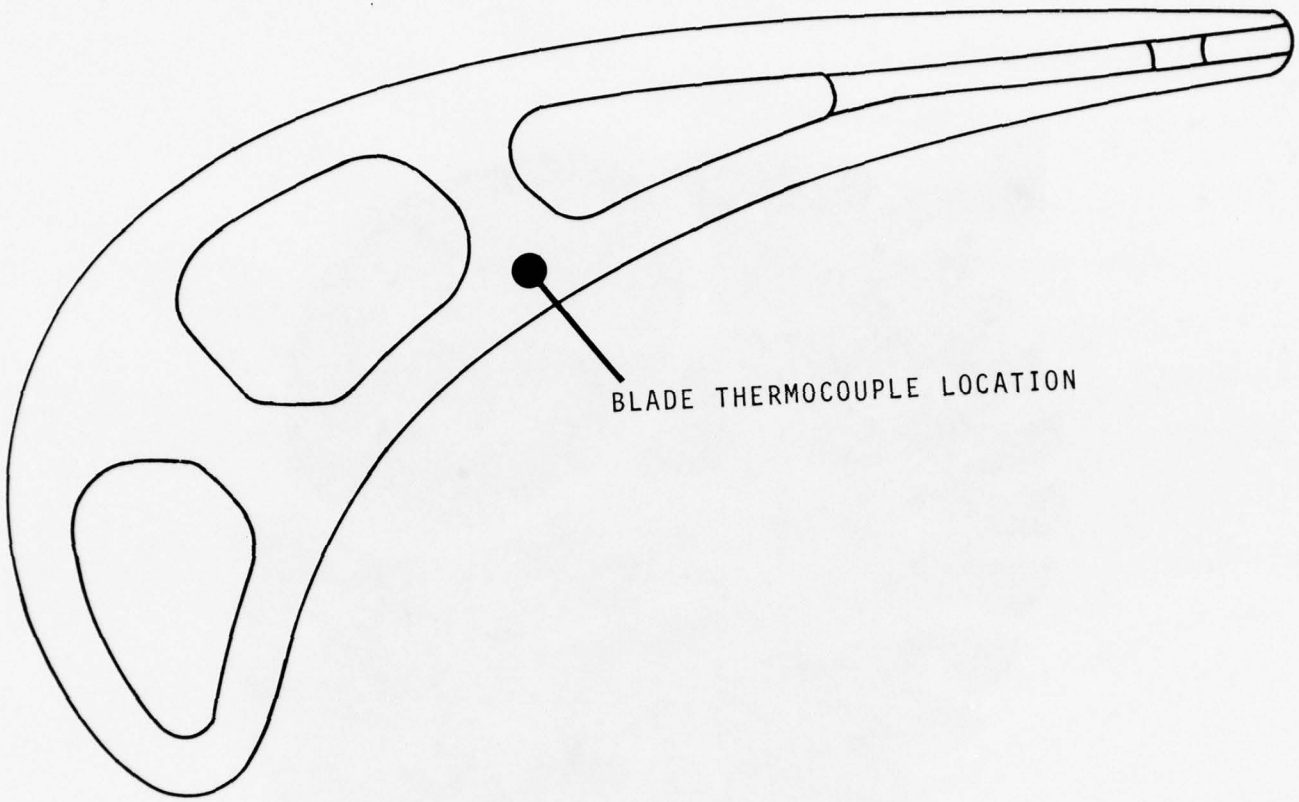

Figure 13. Thermocouple Location in Rotor Blade.

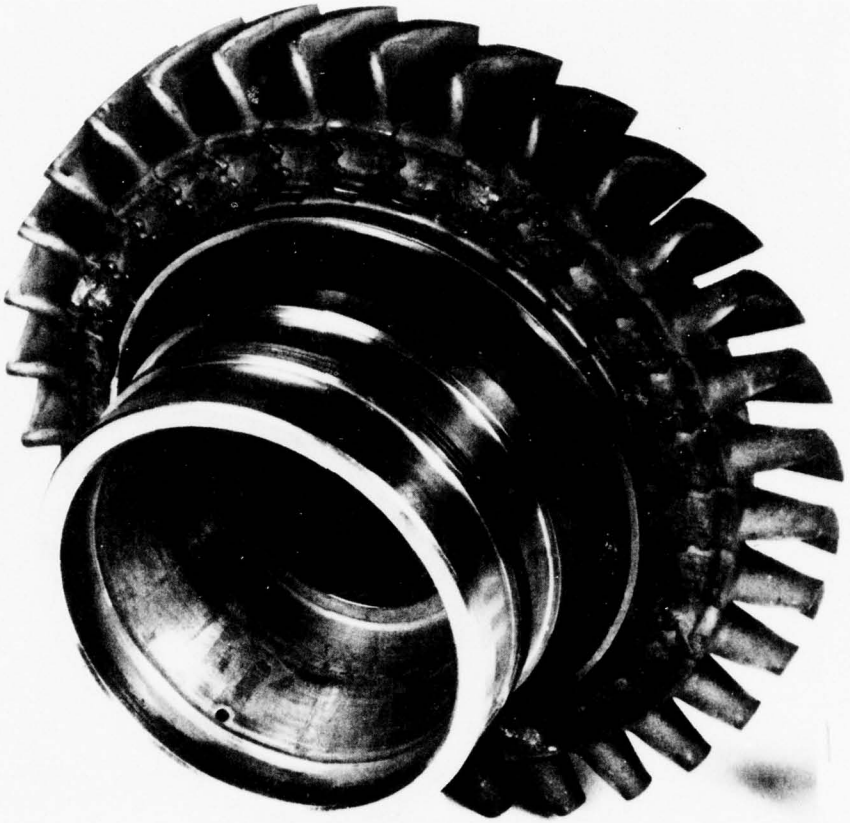

Figure 14. Instrumented Gas Producer Turbine Rotor - Front View.

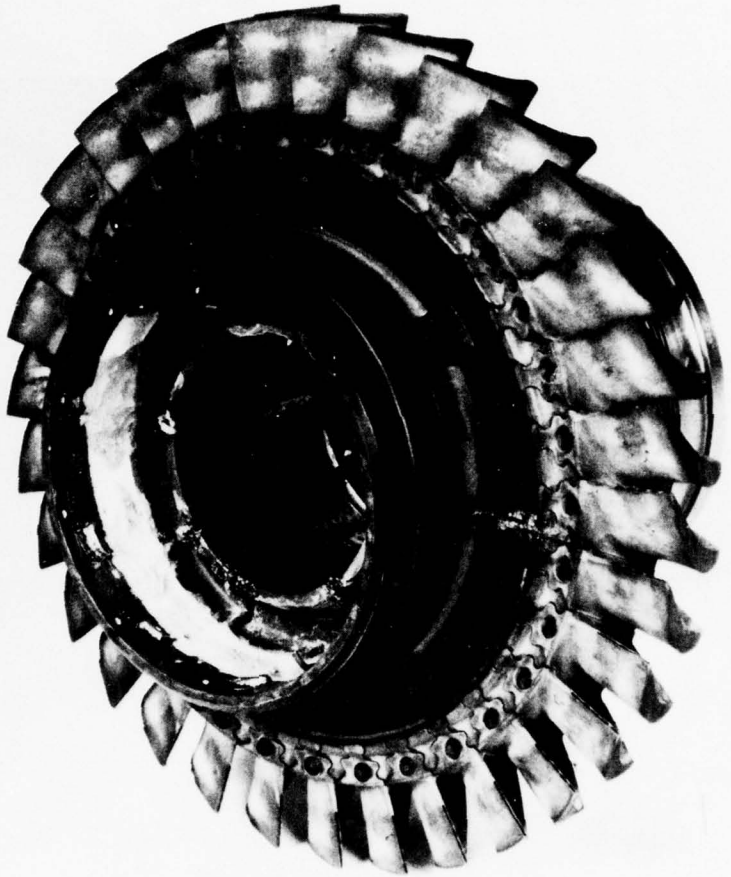

Figure 15. Instrumented Gas Producer Turbine Rotor - Rear View.

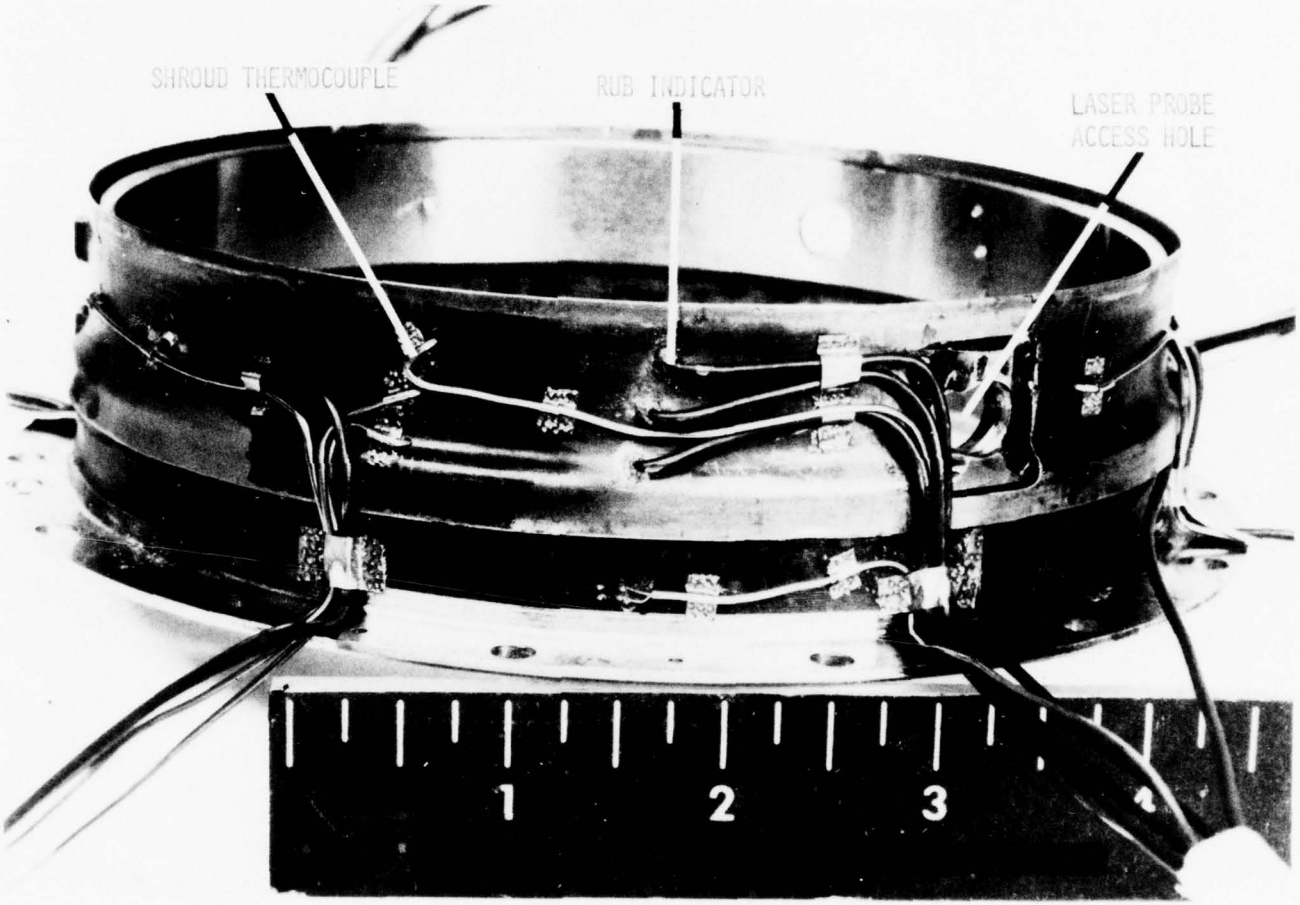

Figure 16. Shroud Thermocouple Installation.

Initial test results indicated a wide spread between measured temperature values, with several thermocouples indicating temperatures clearly too low. This was attributed to conduction error caused by the short insertion depth of the thermocouples into the shroud and the flow of shroud cooling air around the thermocouple leadout. Consequently, the six mid-plane measurement positions were reworked by providing slots in the shroud inner diameter (in the circumferential diameter) into which the thermocouples were placed. The slots were filled with wires tack welded alongside the thermocouple sheath in the same fashion as the blade thermocouple. These thermocouples were used as the basis for shroud temperature determination in the final test series.

BOUNDARY CONDITION INSTRUMENTATION

Overall gas generator performance analysis was done for each steady-state and transient operating condition to achieve definition of component heat-transfer boundary conditions. This was accomplished through the use of performance measuring instrumentation designed and used during the PLT 34 gas generator development program. Measurement of the following parameters was made:

a. Gas generator inlet parameters including airflow, pressure, and temperature

b. Overall operating parameters including rotating speed and fuel flow

c. Compressor exit pressure and temperature

d. Gas producer turbine exit pressure and temperature

e. Cooling airflow pressures and temperatures in the rotor cooling and the shroud cooling networks.

A summary of all gas generator instrumentation is contained in Table 1 and illustrated in Figure 17.

ADDITIONAL INSTRUMENTATION

Normal gas generator mechanical performance monitoring instrumentation was provided to measure vibration levels, oil flow rates, oil pressures, and oil temperatures.

An attempt was made to provide a check of measured tip clearance

TABLE 1. GAS GENERATOR INSTRUMENTATION SUMMARY

Function	Station/Location	Type and Number	
		Pressure	Temperature
Overall Gas Generator Performance	Gas Generator Inlet	4 Total, 8 Static	4
	Combustor Inlet	8 Total	8
	Gas Generator Exit	20 Total	20
Cooling Air Flow Measurement	First Rotor	4	2
	Shroud	4	2
Component Temperature Response	Rotor Blade		3
	Turbine Disc		5
	Shroud		12
	Shroud Support		3

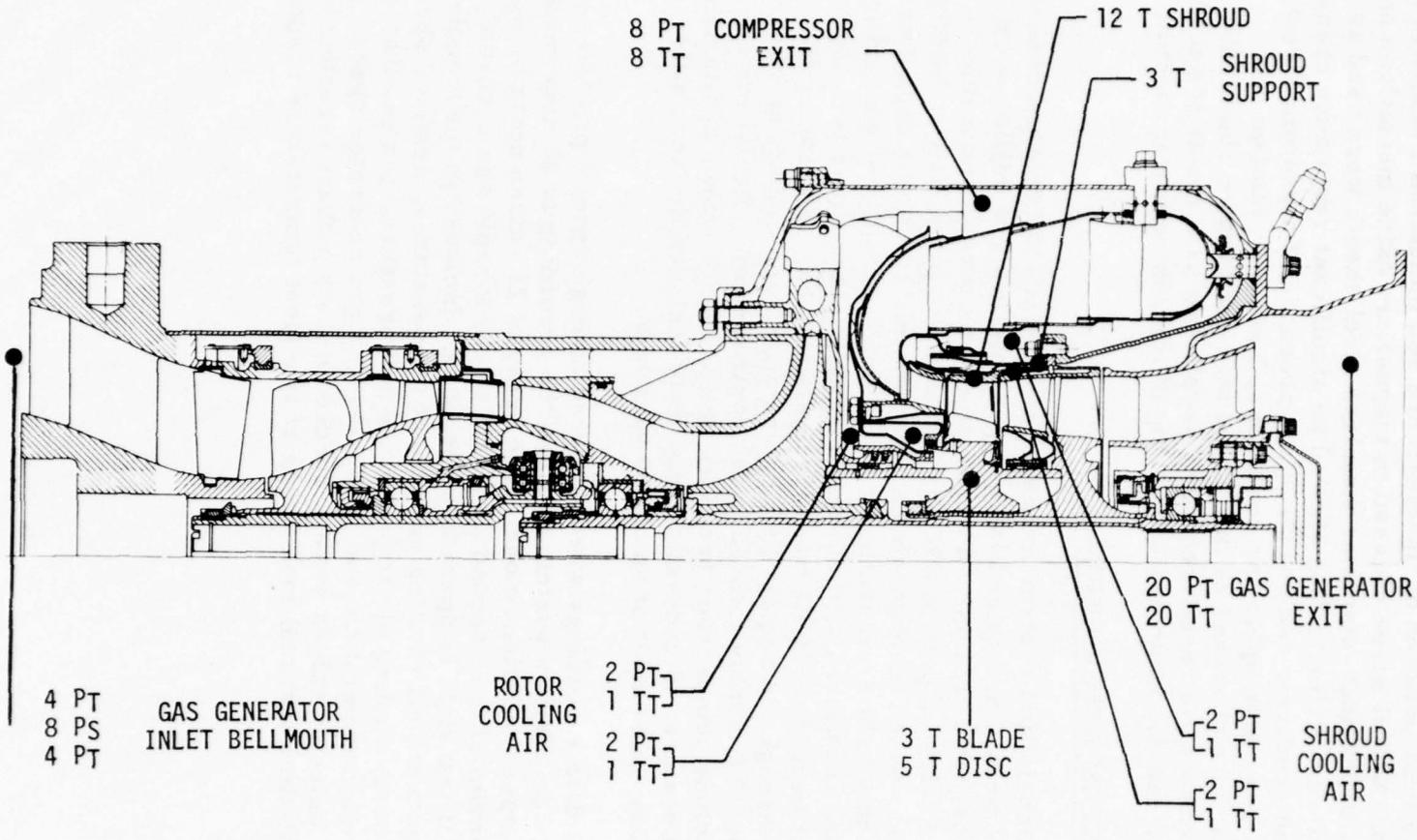

Figure 17. Gas Generator Instrumentation Summary.

through the incorporation of tip-clearance rub indicators installed in the shroud. Nickel wires encased in magnesium oxide insulation contained in a 0.062-inch-diameter stainless steel sheath were used as the rub indicators. Prior testing showed no significant resistance change between the conductor and sheath in the presence of a propane flame. Under gas generator operating conditions, however, random rub indications were observed as the engine was accelerated above idle. This is attributed to resistance paths developing as a result of hot gas ionization, causing improper triggering of the rub indicator circuit.

DATA SYSTEM DESCRIPTION

The data acquisition system consisted of an IBM 1800 data processor with a 32K work memory and is equipped with two 2.9 million word discs, a magnetic tape unit, a card reader and punch, and a line printer. Analog outputs of the data sensors are presented to the IBM multiplexer, which incorporates a relay matrix and flying capacitors to integrate data before presenting it to the analog-to-digital converter. The system allows real-time monitoring of engines under test and the permanent recording of all measured parameters. Monitoring is achieved through the acquisition, computation, and display of 20 variables on a CRT display located in the control room. Real-time computations include compressor pressure ratio, inlet airflow, and turbine inlet temperature. Steady-state capability includes the acquisition, computation, and output of up to 300 variables.

Transient data recordings were achieved through special programming of the data acquisition system to allow the recording of 21 data values in a high-speed transient mode. The array of 21 values could be updated at a maximum of 0.25 second intervals to allow rapid and accurate tracking of transient temperature response. Included in the transient recordings were all rotating component temperatures, selected shroud temperatures, cooling air temperature and pressure, gas generator turbine exit temperature and pressure, and gas generator speed. In addition, selected values were recorded on a strip chart recorder to allow real-time test cell monitoring of transient temperature response.

GAS GENERATOR MODIFICATIONS

GENERAL

In order to accommodate the instrumentation required to determine the response of each component in the rotor/shroud system which affects turbine tip clearance, as well as the devices used to measure the actual steady-state and transient levels of tip clearance, certain modifications to the test vehicle were necessary. These modifications were limited to the minimum required for probe access and component temperature measurement and were analyzed to insure that overall gas generator operation was not affected.

INSTALLATION OF TIP-CLEARANCE MEASUREMENT DEVICE

Because of the reverse-annular combustor design, the laser tip-clearance probes had to penetrate the combustor gas path to reach the turbine shroud. Protection was provided with water-cooled barrels surrounding each probe. A concentric tube design was used, and the barrels were mounted from the combustor outer housing as shown in Figure 18. Gas-filled metal "O" rings were used to avoid leakage at the probe and cooling barrel mounting surfaces, and air seals were provided at the combustor penetration points. A water flow rate of approximately 100 gallons per hour was used for each cooling barrel; temperature measurements showed a maximum water temperature rise of 24° F, which represents approximately 0.4 percent of the total combustor energy release; this did not have significant impact on turbine inlet temperature distribution.

In order to avoid interference with the flow issuing from the compressor diffuser, it was necessary to modify the pipe diffuser extensions in the area of the laser probes. Two pipe extensions were reworked at the entry point of each probe, as shown in Figure 19. The splitters were removed and the flow passages were reblended to divide the flow stream around the probes. No effects on compressor surge margin were detected during the test series due to this modification.

The support member for the first-stage nozzle was modified to allow the incorporation of access holes and slip-joint seals for laser installation. Modification to the shroud consisted of laser probe access holes and the incorporation of mounting lugs for the probe bayonet fitting. The additional material necessary for the probe mounting lugs compensates for the material removed from the holes, resulting in no decrease in shroud stiffness in the area of the probes.

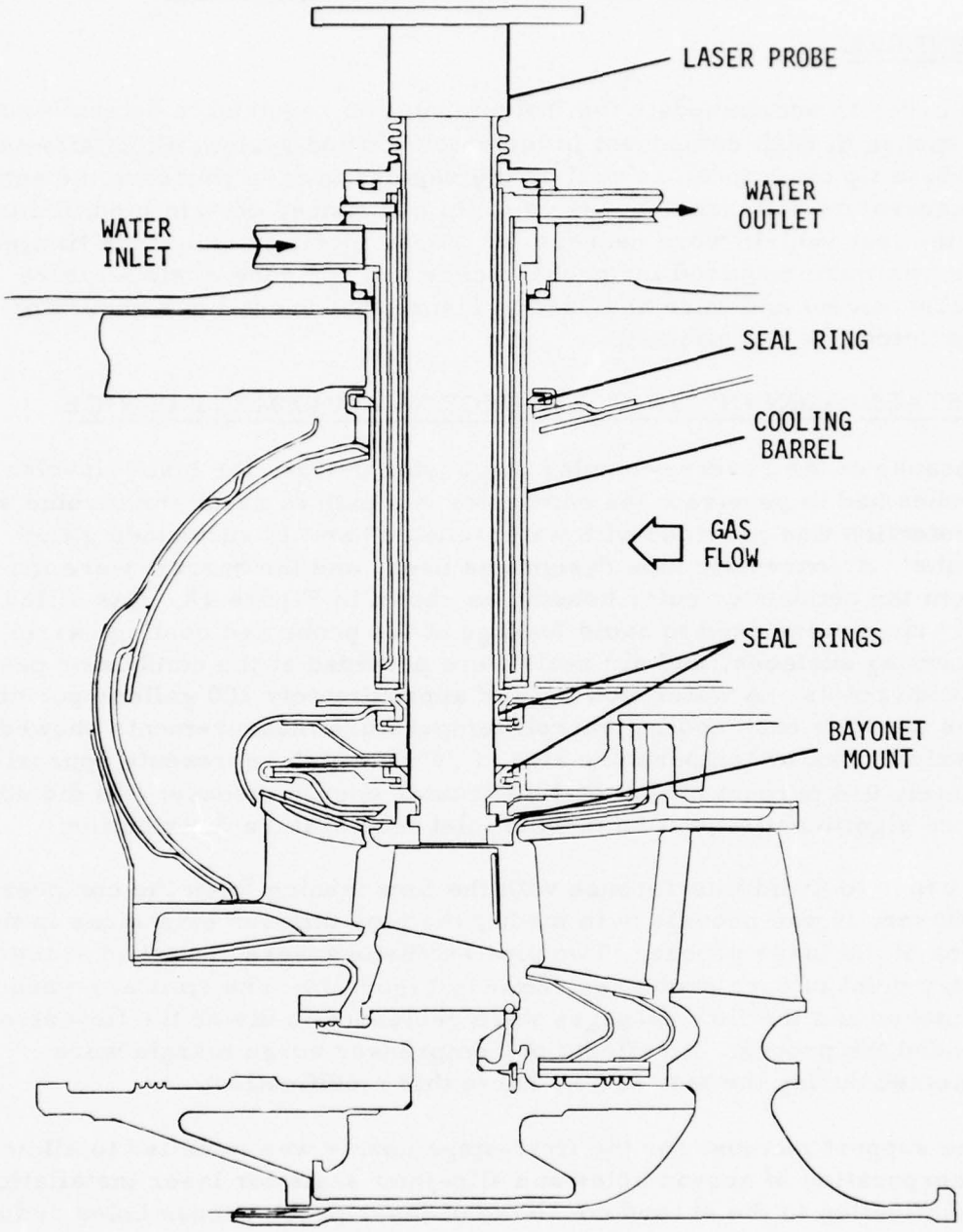

Figure 18. Laser Probe Installation Layout.

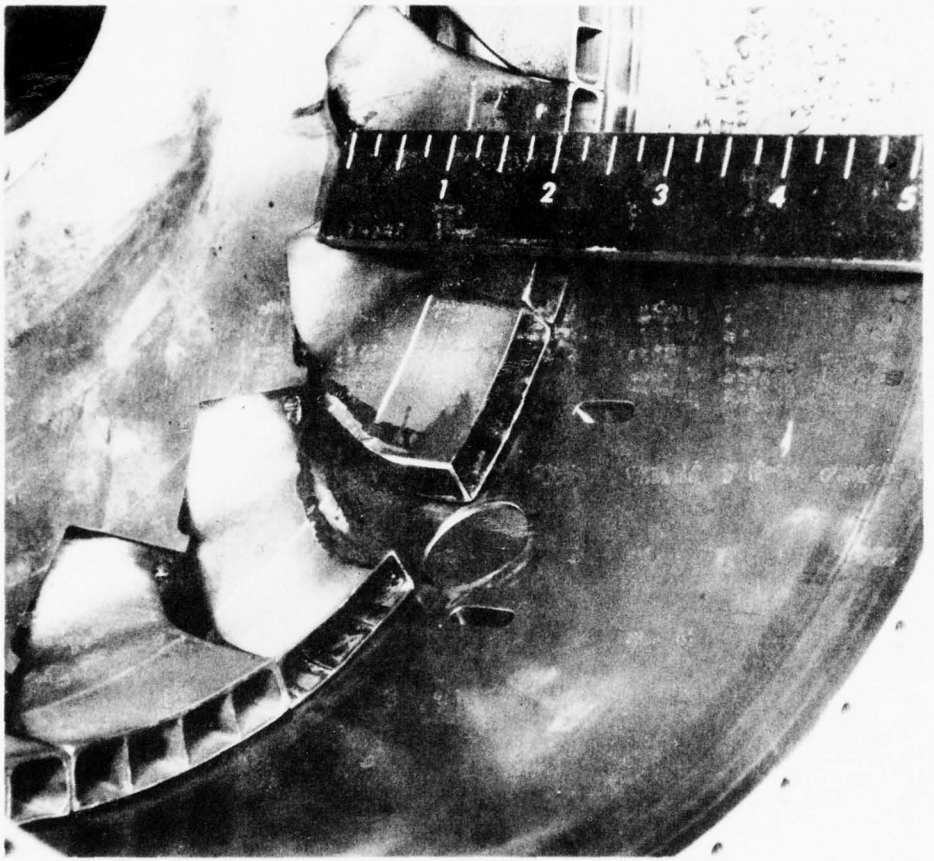

Figure 19. Diffuser Rework.

INSTRUMENTATION INSTALLATION

Thermocouple placement in the rotating components required that the bore diameter of the first disc be increased and holes and slots be incorporated in both discs, as described in the Instrumentation section. Stress analysis conducted on the discs showed a low-cycle fatigue life of 1100 cycles for the first disc, with the critical element being the thermocouple leadout grooves or the disc front face. The second disc has a calculated life of 450 cycles as a result of the 10 holes through the web of the disc.

TEST PROCEDURE

GENERAL

Tip-clearance measurements were made over the full operating range of the gas generator. The sequence of testing began with steady-state operation with very slow transitions from one power level to the next. Test time at maximum continuous power was sufficient to season new turbine parts. After this steady-state test evaluation, an assessment was made of the shroud distortion, the performance of the tip-clearance measurement instrumentation, and the overall gas generator operation. Condition of the test hardware was determined by means of a borescope inspection. After the data was analyzed and compared with the predicted values, moderate accelerations and decelerations were made. The results of the test were extrapolated to determine what the tip clearance would be during the most severe transient. After completion of the analysis, transients were accomplished sequentially in increasing order of severity. The transients included: cold start-up, minimum time acceleration from flight idle to full power, rapid deceleration from maximum power to idle, wave-off, rapid shutdown from full power, and restart immediately after shutdown. Each transient was followed by adequate steady-state hold times to allow component growth and tip clearance to stabilize.

During each test condition, sufficient data were taken to determine the instantaneous growth characteristics of the rotor/shroud system, the transient tip-clearance response, and the gas generator operation boundary conditions.

CALIBRATIONS

Prior to gas generator assembly, the rotor and shroud cooling air supply networks were calibrated to provide a basis for cooling airflow calculation under engine operating conditions. Rotor cooling airflow was correlated to pressure drop across the preswirl nozzle, and shroud cooling airflow was correlated to pressure drop across the metering holes in the first-stage nozzle support.

Test cell instrumentation and data acquisition system transducers were routinely calibrated before each test.

RESULTS

INITIAL ANALYSIS

The initial analytic prediction of tip-clearance response was done using gas generator design operating parameters as boundary conditions to the analytic model. The steady-state results for shroud cooling airflow rates of 0.5 and 1.0 percent are summarized in Table 2. Analysis shows that the steady-state operating clearance will be larger than the assembly clearance and that increasing shroud cooling air results in significant decreases in running tip clearance. Figure 20 illustrates the growth of each component in the rotor/shroud system at all steady-state power points with net tip clearance represented as the differential between shroud growth and the combined growth of the disc, rim, and blade. Calculated component temperature distributions which result in this tip-clearance characteristic are shown in Figure 21.

Transient response characteristics were calculated for start, jam acceleration, snap deceleration, wave-off, shutdown, and restart. The results calculated with 1.0 percent shroud cooling air are shown in Figures 22 through 26. Presented is the change in tip clearance from the assembly clearance value; a negative clearance indicates a value smaller than the assembly level rather than a rub condition. The most severe transient is the shutdown from maximum power and restart. A minimum clearance of 0.0036 inch below the assembly value occurs 36 seconds after initiation of the shutdown. A detailed description of the response of each component during transient is given in the discussion of test results.

An analytical study was conducted to determine the effect of the assumed convective heat-transfer coefficient at the disc bore and the effect of blade cooling air quantity on tip clearance. Maximum power temperature distribution and resulting tip clearance were calculated with the convective heat-transfer coefficient at the disc bore varied from 5.0 to 100.0 about the estimated value of 20 Btu/hr-ft^2 ° F. The results are summarized in the temperature distribution plot of Figure 27. The maximum variation in disc bore temperature of 40° F represents a tip-clearance change of only 0.0006 inch.

Additionally, the variation in blade-to-blade temperature as a result of variations in blade-to-blade cooling air quantity was analyzed to determine if a misleading radial temperature distribution could be obtained with individual blades selected for each radial measurement position rather than having all thermocouples installed on a single blade. Vari-

TABLE 2. STEADY-STATE TIP-CLEARANCE ANALYSIS RESULTS

Power Point	Differential Tip Clearance (inches)	
	0.5% Shroud Cooling	1.0% Shroud Cooling
Ground Idle	0.0054	0.0034
Flight Idle	0.0045	0.0023
30%	0.0044	0.0021
60%	0.0061	0.0033
100%	0.0104	0.0051

Differential Tip Clearance = Change in clearance from the assembly clearance.

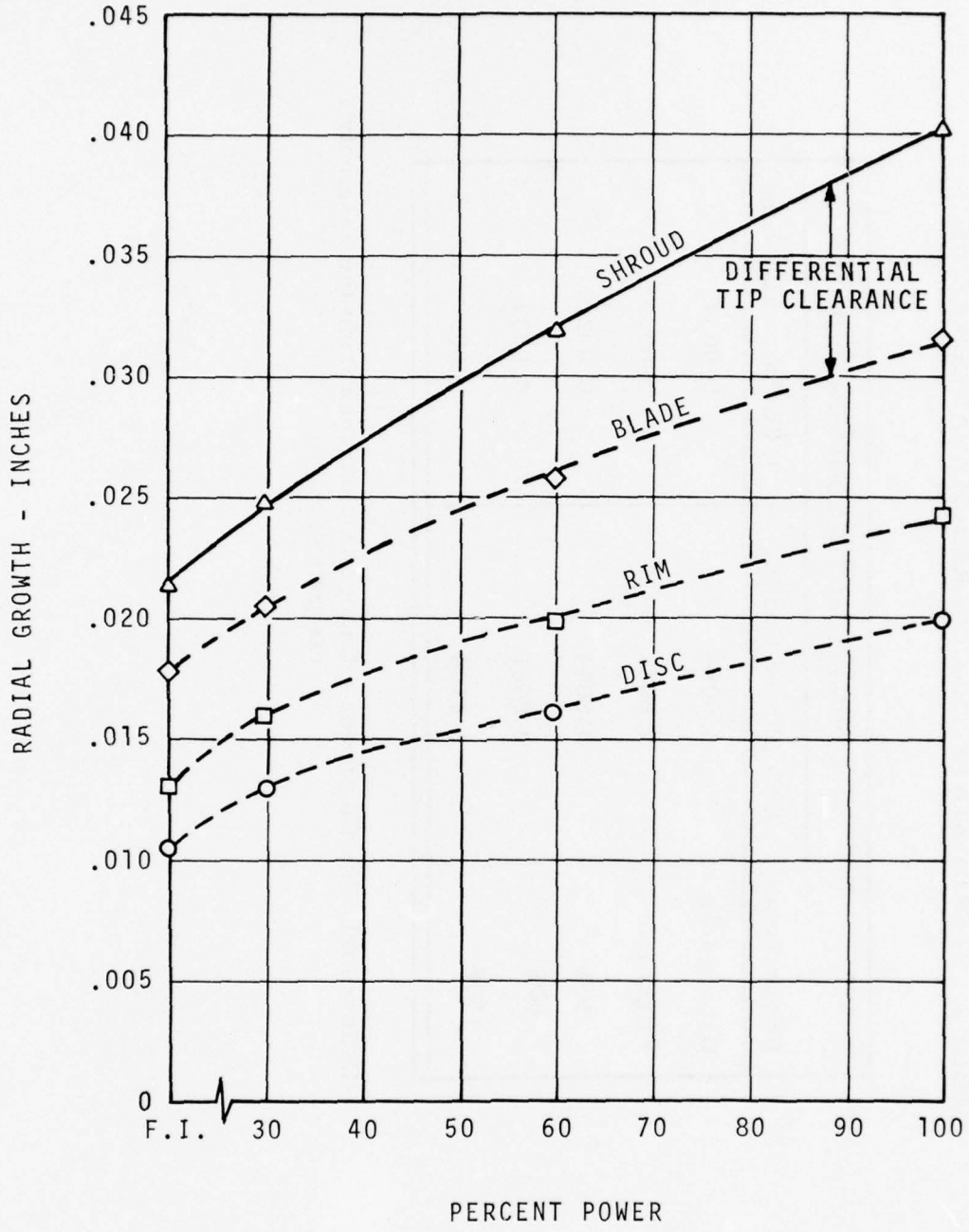

Figure 20. Calculated Component Growth Characteristics - Initial Analysis, 0.5 Percent Shroud Cooling Air.

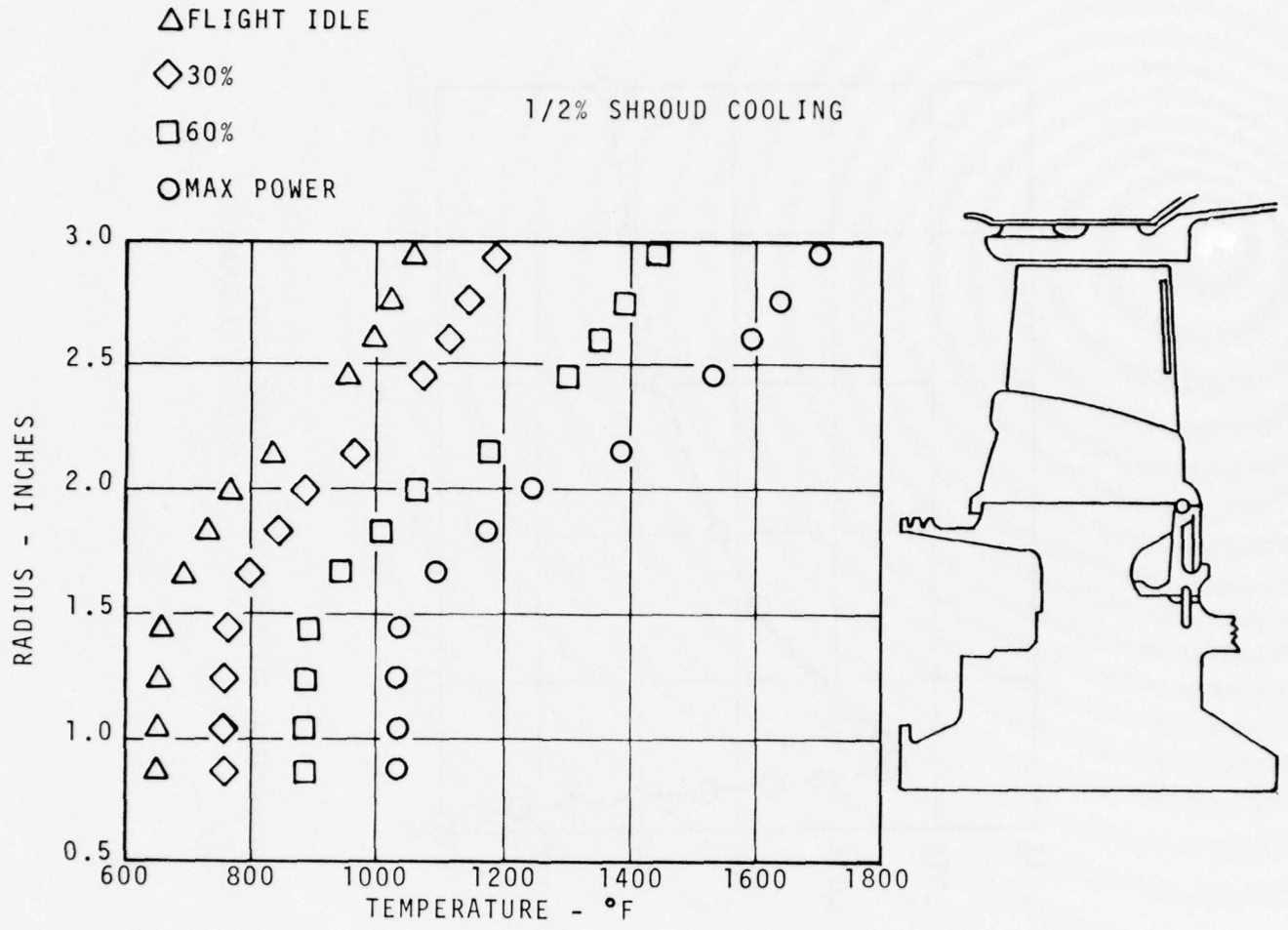

Figure 21. Calculated Component Temperature Distribution - Initial Analysis, 0.5 Percent Shroud Cooling Air.

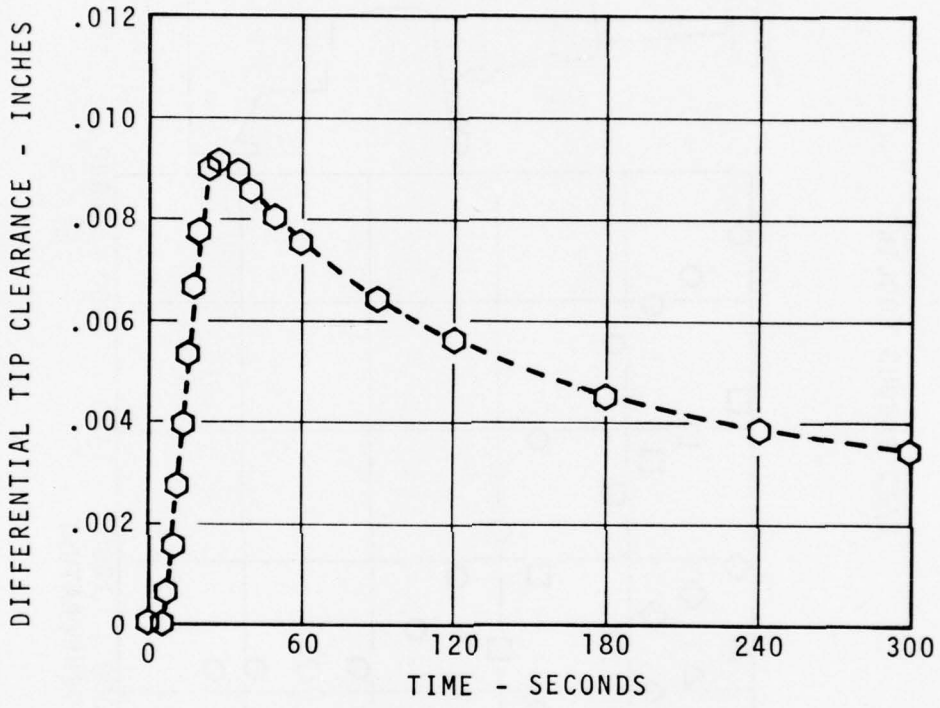

DIFFERENTIAL TIP CLEARANCE = CHANGE FROM ASSEMBLY CLEARANCE

Figure 22. Calculated Tip-Clearance Response - Start.

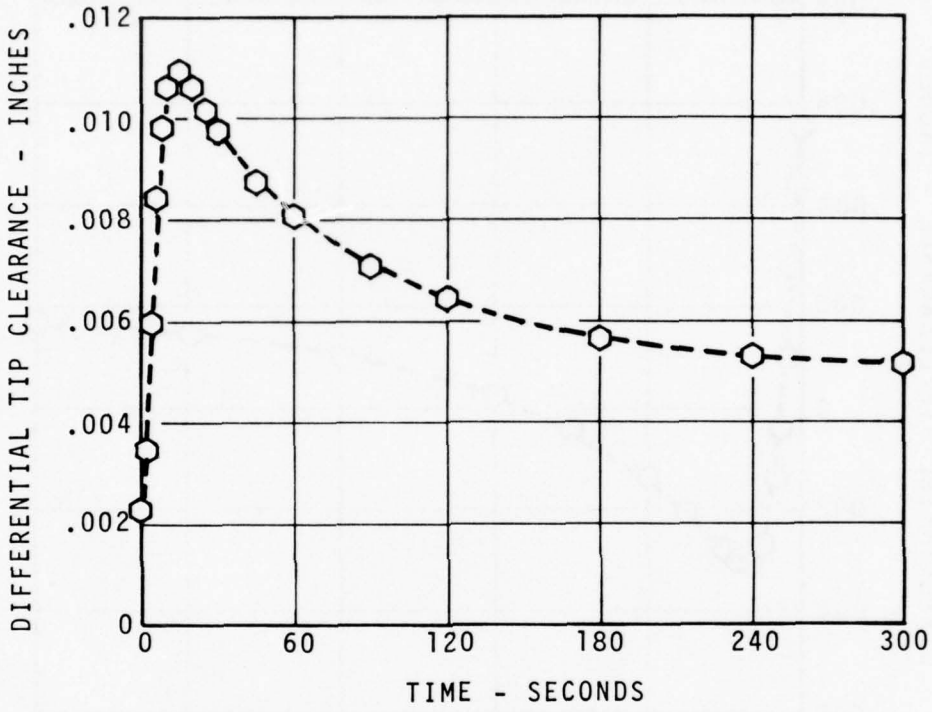

DIFFERENTIAL TIP CLEARANCE = CHANGE FROM ASSEMBLY CLEARANCE

Figure 23. Calculated Tip-Clearance Response - Jam Acceleration.

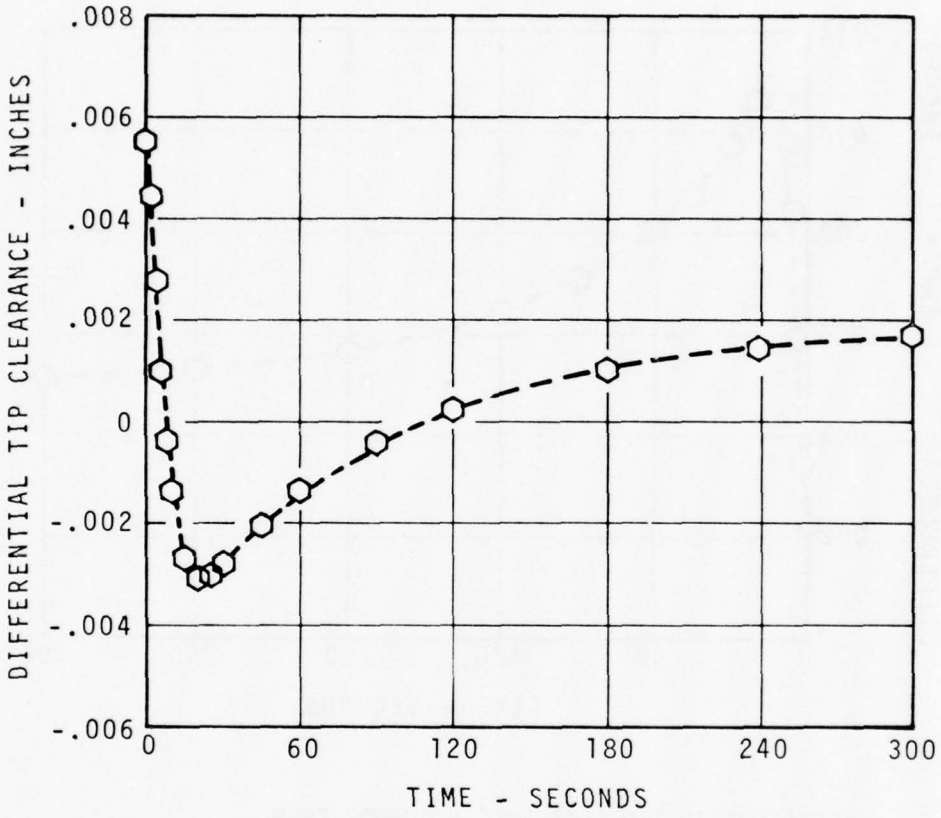

DIFFERENTIAL TIP CLEARANCE = CHANGE FROM ASSEMBLY CLEARANCE

Figure 24. Calculated Tip-Clearance Response - Snap Deceleration.

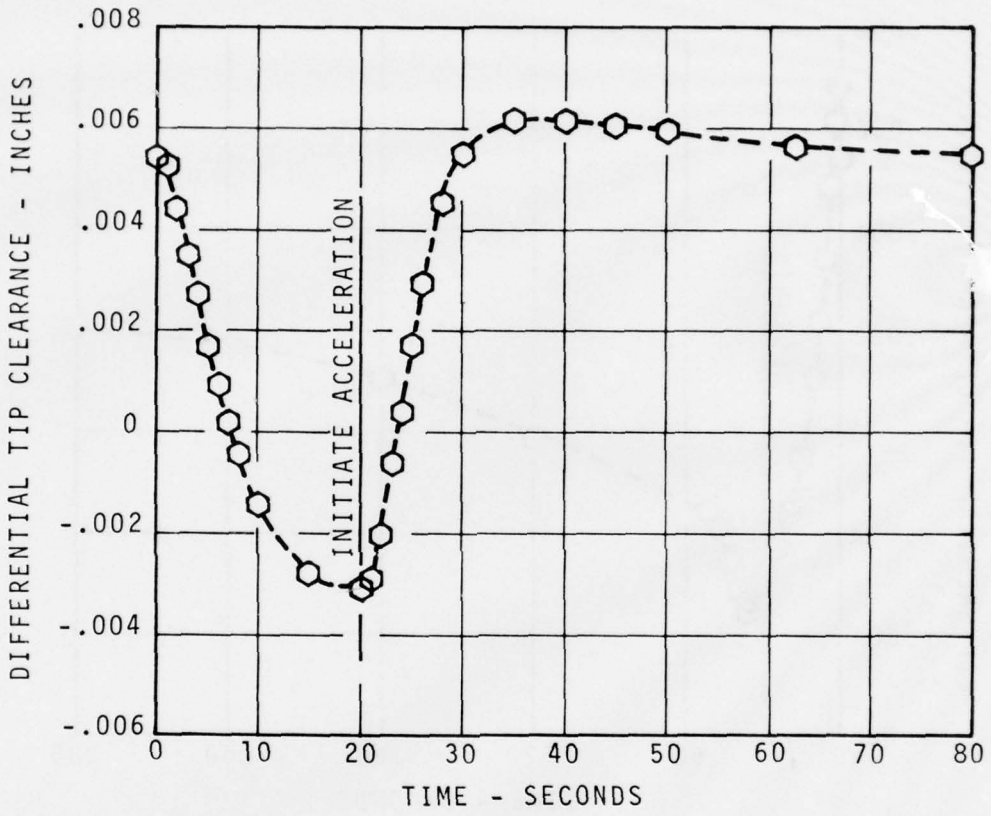

Figure 25. Calculated Tip-Clearance Response - Wave-off.

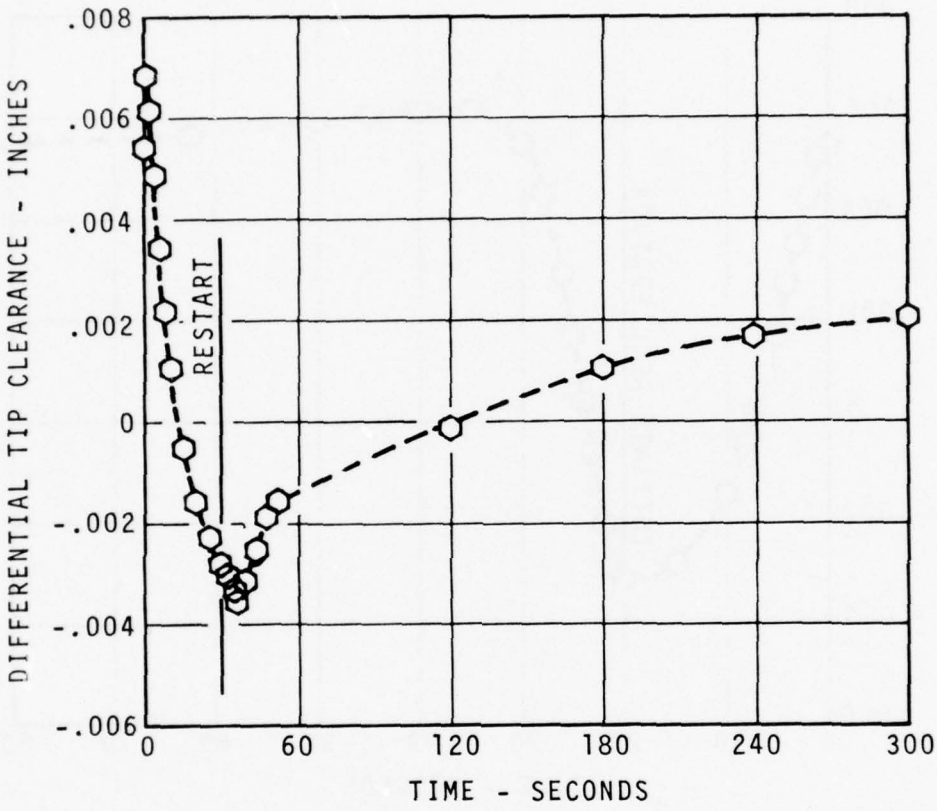

DIFFERENTIAL TIP CLEARANCE = CHANGE FROM
ASSEMBLY CLEARANCE

Figure 26. Calculated Tip-Clearance Response - Shutdown and Restart.

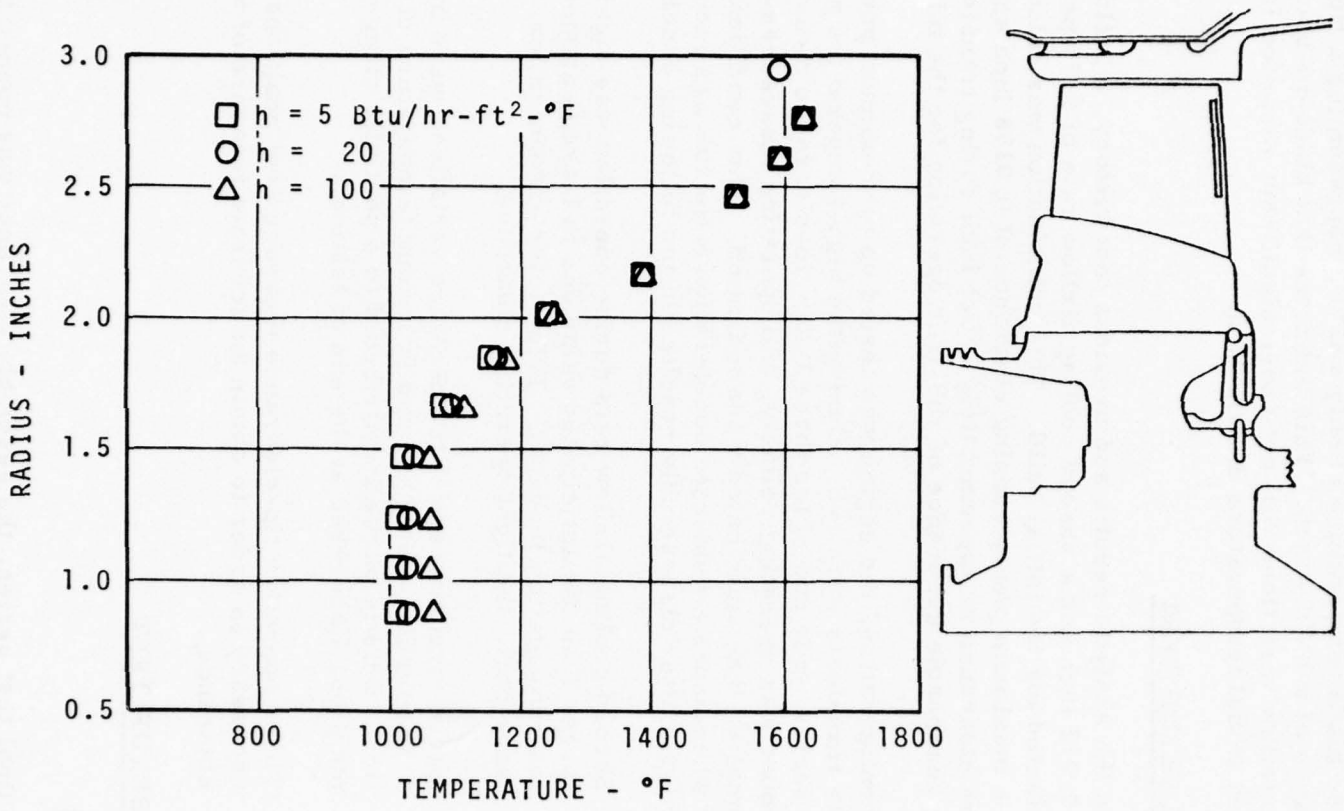

Figure 27. Effect of Convective Heat Transfer Coefficient at the Disc Bore on Calculated Temperature Distribution.

ation of cooling airflow rate over a ± 20% range resulted in a change in calculated blade temperature of only ± 42° F, representing a tip-clearance change of ± 0. 0004 inch. This indicates that blade-to-blade cooling airflow variations will not cause significant variation in measured radial temperature distribution.

INITIAL SETUP TEST

Based on the analytic results and previous test history, a build clearance of 0. 012 inch and a shroud cooling airflow rate of 0. 75 percent were selected for the initial build. This combination was calculated to yield a maximum power running clearance of 0. 0198 inch and a minimum clearance of approximately 0. 011 inch during transients, offering reasonable assurance of rub-free operation for the initial test.

In this configuration, the engine was tested up to maximum power and moderate transients were run. During the high-temperature phase of the test series, only one of the three laser tip-clearance measurement probes was operating reliably, and operating clearances significantly smaller than anticipated were indicated. This condition was verified when under a moderate deceleration a tip rub was incurred. Data analysis after disassembly resulted in the following conclusions:

a. Shroud cooling airflow rate during operation was significantly larger than the anticipated value due to leakage around the instrumentation leadouts. This factor accounted for, in large part, the tight operating clearance.

b. Large circumferential temperature variations were measured at the turbine exit plane and in shroud temperature distribution. This is partially attributed to a partially clogged fuel manifold discovered at the end of testing.

c. Three operative tip-clearance measurement positions are necessary in order to obtain an accurate measure of average clearance.

FINAL SETUP TEST

General

For the final test series, the assembly clearance was opened to 0. 015 inch as a result of regrinding the rotor to clean up the blade tips. Shroud cooling airflow rate was set at 0. 47 percent, and all instru-

mentation leadout paths were sealed with ceramic cement. The gas generator was tested up to maximum power conditions, and all required transients were run.

Steady-State Operation

Steady-state clearance was measured for operating conditions from idle to full power, and calculations were repeated for these points using actual operating parameters as boundary conditions to the analytic technique. The results are summarized in Table 3, which presents the clearance measured by each probe as compared with the calculated value. Analytic results are based on calculated component temperatures because rotating thermocouple failures which occurred during the final test series did not allow definition of complete component temperature distributions for these operating conditions. A plot of average tip clearances as a function of percent power is presented in Figure 28. Calculated clearance is based on change from the effective assembly clearance of 0.0148 inch which represents the average measured clearance under cold cranking conditions. This is slightly smaller than the average static assembly clearance due to the centrifugal loading that tightens the blades in their root slots. The measured and calculated clearances follow the same general characteristic, with clearance at idle larger than the assembly level and clearance decreasing at intermediate power and increasing again at maximum power. At all power points, the calculated clearance was larger than the measured clearance.

The three major factors influencing the comparison between measured and calculated clearances are component temperature, distortion, and shroud thermal stresses.

Component Temperature Distribution - The comparison between calculated and measured component temperature distributions at maximum power is shown in Figure 29. This data was recorded during the initial test series because of the rotating thermocouple failures that occurred during the final test series. The data are presented only to illustrate the comparison between measured and calculated component temperatures. Clearances calculated for this operating condition cannot be compared directly with clearances measured during the final test series because of differences in thermodynamic boundary conditions. Agreement between calculated and measured disc and blade temperatures was very good. The measured disc temperature was 70° F higher than the calculated value at the bore, reached exact agreement in the web area at a radius of 1.6 inches, and exceeded the calculated value in the aft rim area. Measured and calculated blade temperatures agreed to

TABLE 3. STEADY-STATE TIP-CLEARANCE TEST RESULT COMPARISON

Power Point	% RPM	Tip Clearance (inches)				
		Probe No. 1 (3 o'clock)	Probe No. 2 (7 o'clock)	Probe No. 3 (11 o'clock)	Measured Average	Analytic * Result
In-Place Calibration	0	0.0155	0.018	0.0145	0.016	
Crank	15.0	0.0135	0.0175	0.0135	0.0148	0.0148
Flight Idle	73.0	0.021	0.018	0.013	0.0173	0.0196
46%	87.0	0.020	0.018	0.0115	0.0165	0.0185
54%	89.5	0.0185	0.018	0.0115	0.016	0.0186
81%	93.9	0.0195	0.0165	0.0115	0.0158	0.0200
98%	96.0	0.021	0.019	0.009	0.0163	0.0218

*Analytic Result Based on Calculated Component Temperatures

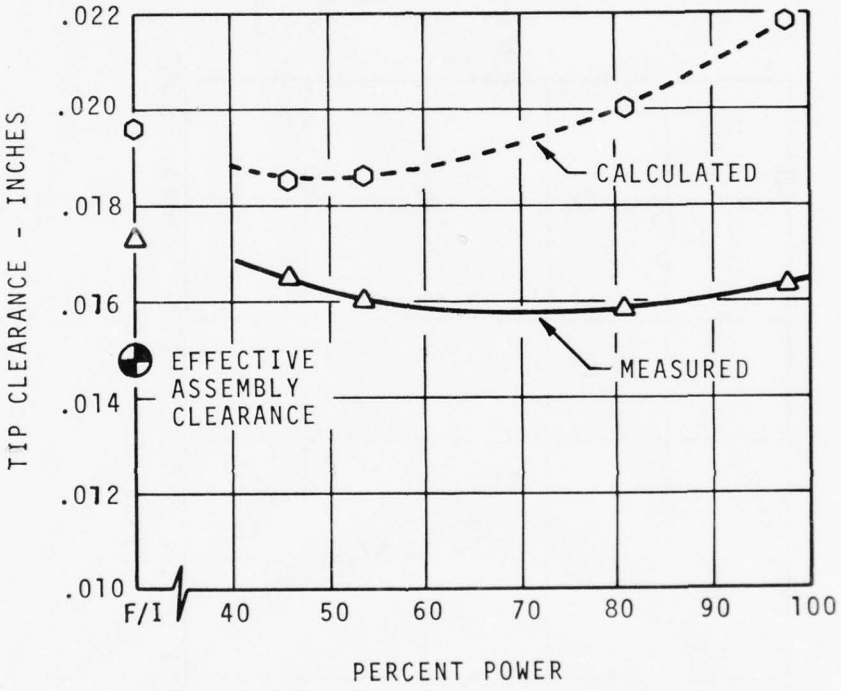

Figure 28. Steady-State Tip-Clearance Comparison.

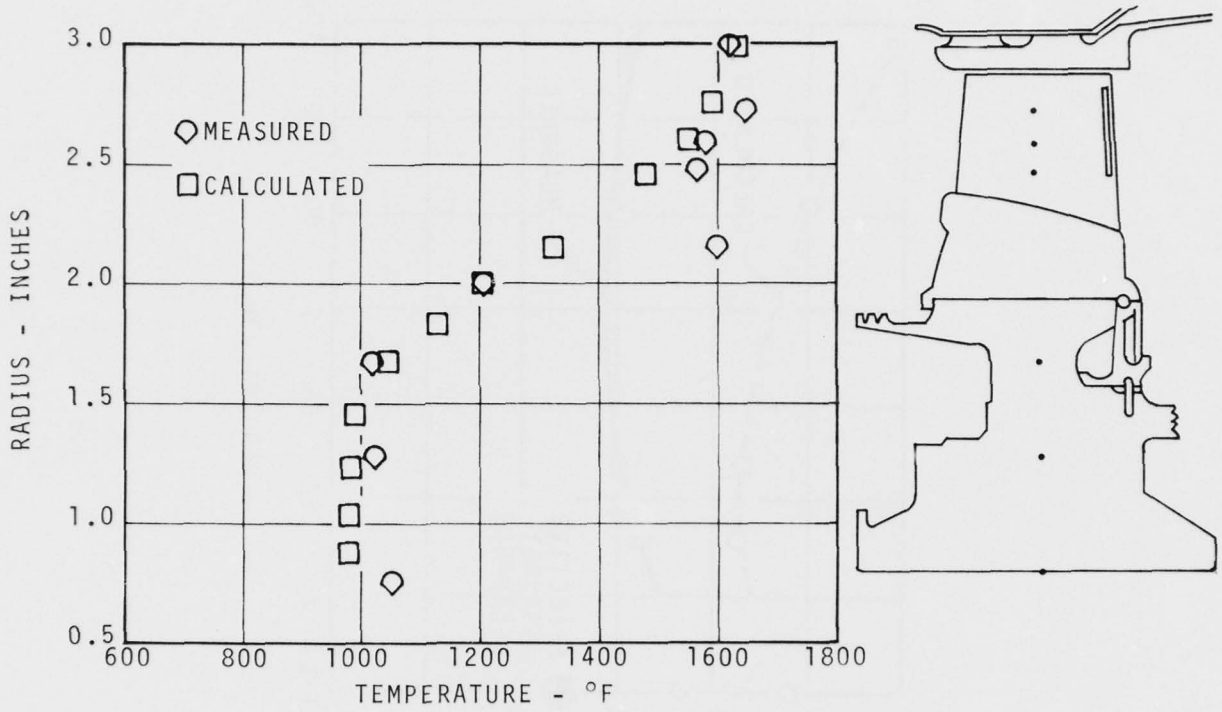

Figure 29. Component Temperature Distribution Comparison - Maximum Power.

within 35° F at the midspan location and to within 70° F at the hub and tip. Included in the comparison is the shroud temperature measured and calculated for the maximum power point during the final test series. The average measured temperature of 1611° F agrees well with the calculated average of 1607° F.

Component growth values determined for the measured and calculated temperature distributions are presented in Table 4. As can be seen, the calculated-to-measured temperature differentials result in small changes in component growth. The net effect of the disc and blade measured temperatures being higher than calculated is that total rotor growth based on calculated component temperatures was 0.0013 inch less than the growth based on measured temperatures. Shroud growth agreement is within 0.0001 inch. This results in the tip clearance based on calculated component temperatures being 0.0012 larger than the clearance that would result from measured temperatures. At maximum power, this accounts for 22 percent of the total variation of 0.0055 inch between analysis and measurement.

Distortion - Component distortion was found to be a significant factor influencing the tip clearance of the turbine stage. The tabulation of measured tip clearance as a function of power, presented in Table 3, illustrates the variation in tip clearance recorded by the probes at three circumferential positions. At maximum power, this variation reached 0.012 inch, with a maximum local clearance of 0.021 inch and a minimum local clearance of 0.009 inch. The circumferential variation in clearance is a significant fraction of the average clearance level of 0.0163 inch. The shroud distortion pattern is summarized in Figure 30 which illustrates the measured shroud runout pattern at build and teardown, as well as the relative tip-clearance measurement results at build, idle, and maximum power. Tip-clearance distortion is comprised of two elements: distortion in shroud shape and shroud eccentricity. Both factors are indicated by the measured distortion pattern. Shroud distortion is evident as a flattening of the shroud shape along a diagonal axis. This progressed from 0.003 to 0.006 inch out-of-round during testing as measured by shroud runouts taken at assembly and teardown. The three laser tip-clearance probes showed a similar pattern with the addition of an apparent centerline shift between shroud and rotor. This is evident as a consistent increase in clearance at the 3 and 7 o'clock circumferential positions coupled with the decrease in clearance measured at the 11 o'clock position. It is apparently due to nonuniform growth in the shroud support structure and is not fully understood. Circumferential variation in the temperature of the aft housing support struts, the combustor housing inner wall, or the shroud cantilever support

TABLE 4. STEADY-STATE COMPONENT GROWTH COMPARISON

Component	Radial Growth at Maximum Power (inches)	
	Based on Analytic Temperature Distribution	Based on Measured Temperature Distribution
Disc	0.0182	0.0186
Rim	0.0048	0.0054
Blade	0.0071	0.0074
Shroud	0.0378	0.0379
Net Differential Tip Clearance	+0.0077	+0.0065

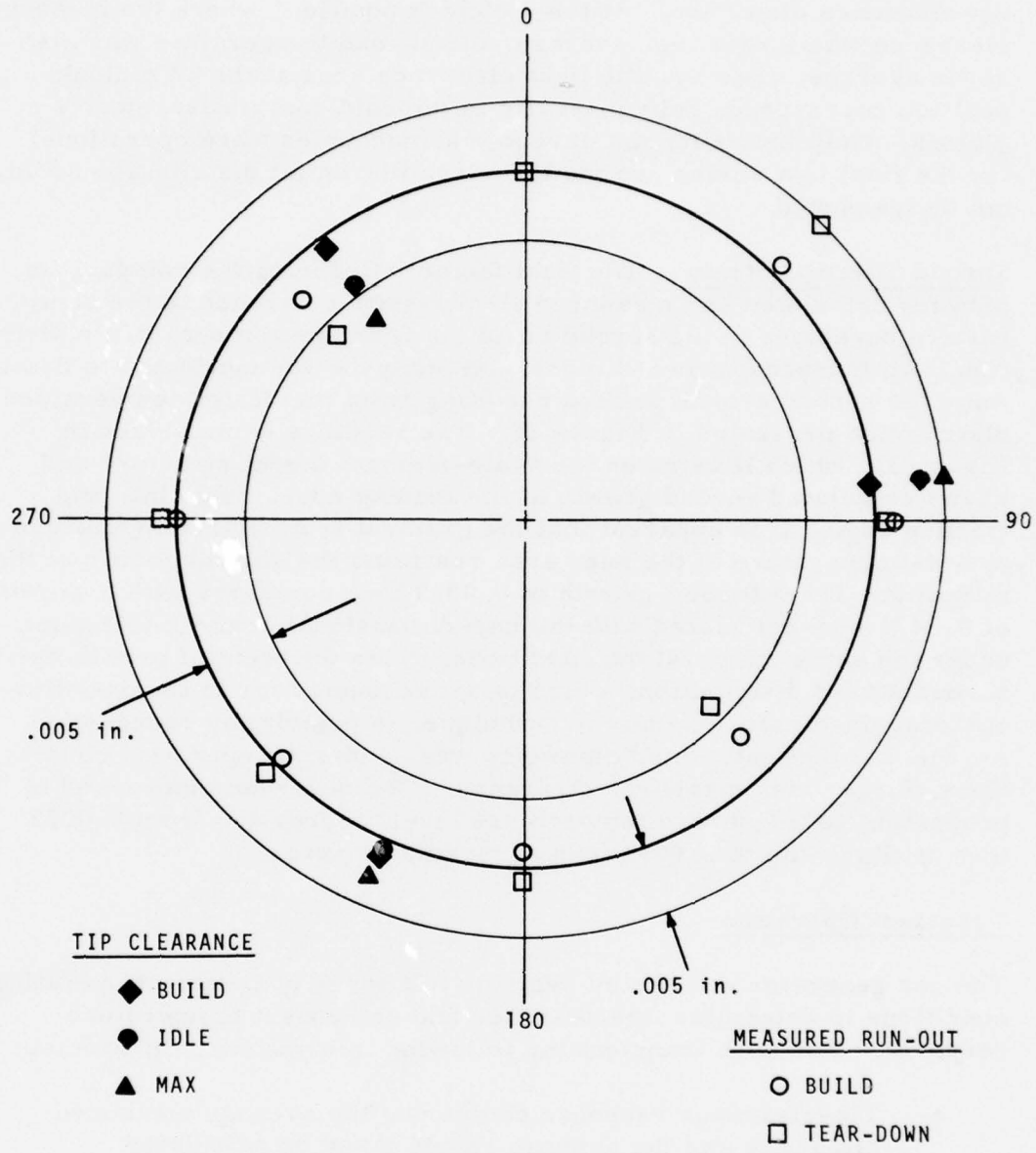

Figure 30. Shroud Distortion Pattern.

could cause the shroud to shift relative to the rotor. Inspection of the shroud temperature distribution measured at maximum power (Figure 31) shows only a slight correlation between temperature distribution and tip-clearance distortion. At the 3 o'clock position, where the measured clearance was larger than average, the shroud temperature was also above average; however, the tight clearance area at the 11 o'clock position corresponds only generally to the cold spot measured at 9 o'clock. Only four midpoint shroud thermocouples were operational for the final test series, so the full circumferential distribution could not be measured.

Shroud Thermal Strain - The final factor influencing the comparison between calculated and measured steady-state clearance is the strain pattern developed in the shroud resulting from the temperature distribution. An independent two-dimensional analysis was conducted to determine the shroud growth pattern resulting from the design temperature distribution presented in Figure 32. The result is summarized in Figure 33, which illustrates the finite-element model structure and shows calculated shroud growth at the leading edge, midpoint, and trailing edge. It is apparent that the gradient from high-temperature to low-temperature in the knee area restrains the shroud growth at the midpoint. The midpoint growth of 0.0363 inch compares with a growth of 0.0421 inch calculated with the one-dimensional analytic technique under the same temperature conditions. This differential growth due to shroud stress distribution, which is not accounted for in the one-dimensional tip-clearance analytic technique, is principally responsible for the fact that calculated clearance was, under all operation conditions, larger than measured clearance. The difference increased in proportion to the shroud temperature level, increasing from 0.0023 inch at flight idle to 0.0055 inch at maximum power.

Transient Operation

The gas generator was tested over the full range of transient operating conditions to determine tip-clearance and component temperature response. For each transient the following information is presented:

a. Tip-clearance response comparing the average measured clearance and the analytic result based on calculated component temperature distribution. Gas generator speed as a function of time during the transient is also included.

b. Measured tip-clearance response of each tip-clearance probe.

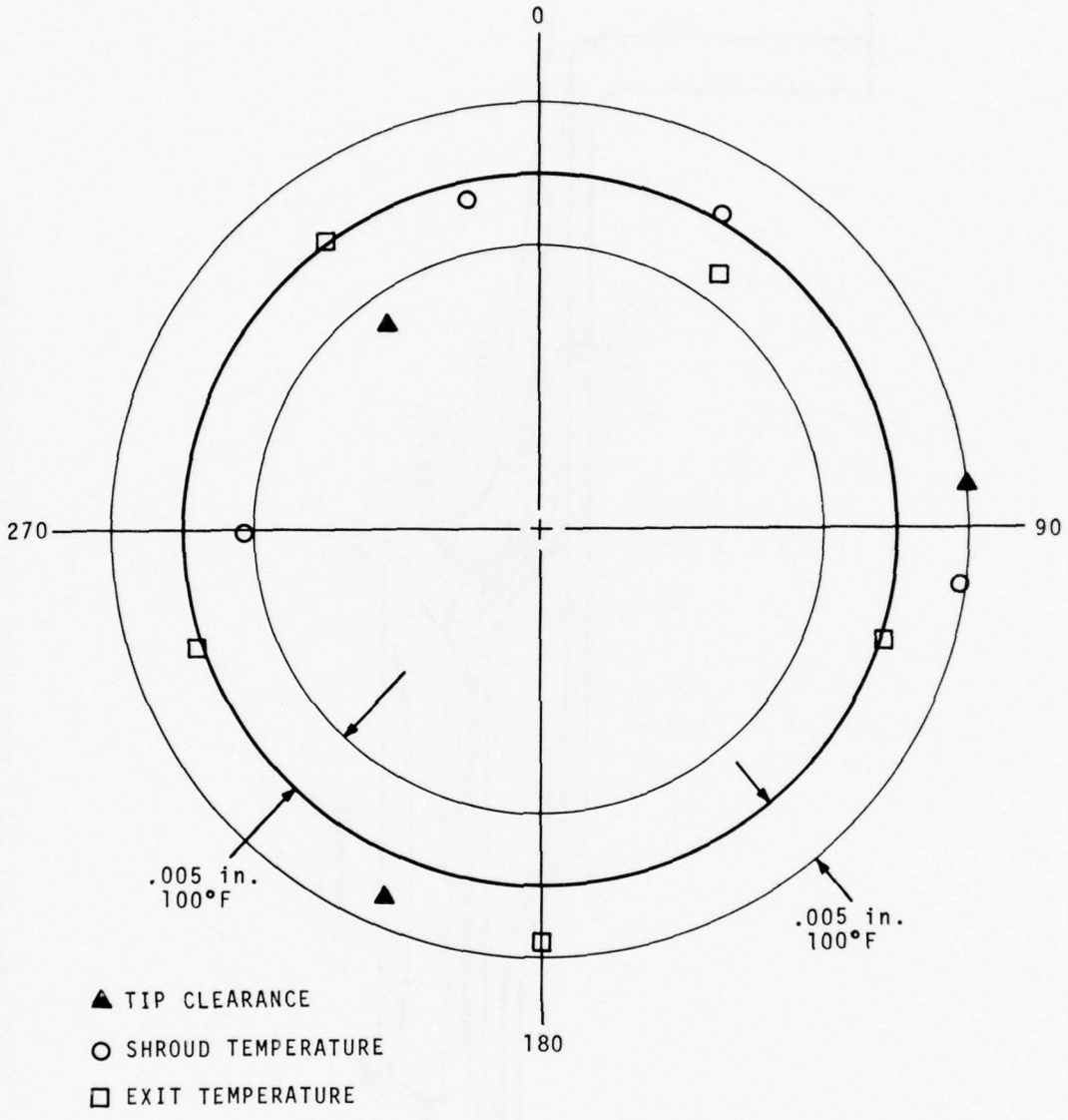

Figure 31. Measured Temperature Distortion Pattern - Maximum Power.

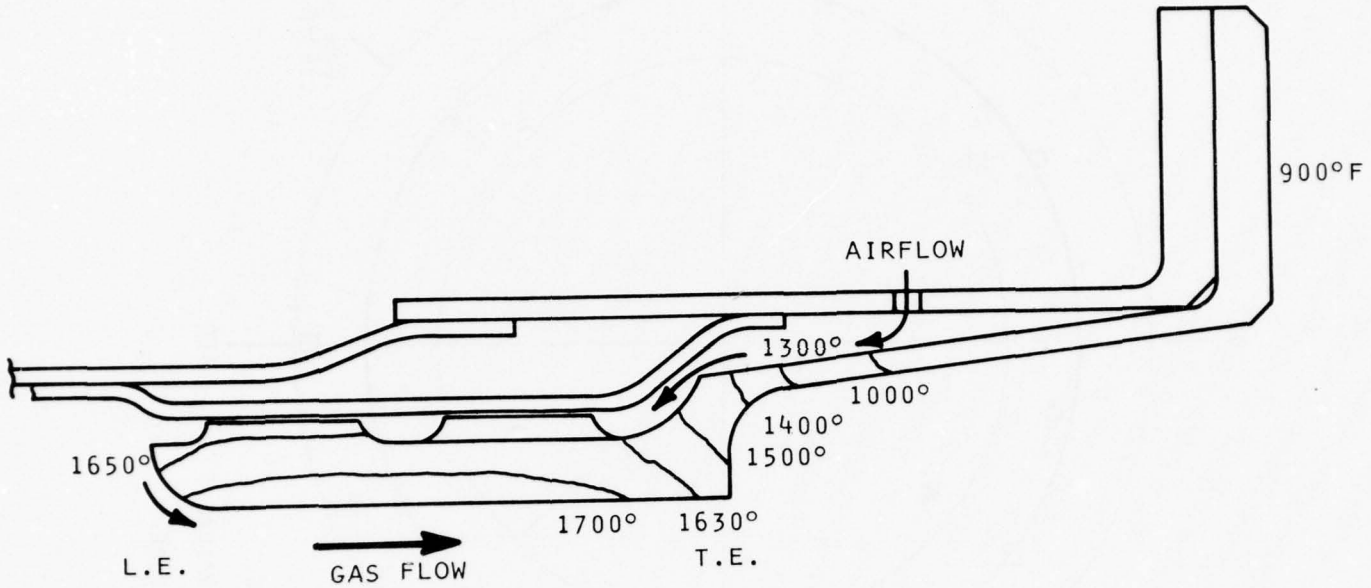

Figure 32. Shroud Design Point Temperature Distribution.

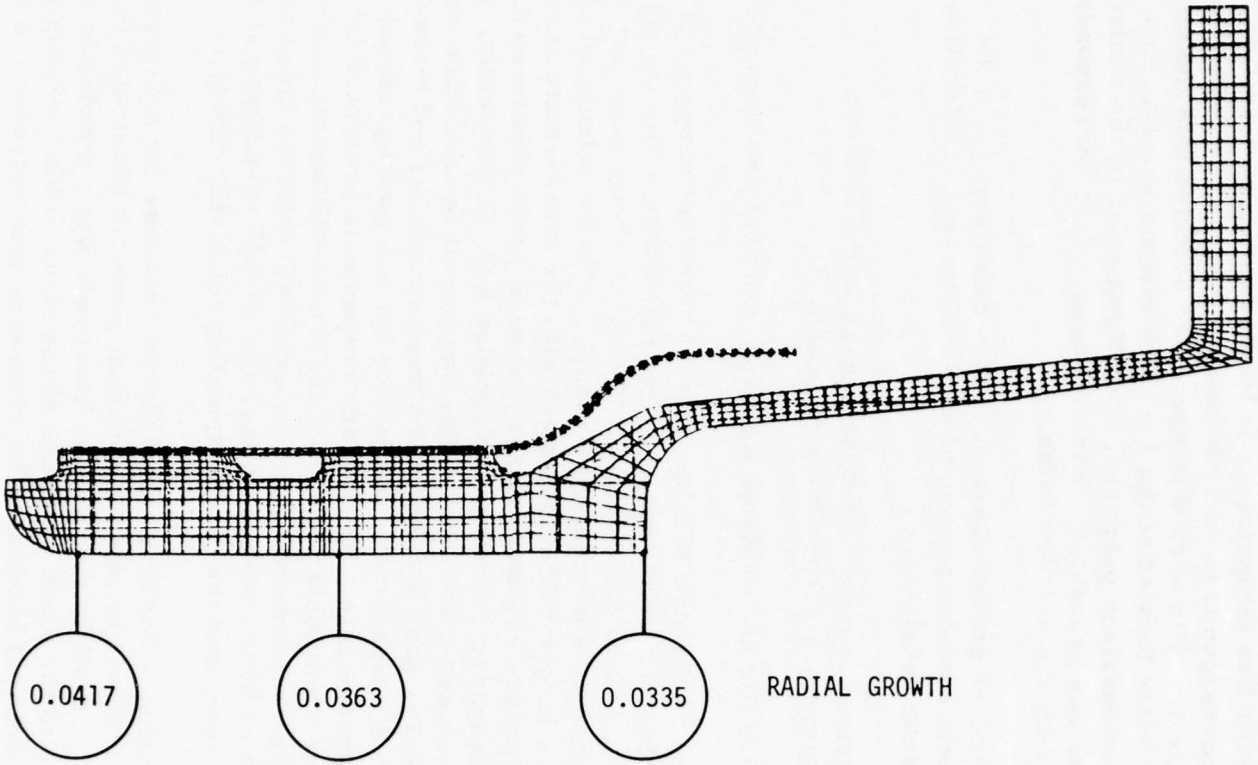

Figure 33. Shroud Finite Element Analysis Result - Design Temperature Distribution.

c. Component temperature response of the rotor and shroud comparing the measured and analytical results. The selected disc temperature is located in the mid-section and corresponds to analytic node number 42 as defined in Figure 3. The shroud temperature selected was the mid-point value located at the 1 o'clock circumferential position. For comparison purposes, node Number 62 of the analytic model was presented. Each of these values corresponds well with the average value.

d. Component growth characteristics calculated from the analytic model - presented only for the jam acceleration and snap deceleration.

e. Transient boundary conditions used in the analytic technique are presented in Appendix D.

The detailed results and analysis for each transient are presented below:

Start - Figures 34 through 37 illustrate the transient response of the gas producer turbine to a start from ambient conditions. The comparison between measured and calculated tip clearance shows excellent agreement of response rate of clearance change, with the calculated clearance stabilizing at a larger value consistent with the steady-state results. Measured clearance response shows that each probe measured an increase in clearance at the time of ignition and, subsequently, decreased to the idle steady-state level. The component temperature response comparison shows good agreement between calculated and measured disc and shroud temperature, accounting for the good agreement in tip-clearance response rate. Rotor blade response is presented for this transient since the midblade thermocouple was still operational during the start. The response rates are as expected, with the blade following gas temperature with virtually no lag, the shroud responding at an intermediate rate, and the disc responding relatively slowly.

Jam Acceleration - Turbine rotor/shroud response for a 6-second jam acceleration from flight idle to maximum power is illustrated in Figures 38 through 42. A slight decrease in clearance was recorded in the first 3 seconds due to the rapid response of the blade to the increased temperature and centrifugal loading. The clearance then increased to 0.021 inch and gradually returned to the maximum power steady-state value. Response rate agreement between the analysis and measurement was excellent as illustrated by the component temperature response comparison. Component growth characteristics determined from the calculated

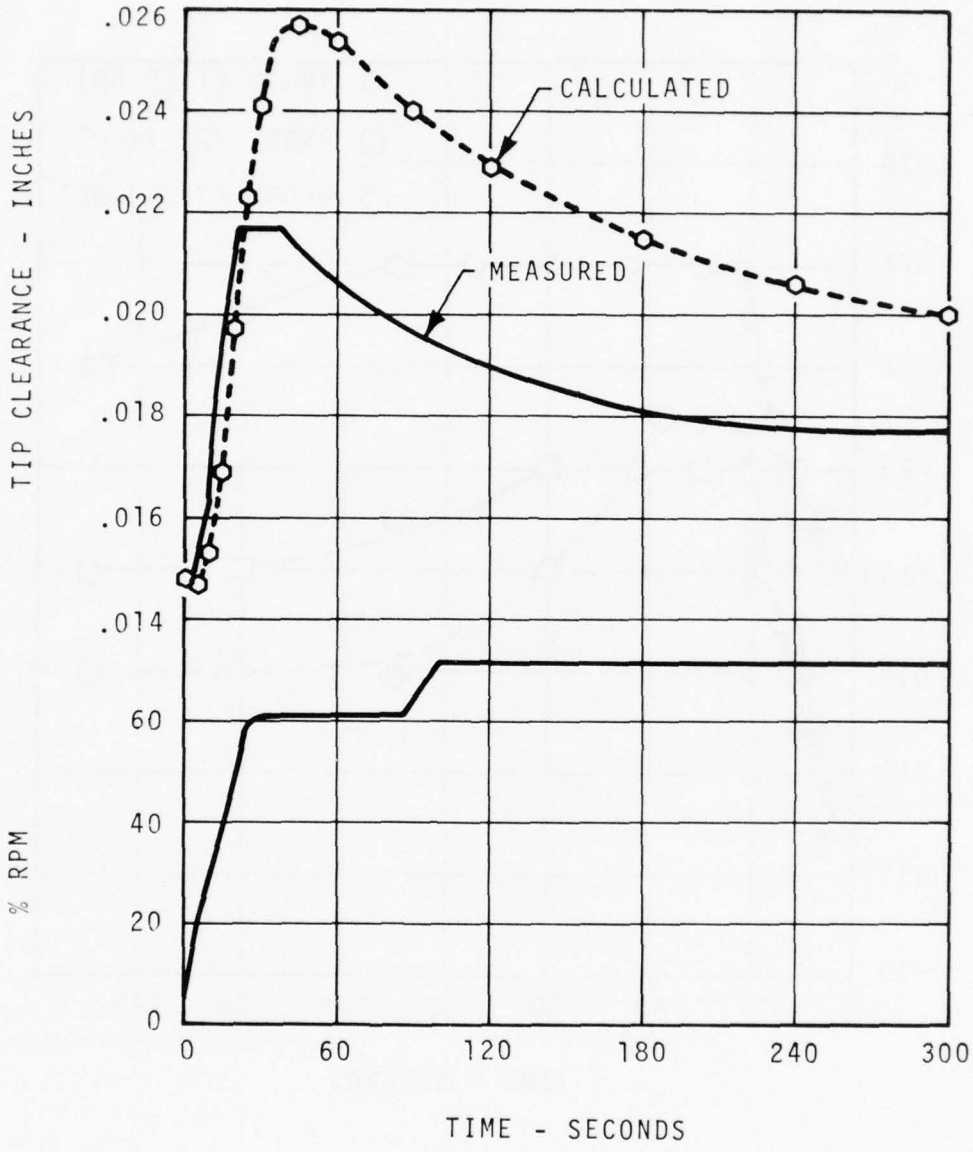

Figure 34. Transient Tip-Clearance Response - Start.

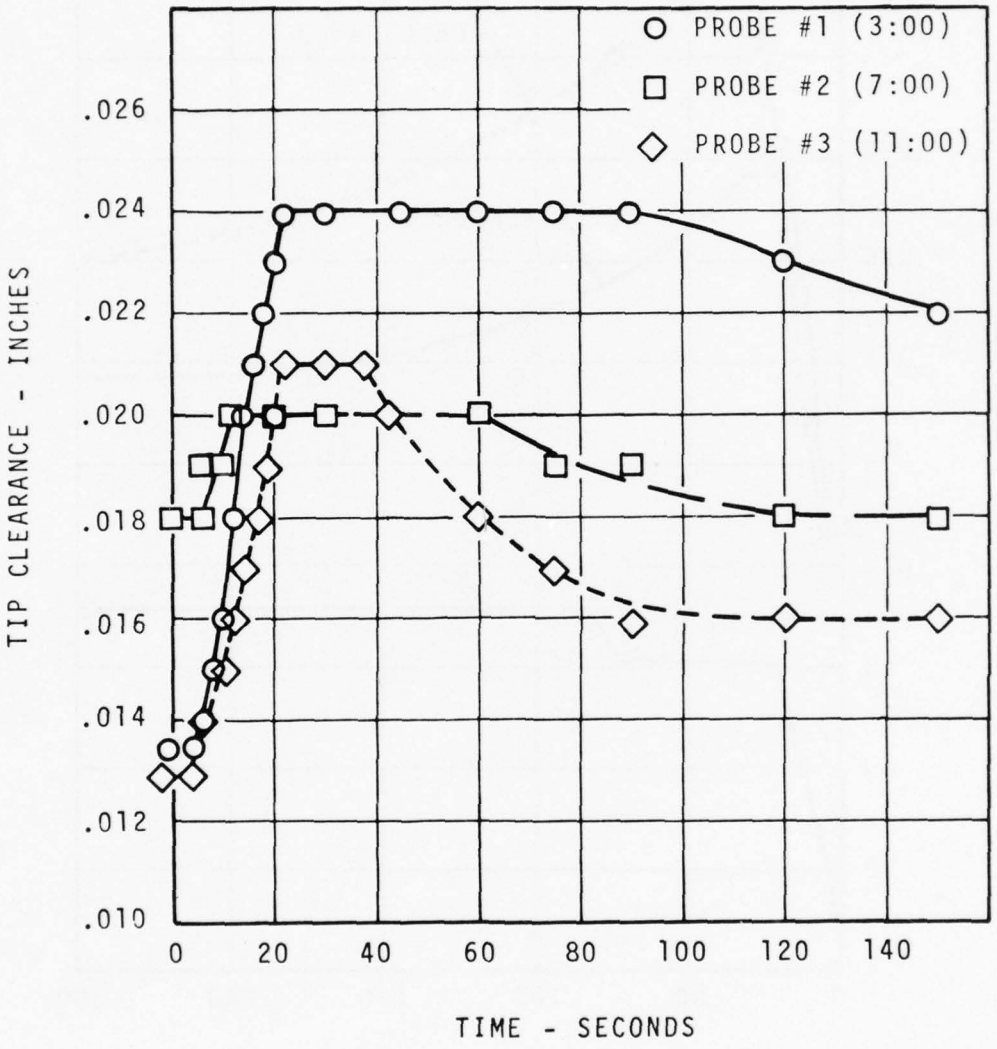

Figure 35. Measured Tip Clearance - Start.

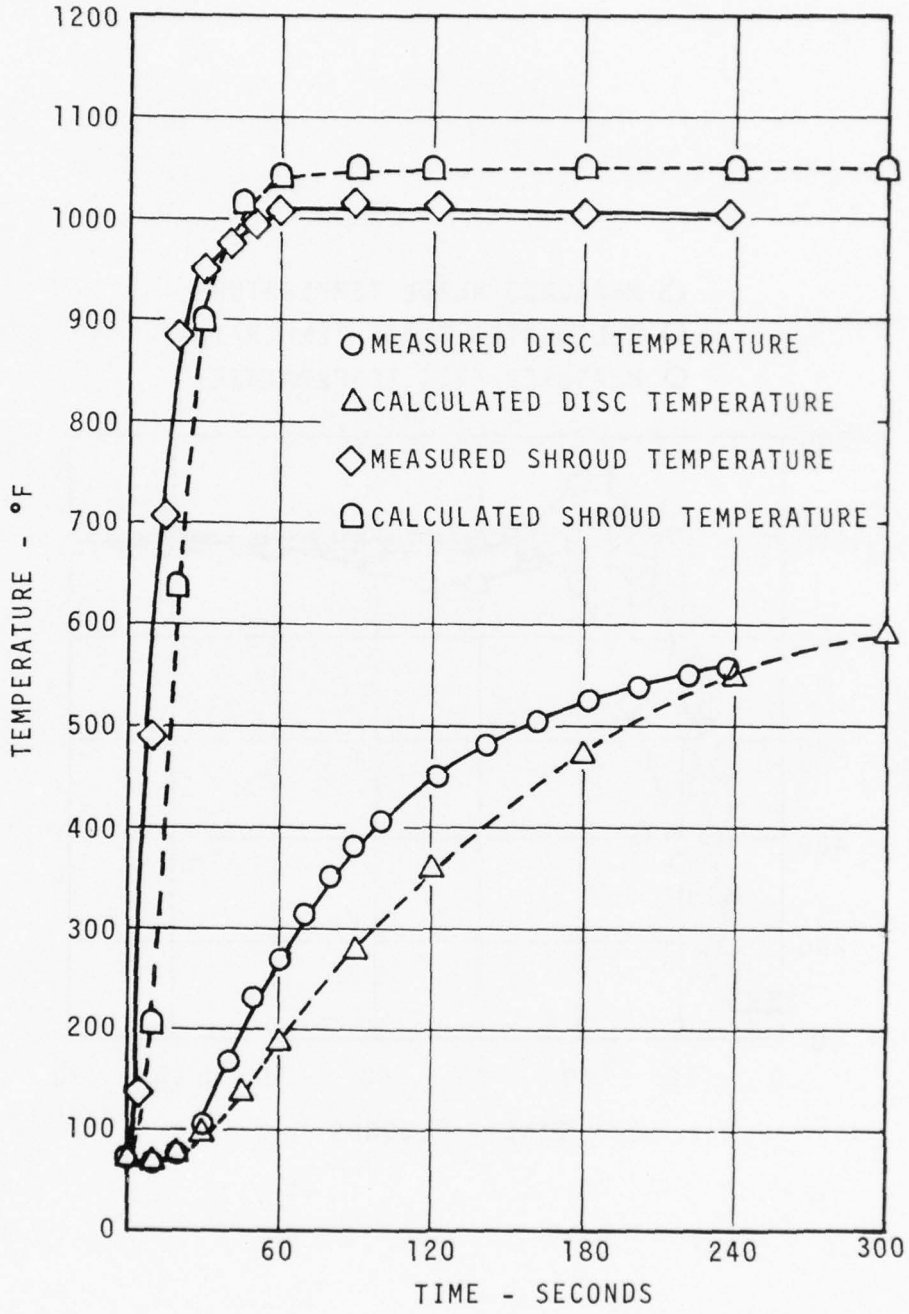

Figure 36. Component Temperature Response - Start.

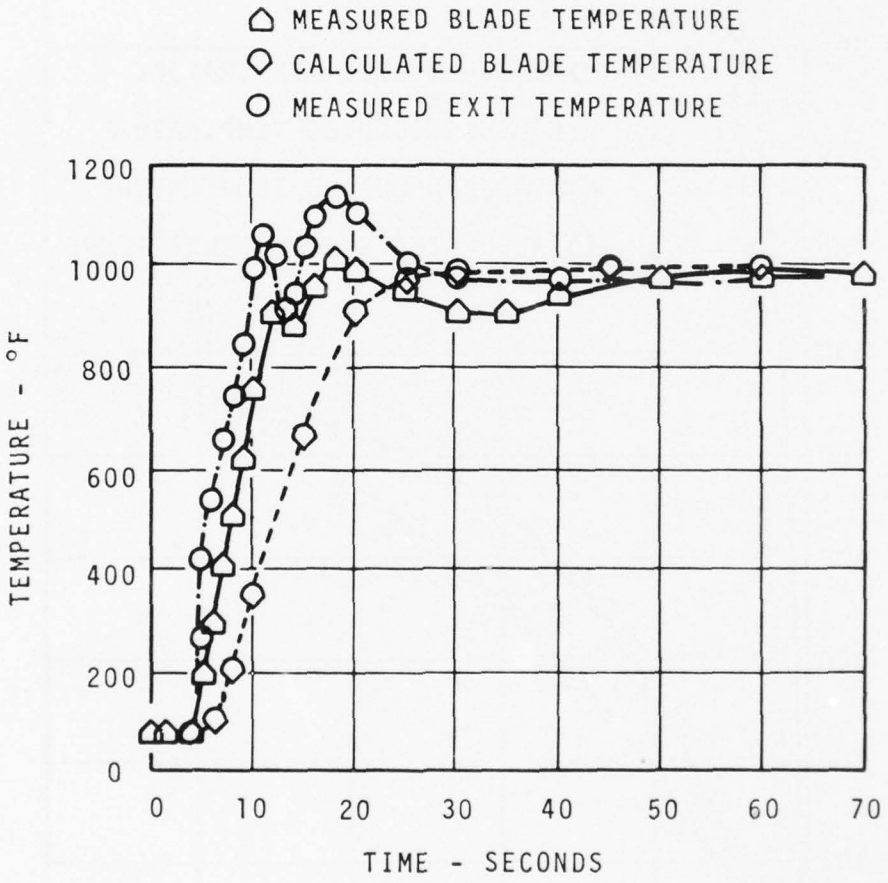

Figure 37. Blade Temperature Response - Start.

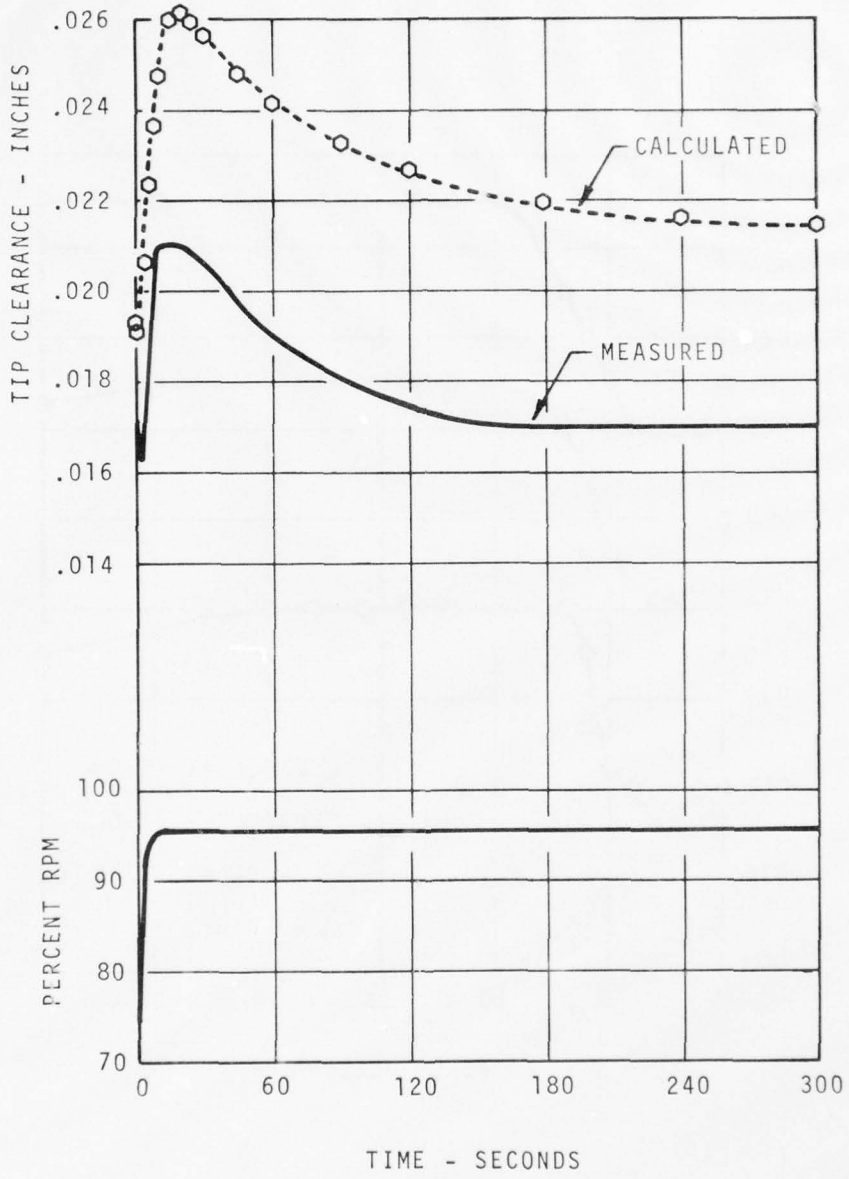

Figure 38. Transient Tip-Clearance Response - Jam Acceleration.

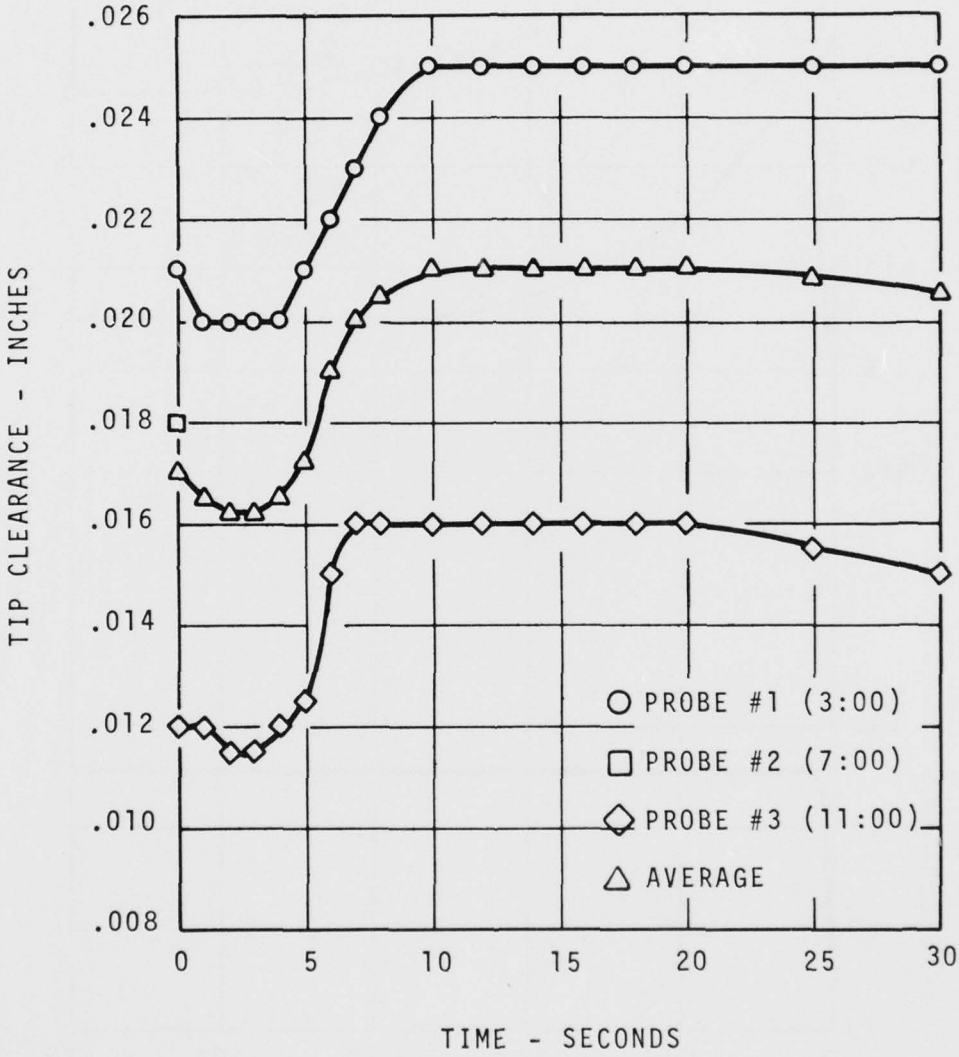

Figure 39. Measured Tip Clearance - Jam Acceleration.

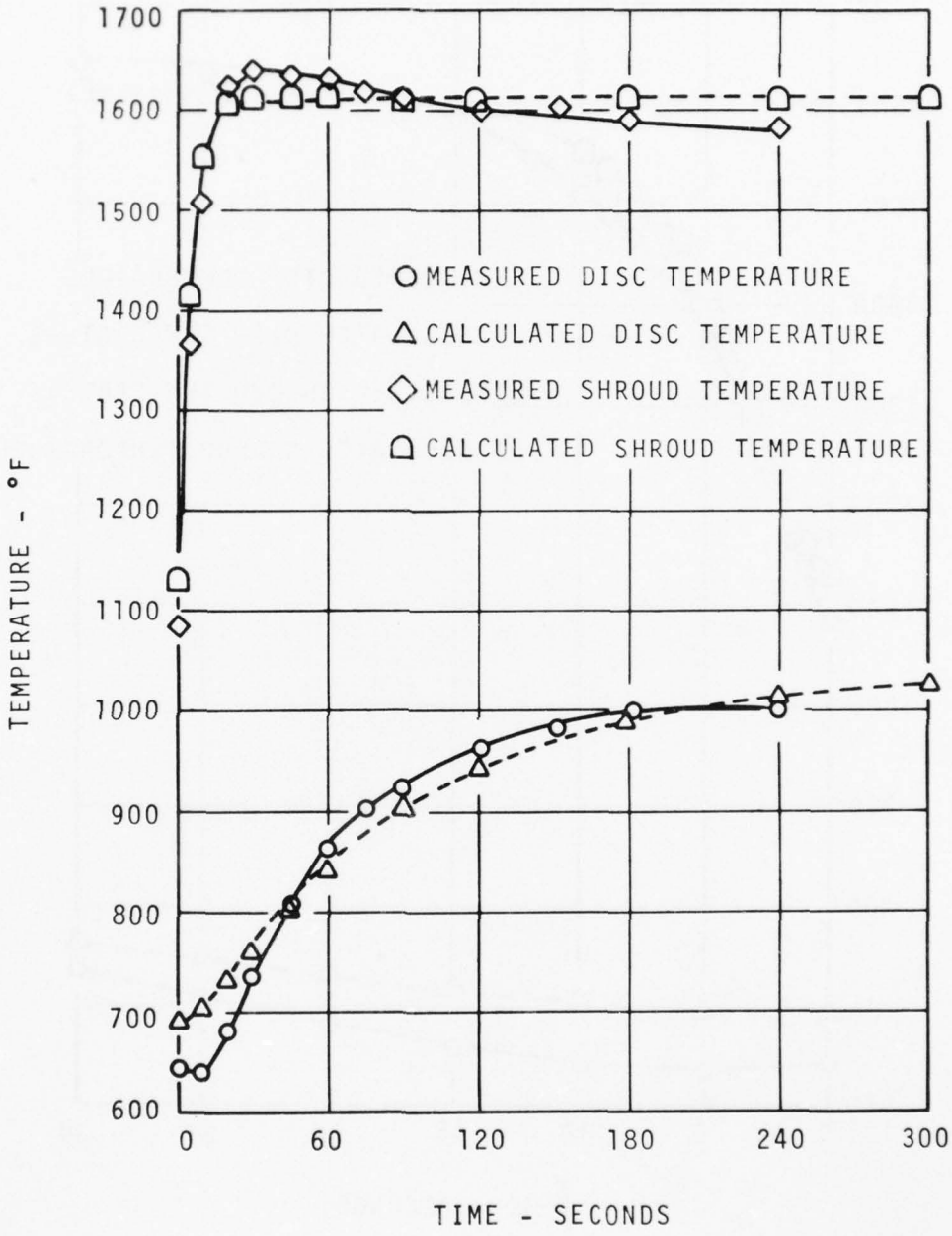

Figure 40. Component Temperature Response - Jam Acceleration.

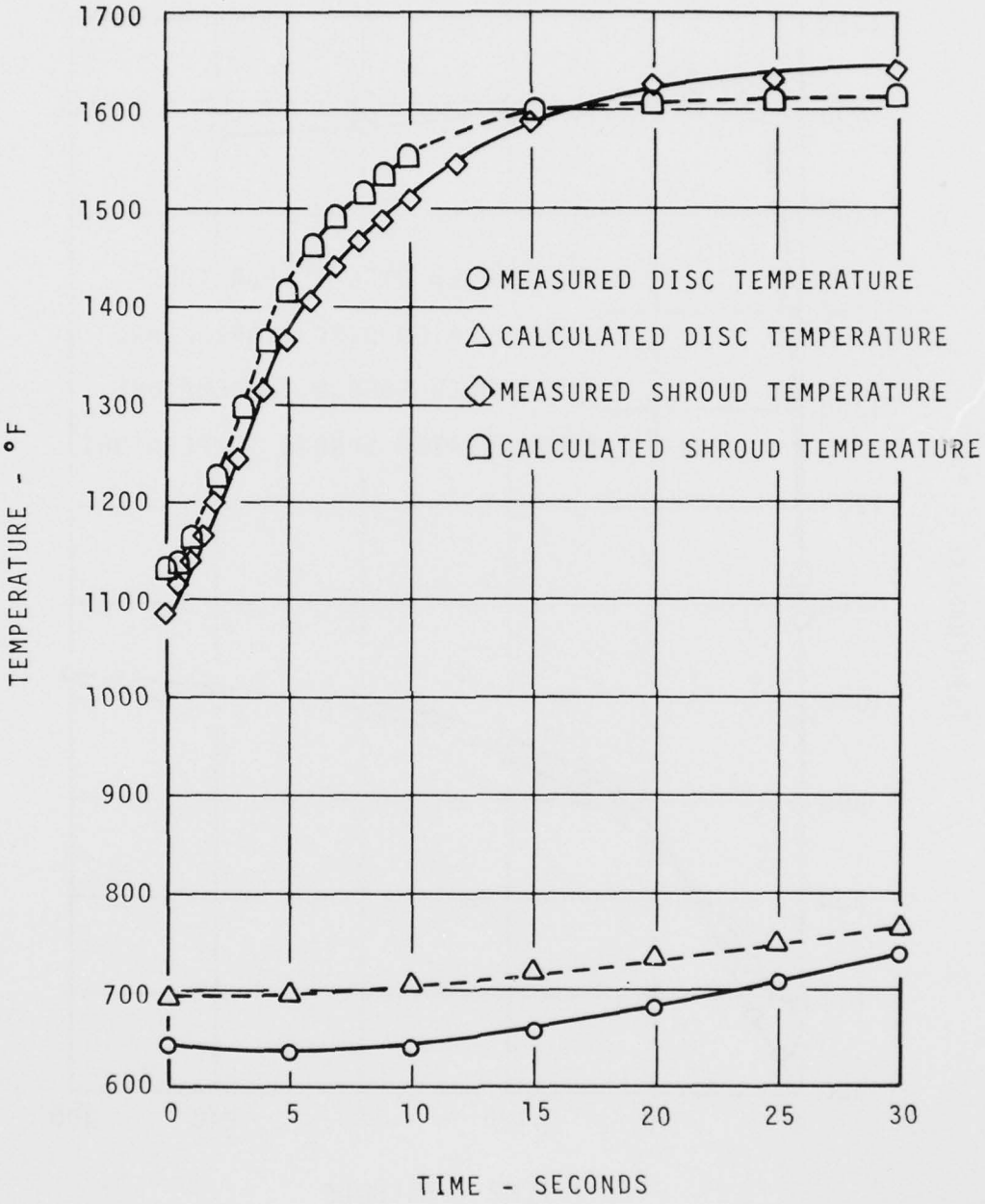

Figure 41, Component Temperature Response - Jam Acceleration.

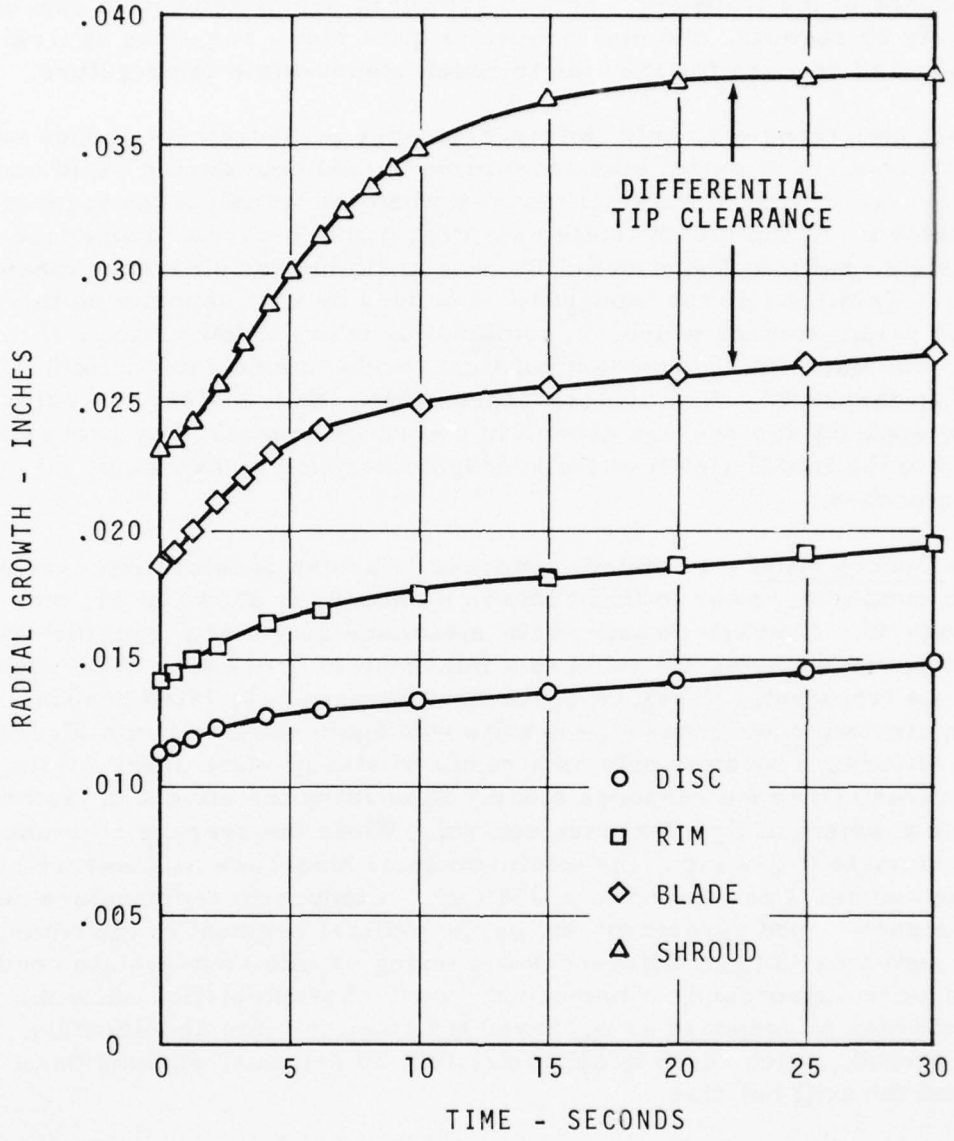

Figure 42. Component Growth Characteristics - Jam Acceleration.

temperatures illustrate the order of response. Blade growth, illustrated as the differential between total blade tip growth and disc rim growth, is very rapid, with most of the change occurring within the first 5 seconds of the transient. Shroud growth is completed within approximately 20 seconds, and disc growth is quite slow, requiring approximately 180 seconds for the disc to reach steady-state temperature.

During this transient, only two tip-clearance measurement probes were operational. The output spot from probe 2 faded out during rapid acceleration conditions on the final test day when the transient testing was conducted. At the steady-state operating points before and after the transient, sufficient spot definition was available for clearance measurement. This behavior is thought to be caused by soot deposits on the probe prism surface which, in combination with the low reflectivity from the blade tip, reduced output light levels to below the optical system threshold. Average clearance during the transient was calculated by applying the average change in clearance measured by probes 1 and 3 to the initial steady-state average clearance measured by all three probes.

Snap Deceleration - Transient response to a snap deceleration executed from maximum power to flight idle in 6 seconds is shown in Figures 43 through 48. Average measured tip clearance decreased from the maximum power steady-state value to a minimum of 0.012 inch at 20 seconds into the transient. Excellent agreement between calculated response characteristics and measured results was again observed with significant difference existing only as a result of steady-state differentials. Measured clearance response clearly illustrates the effects of distortion on the problem of tip-clearance control. While the average clearance decreased to 0.012 inch, the minimum local clearance as measured by probe number 3 decreased to 0.004 inch. Component temperature response shows good agreement during the critical segment of the transient, with somewhat larger differences occurring as idle steady-state conditions were approached. Component growth characteristics show the same order of response as observed for start and jam acceleration. The shroud, which cools in approximately 30 seconds, shrinks down around the still hot disc.

Wave-Off - The wave-off (illustrated in Figures 49 through 51) consisted of a rapid decleration from maximum power to flight idle and an immediate acceleration back to maximum power. The deceleration leg was completed in 3.8 seconds, and maximum power was attained after a total time of 7.0 seconds. A minimum average clearance of 0.013 inch was measured 6.0 seconds after initiation of the transient with a

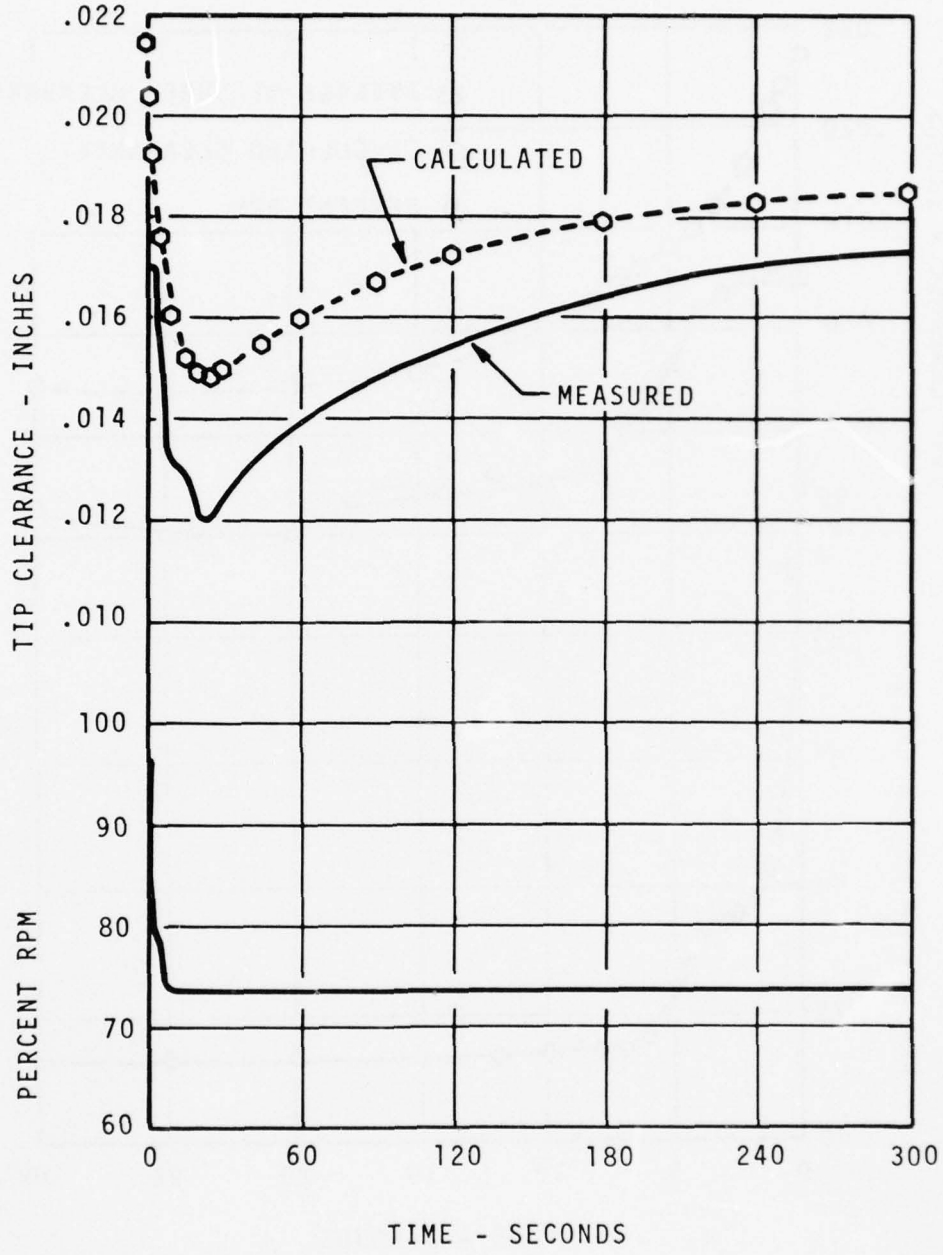

Figure 43. Transient Tip-Clearance Response - Snap Deceleration.

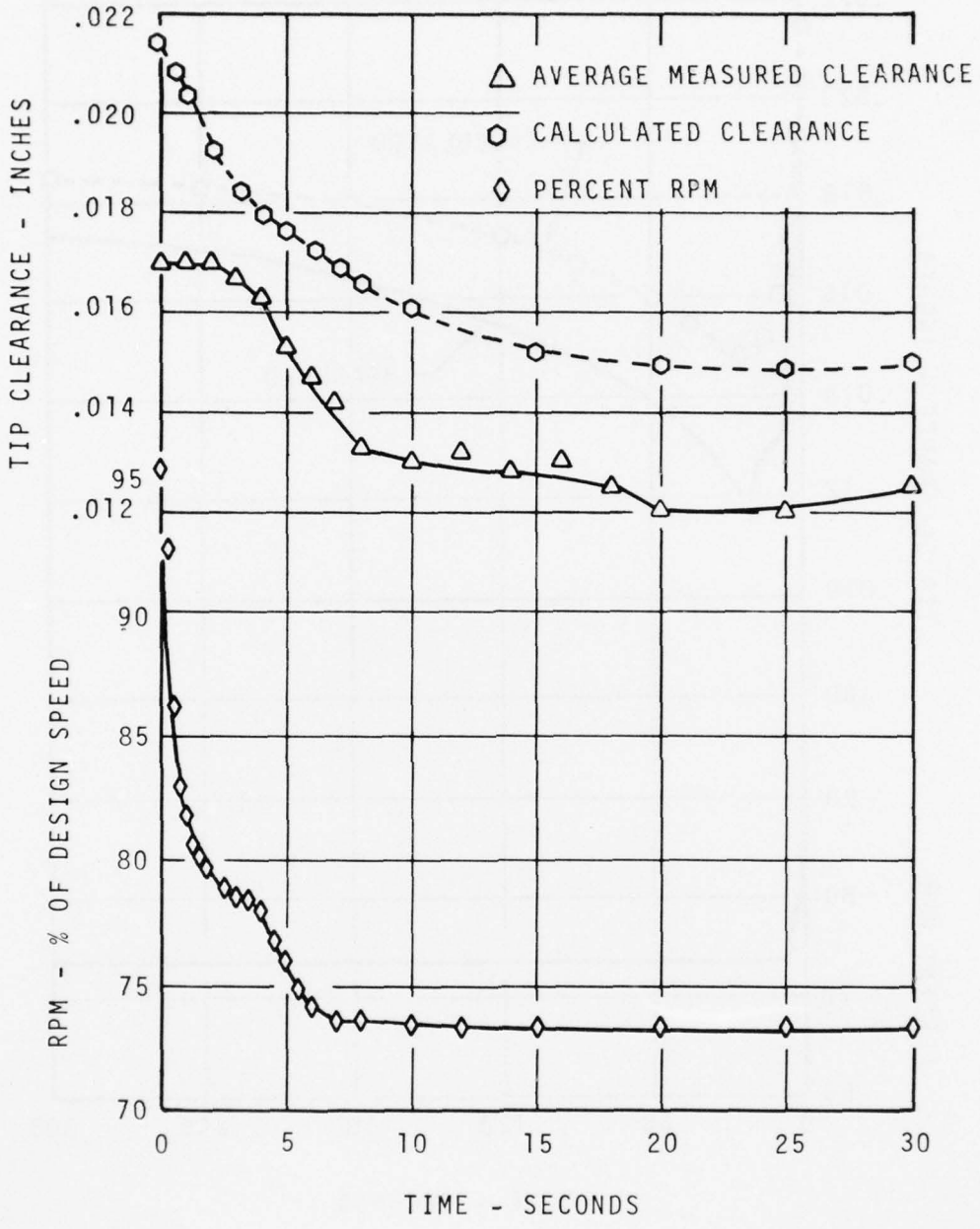

Figure 44. Transient Tip-Clearance Response - Snap Deceleration (0 -30 Seconds).

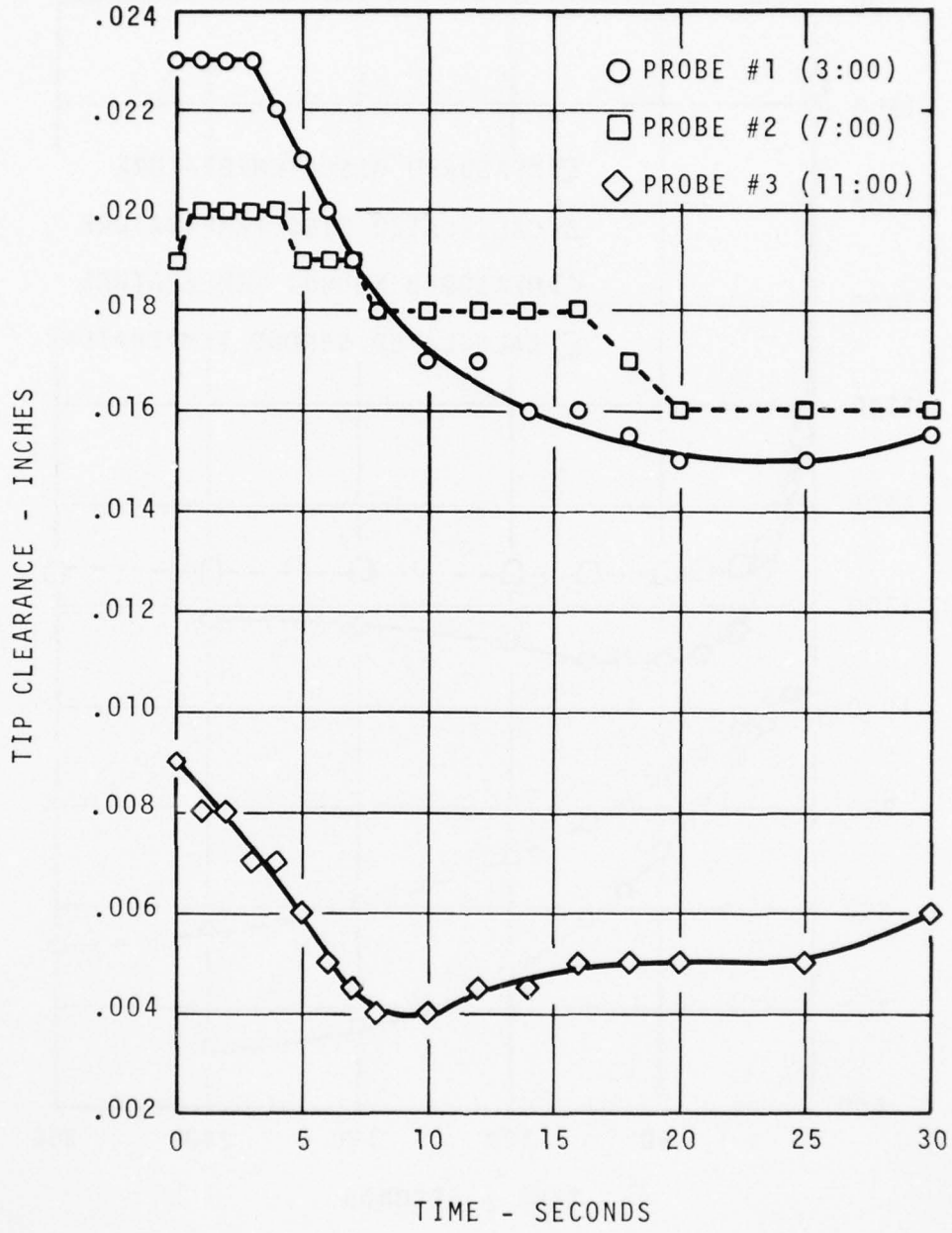

Figure 45. Measured Tip Clearance - Snap Deceleration.

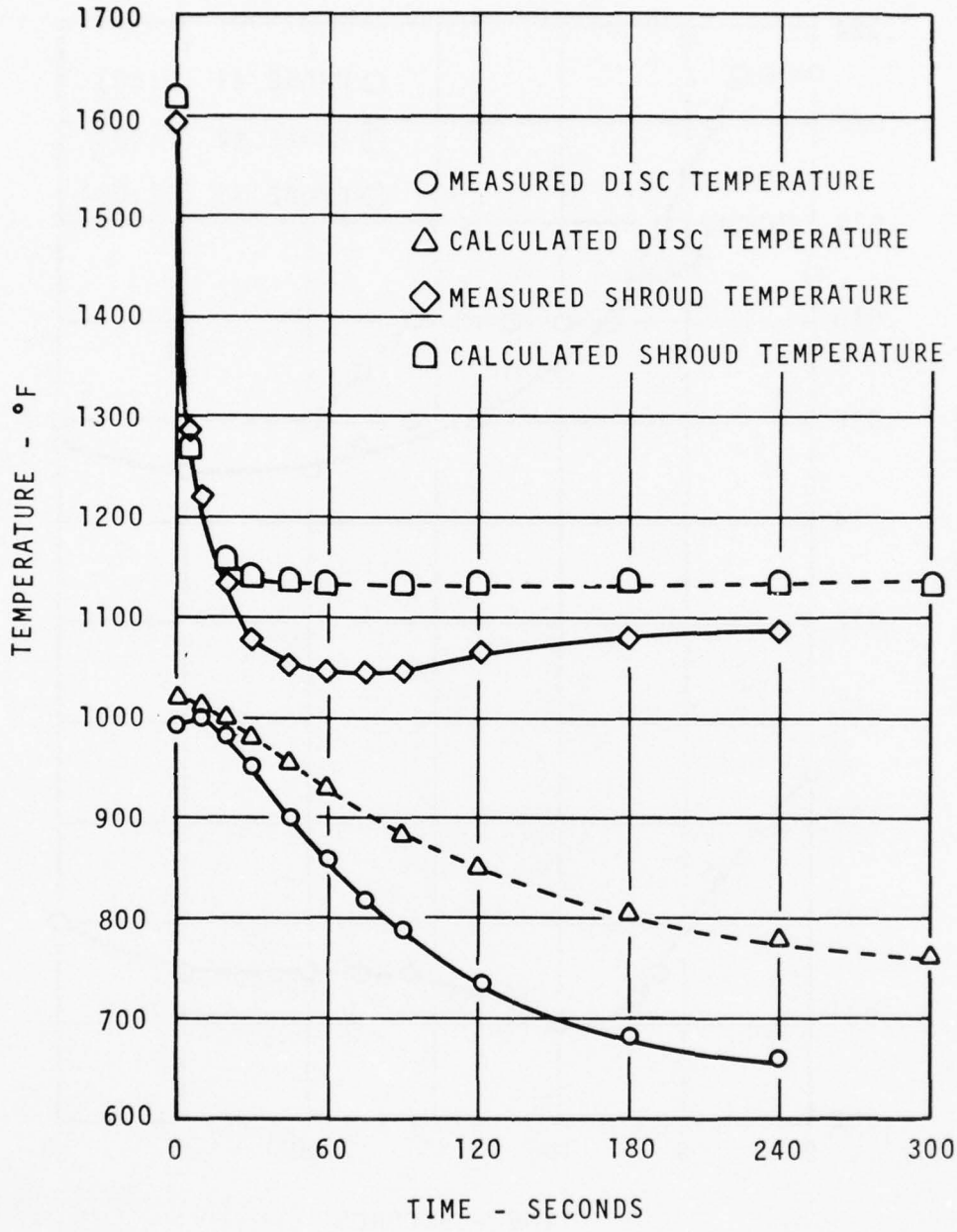

Figure 46. Component Temperature Response - Snap Deceleration.

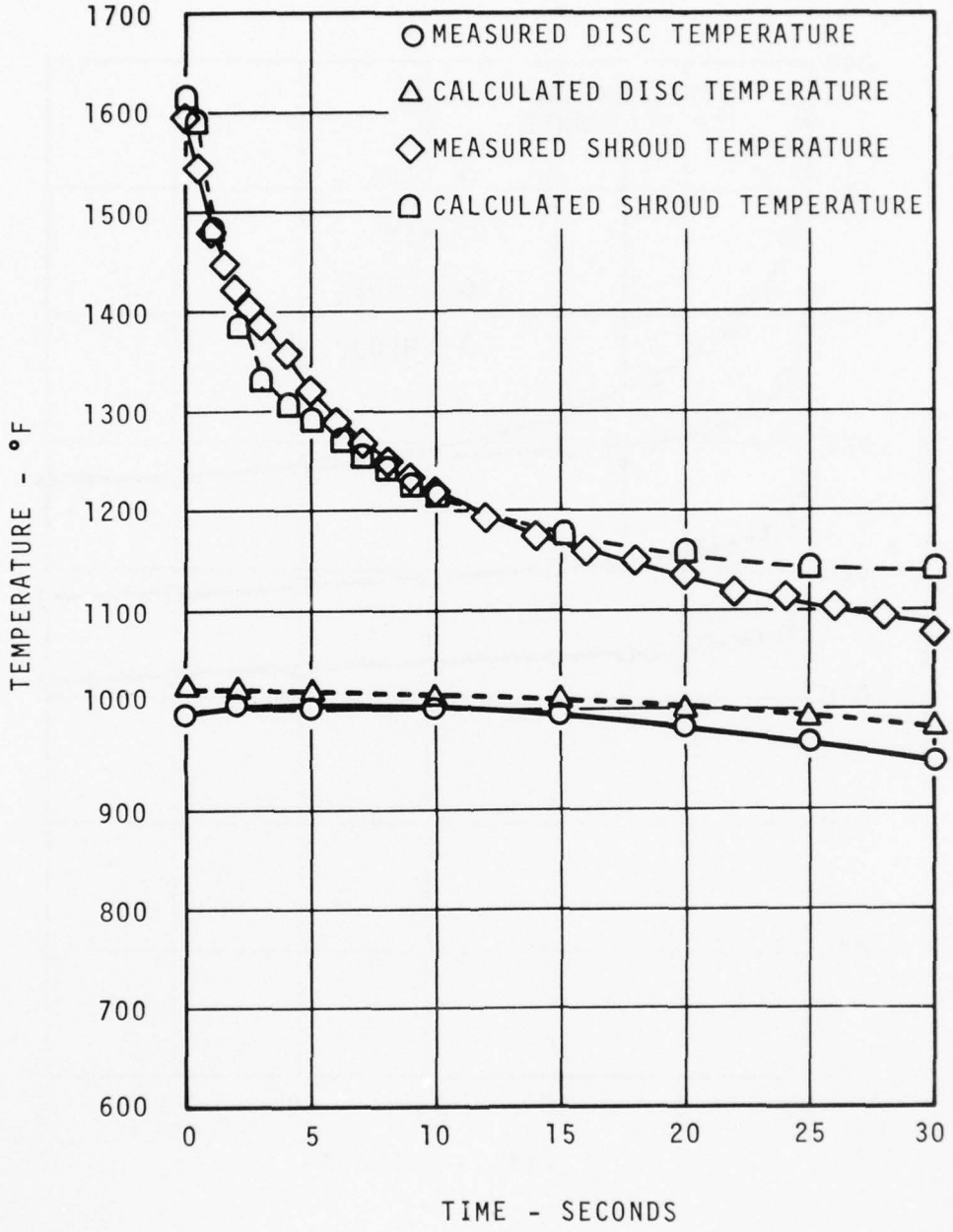

Figure 47. Component Temperature Response - Snap Deceleration (0-30 Seconds).

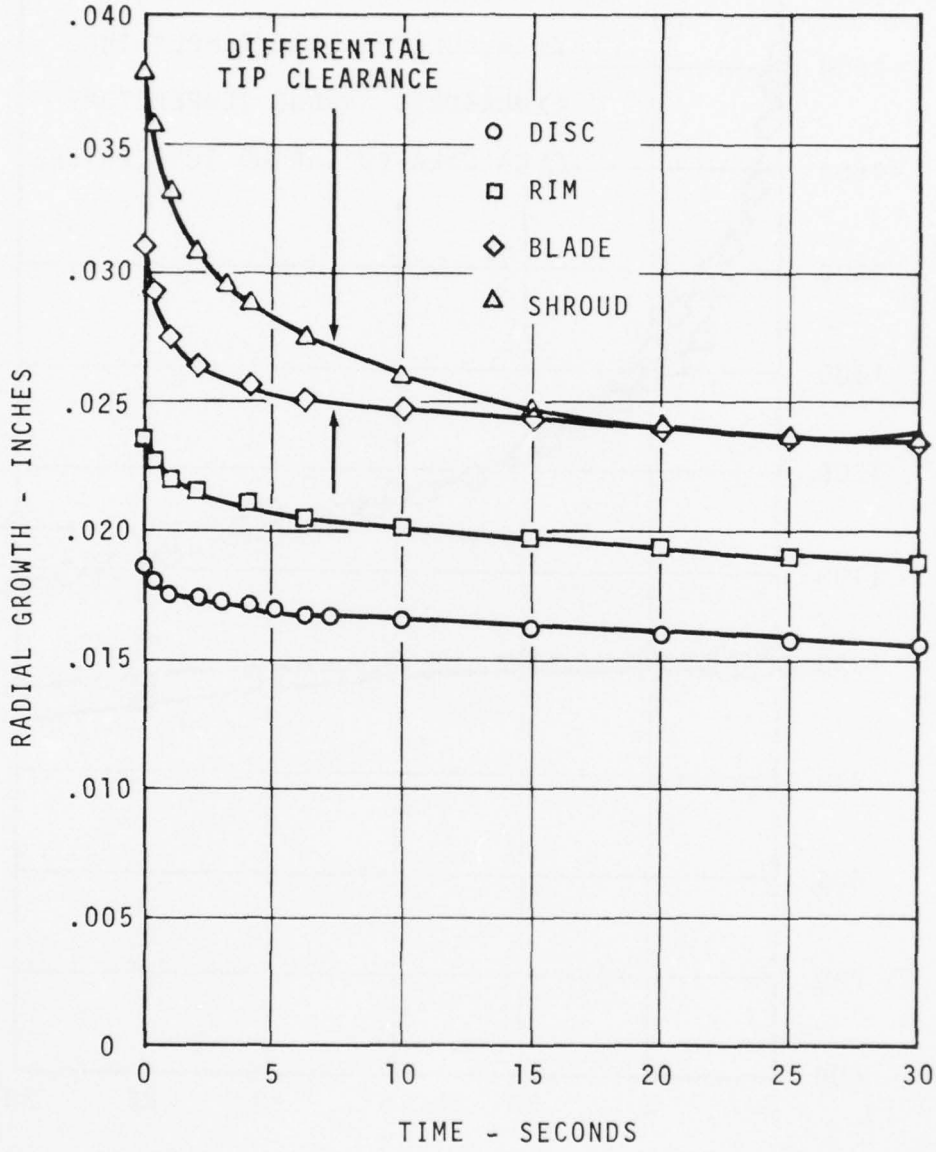

Figure 48. Component Growth Characteristics - Snap Deceleration.

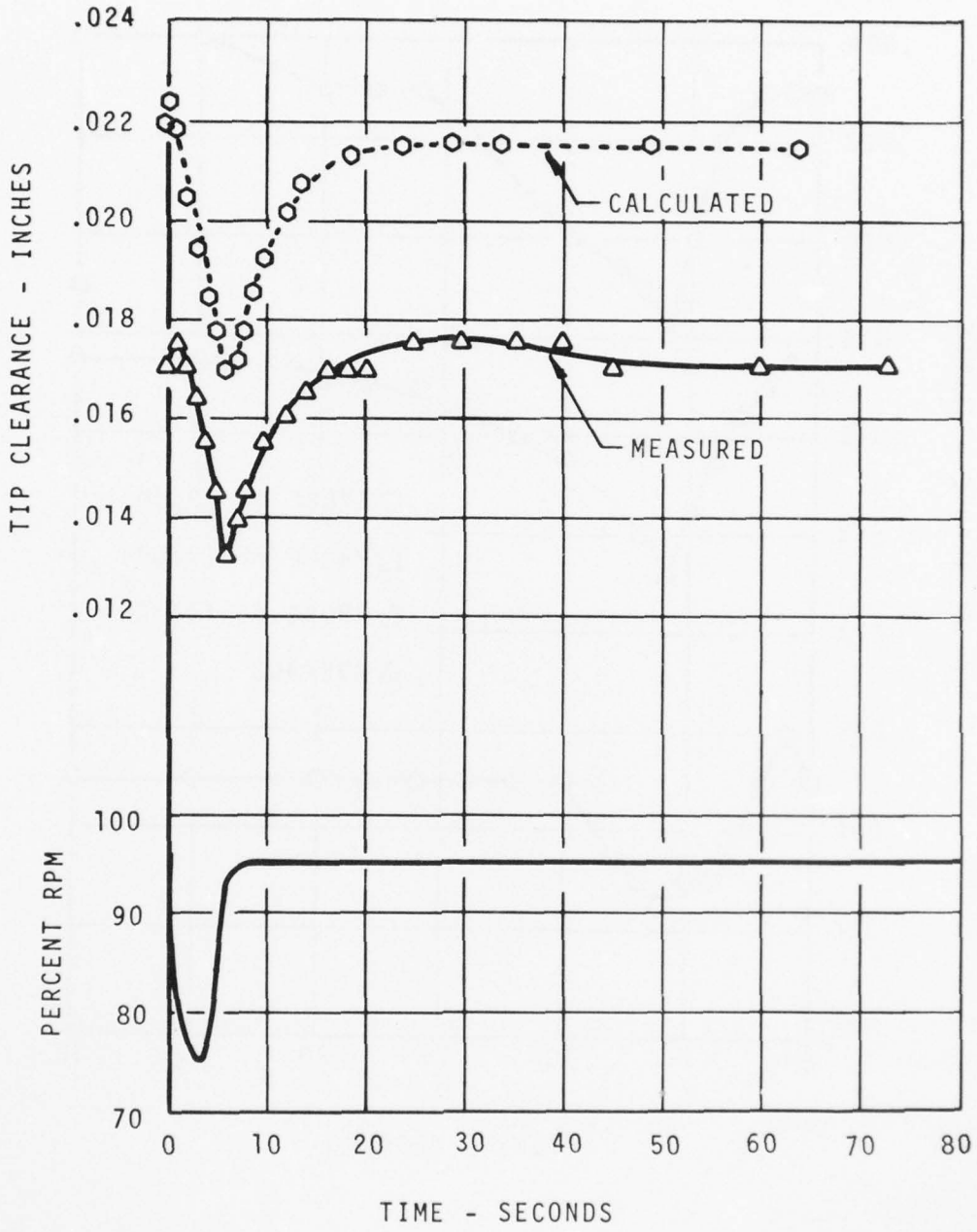

Figure 49. Transient Tip-Clearance Response - Wave-off.

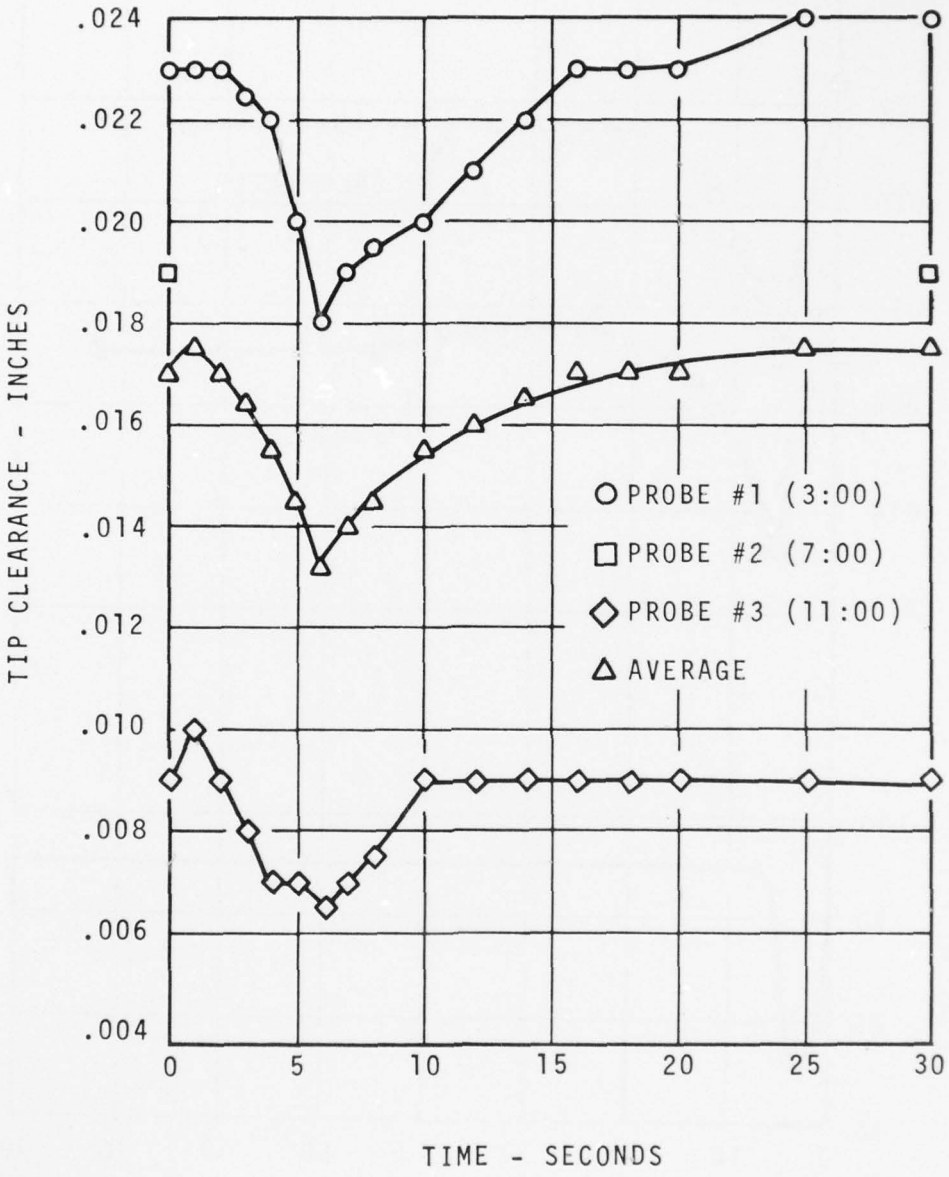

Figure 50. Measured Tip Clearance - Wave-off.

AD-A052 042 AVCO LYCOMING DIV STRATFORD CONN F/G 21/5
TURBINE TIP-CLEARANCE MEASUREMENT.(U)
DEC 77 S D WHITE DAAJ02-75-C-0051
UNCLASSIFIED LYC-77-46 USARTL-TR-77-47 NL

2 OF 2
AD A052 042

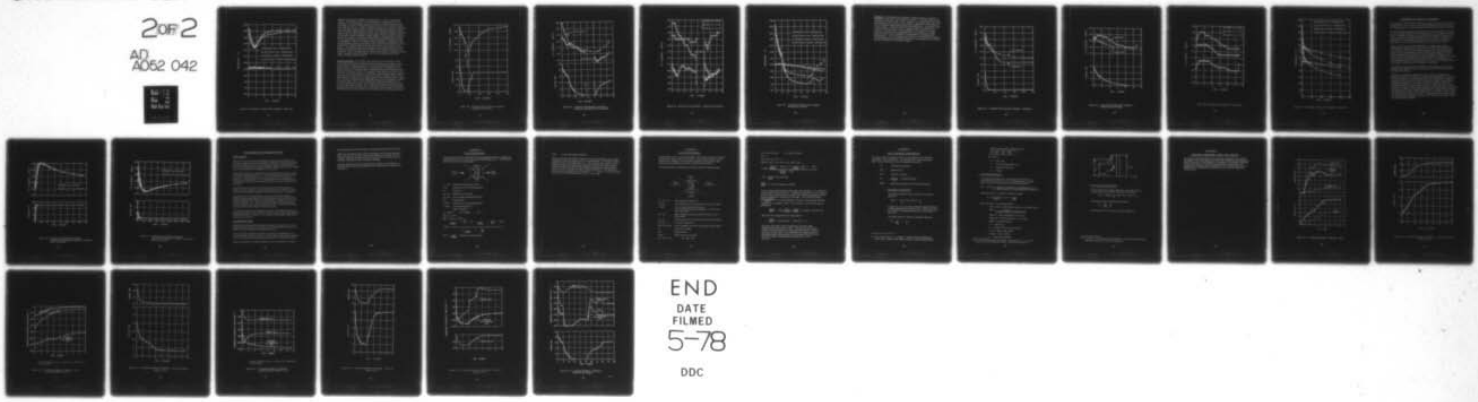

END
DATE FILMED
5-78
DDC

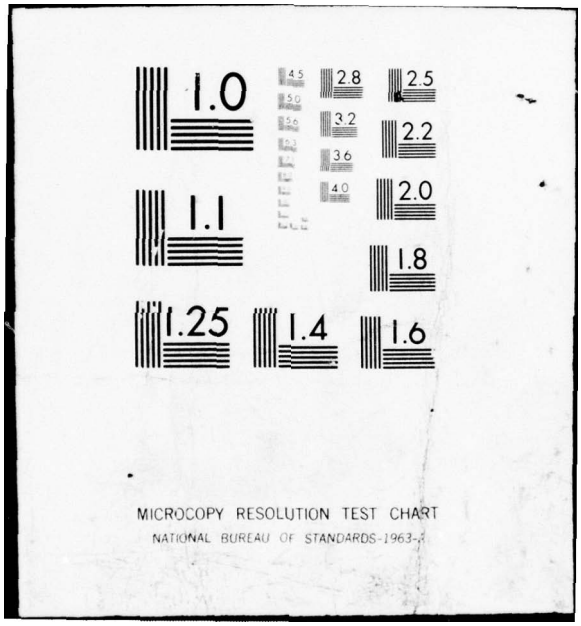
1.0
1.1
1.25
1.4
1.6
1.8
2.0
2.2
2.5
2.8
3.2
3.6
4.0
4.5
5.0
5.6
MICROCOPY RESOLUTION TEST CHART
NATIONAL BUREAU OF STANDARDS-1963-A

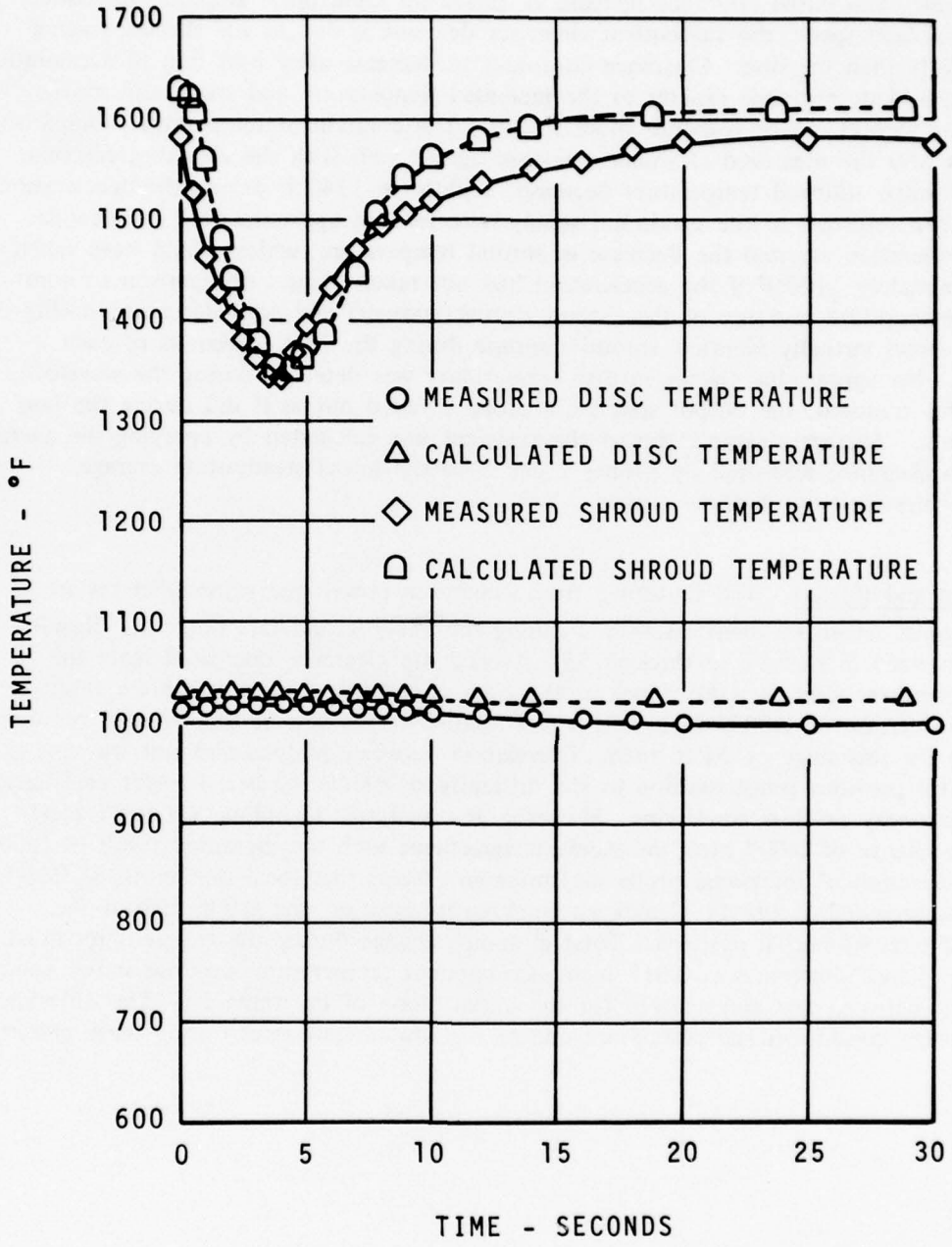

Figure 51. Component Temperature Response - Wave-off.

minimum local clearance of 0.0065 inch measured at the 11 o'clock circumferential location. The minimum clearance occurs approximately 2 seconds after the start of acceleration. The initial clearance increase is caused by rapid blade response to reduce temperature and speed; the subsequent clearance decrease is due to the shroud cooling more rapidly than the disc. Clearance continues to decrease after initiation of acceleration because the blade responds rapidly to the increased temperature and speed and moves toward the shroud, which responds more slowly. The component temperature comparison illustrates why the measured clearance response agrees well with the clearance response analysis results. Shroud temperature decreased rapidly to 1340°F during the deceleration leg and then returned to the maximum steady-state level in approximately 20 seconds. The reacceleration arrested the decrease in shroud temperature, which would have fallen to approximately 1100°F if the acceleration had not taken place. Comparison of component temperature response of the shroud during wave-off and snap deceleration (Fig 51 and 46) shows virtually identical shroud response during the first 4 seconds of each transient. No appreciable change in disc temperature was detected during the wave-off. During this transient, the output spot from probe 2 faded out as it did during the jam acceleration. Average clearance during the transient was calculated by applying the average change in clearance measured by probes 1 and 3 to the initial steady-state average clearance measured by all three probes.

Shutdown and Restart - The shutdown from maximum power and subsequent restart was the most severe transient discovered during the analytic and test program. Results are summarized in Figures 52 through 55. Average tip clearance decreased from the maximum power level to 0.0095 inch at the time of restart. This represents a total clearance decrease of 0.0075 inch, which is a significant fraction of the targeted running clearance for this stage of 0.010 inch. Correlation between analysis and test was not as close as for previous transients due to the difficulty of predicting heat-transfer coefficients under stationary no-flow conditions. However, the analytic technique yielded a total clearance change of 0.009 inch, an excellent agreement with the measured result of 0.0075 inch. Inspection of individual probe measurements shows that local minimums of 0.005 inch were recorded at the 11 o'clock circumferential position and 0.006 inch at the 3 o'clock circumferential position. Total clearance change during the transient recorded at the 3 o'clock position was 0.017 inch. Component temperature response shows good agreement between test and analysis for the initial phase of the transient. The differences noted during coastdown and restart are due to the low airflow rates during these phases.

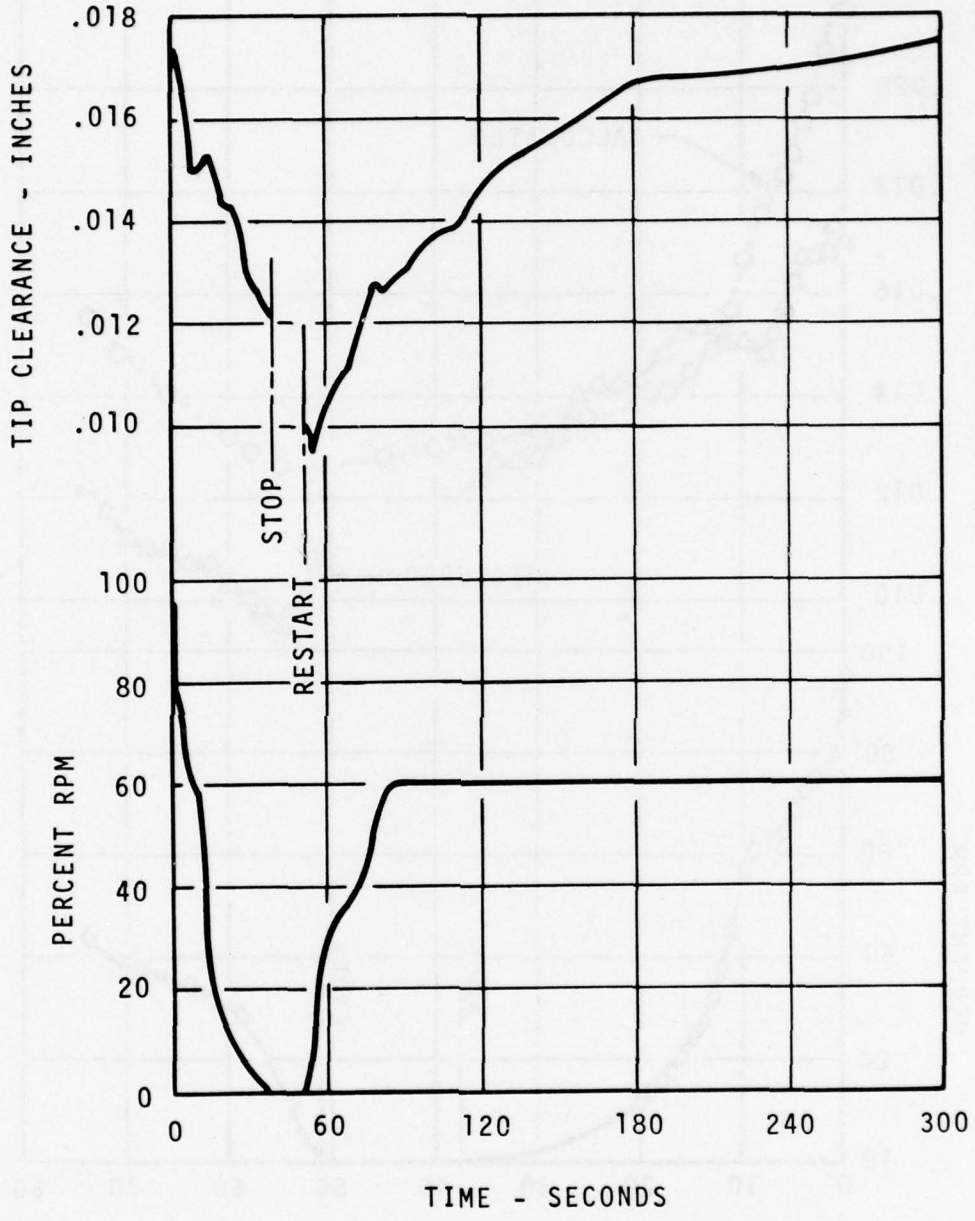

Figure 52. Transient Tip-Clearance Response - Shutdown and Restart.

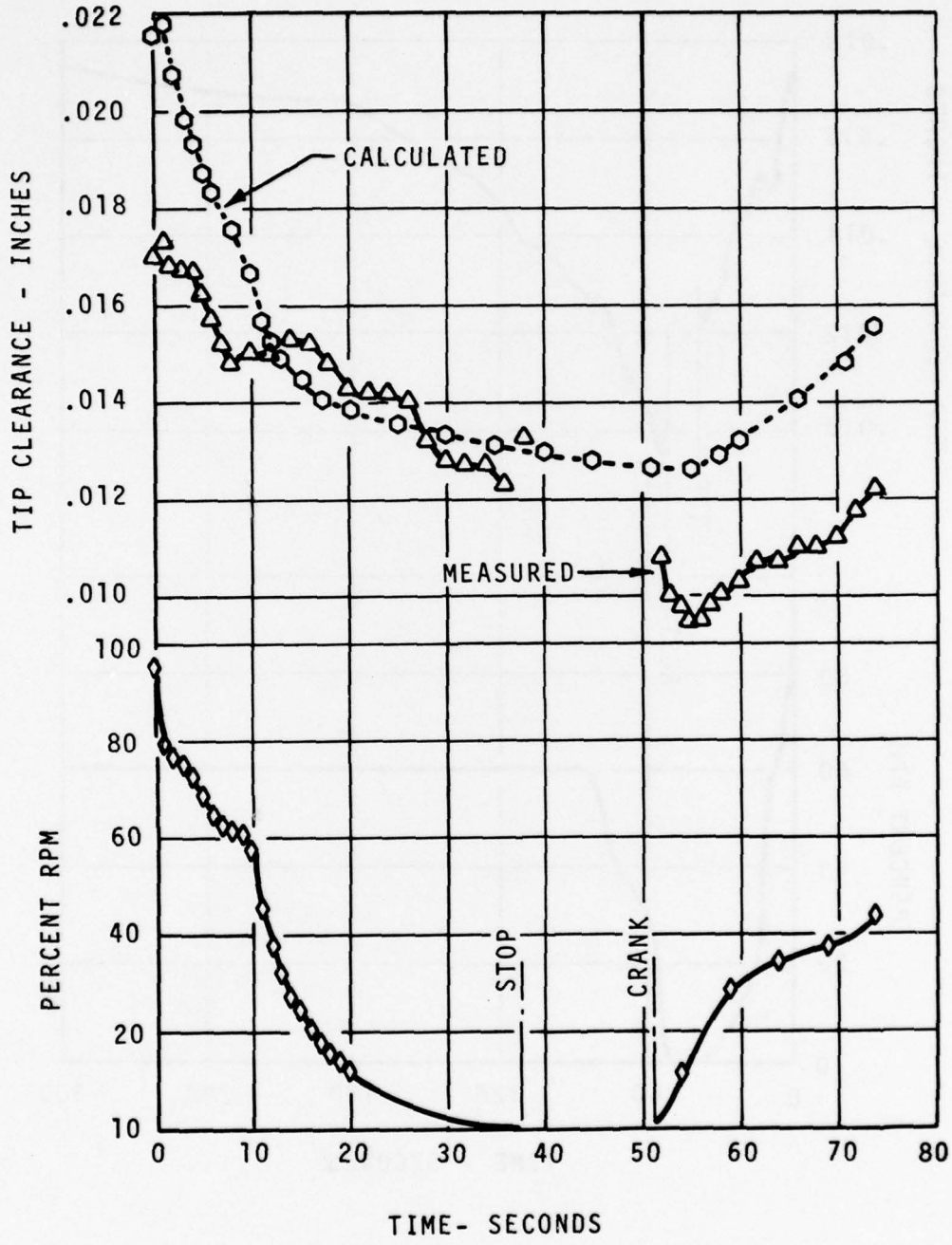

Figure 53. Transient Tip-Clearance Response - Shutdown and Restart (0-70 Seconds).

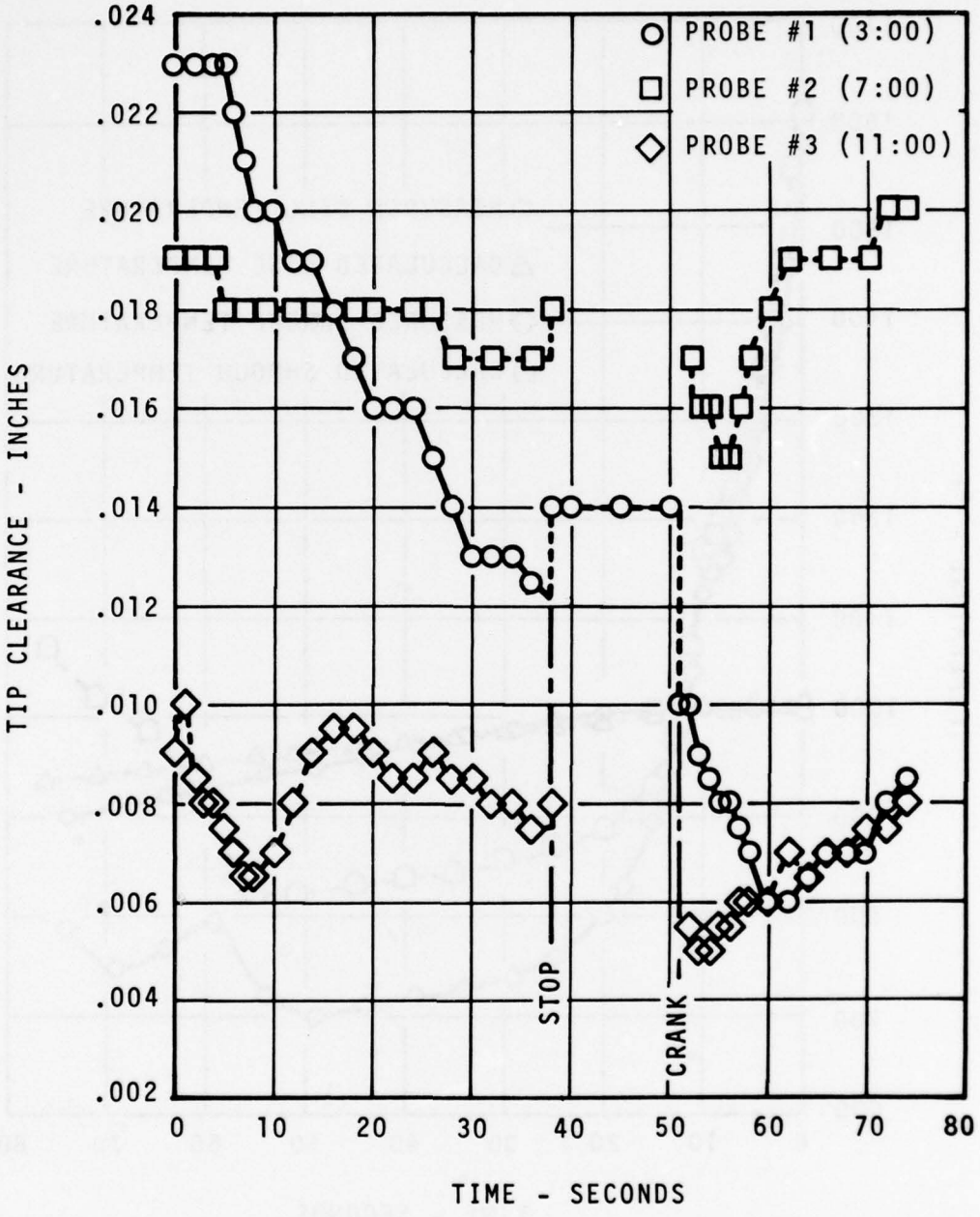

Figure 54. Measured Tip Clearance - Shutdown and Restart.

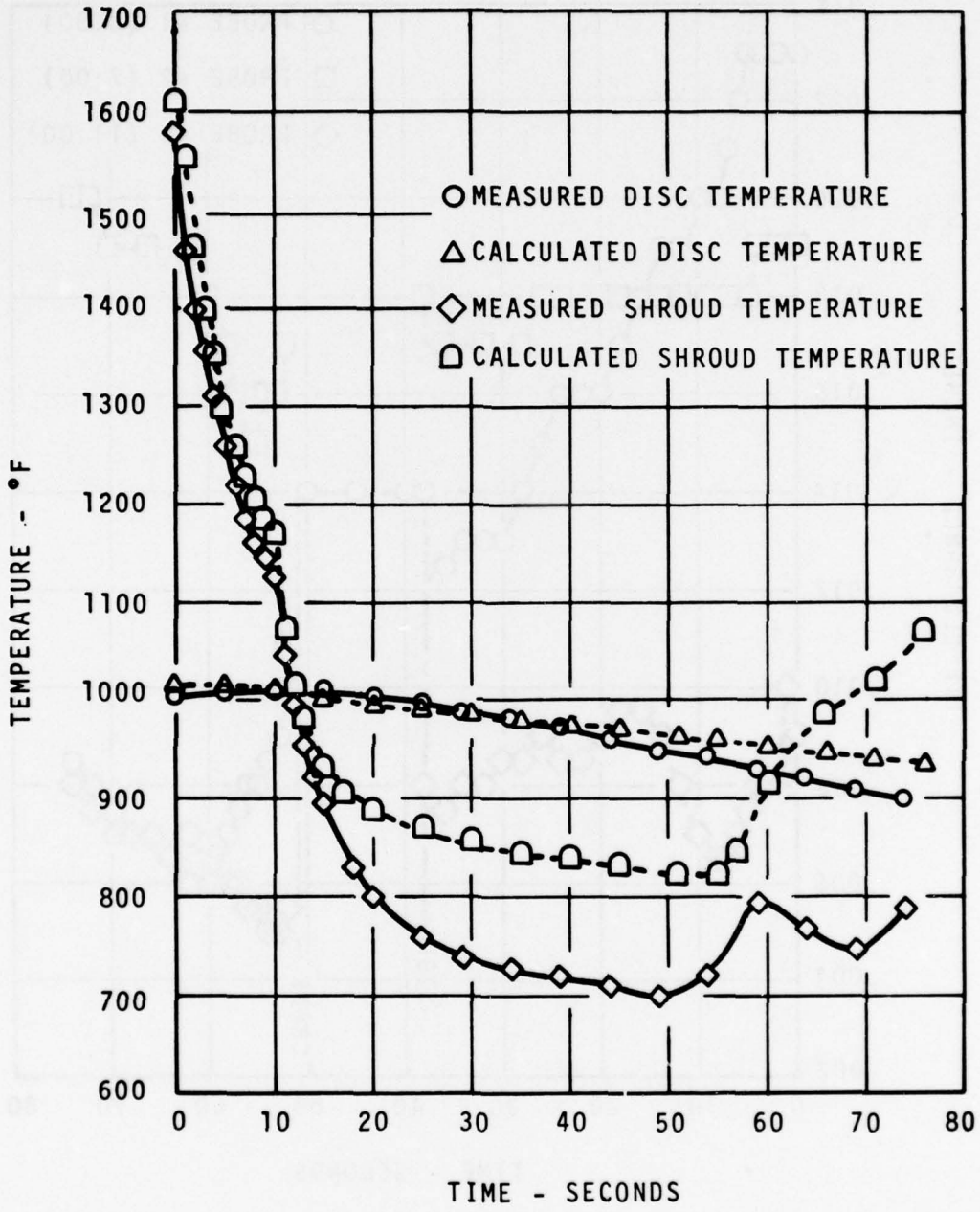

Figure 55. Component Temperature Response - Shutdown and Restart.

Shutdown - The shutdown tip-clearance response shown in Figures 56 through 59 is similar to the previous transient. Average minimum tip clearance was 0.0105 inch. This, however, is based on only one probe measurement after gas generator rotation stopped since all blades are not in the probe measurement planes simultaneously. Clearance measured by probe 1, located at the 3 o'clock position, decreased from 0.019 to 0.013 inch after rotation stopped. The minimum average clearance is based on the assumption that the reduction in average clearance after rotation stopped corresponded to the single probe measurement. As for the previous transient, measured and calculated shroud temperatures agreed well during the initial phase of the transient and then diverged as the airflow stopped.

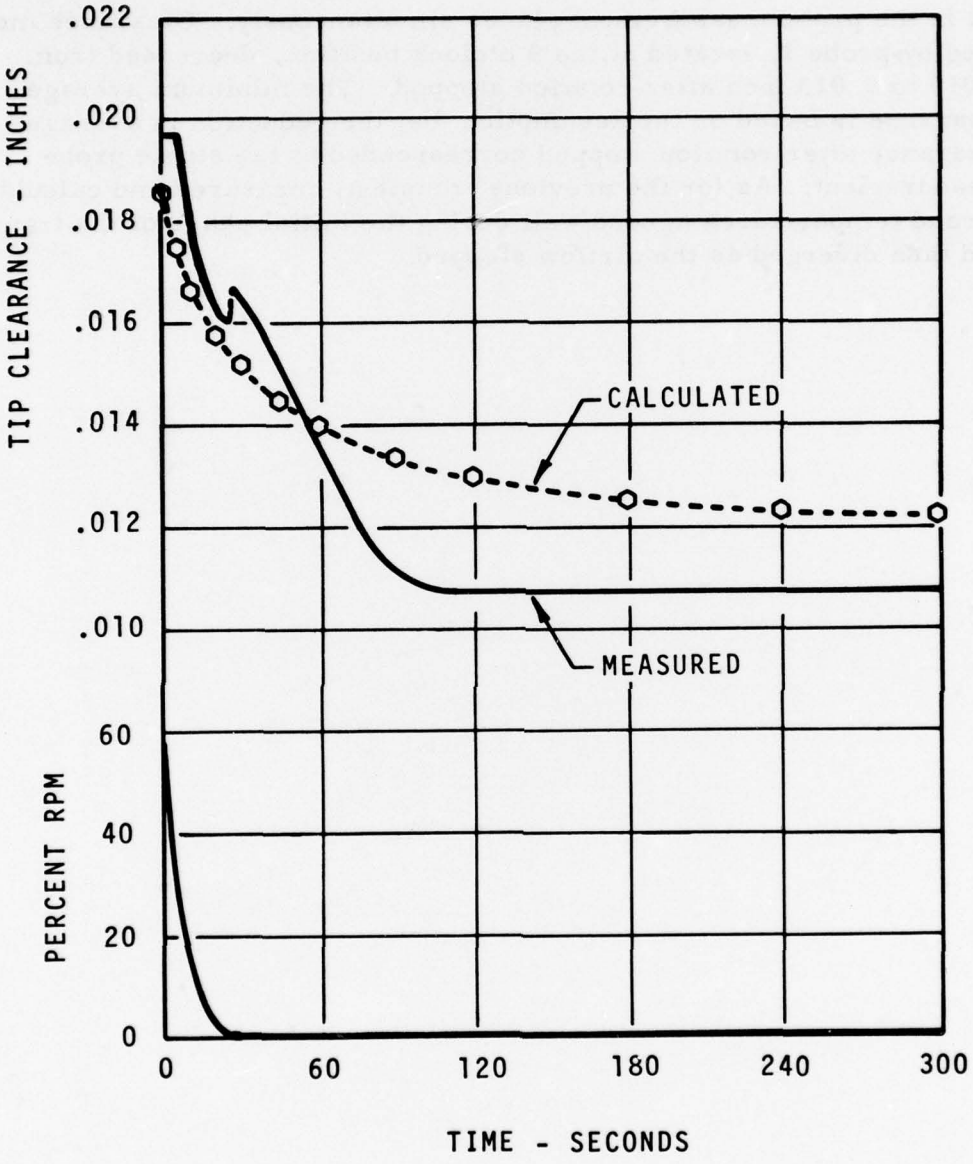

Figure 56. Transient Tip-Clearance Response - Shutdown.

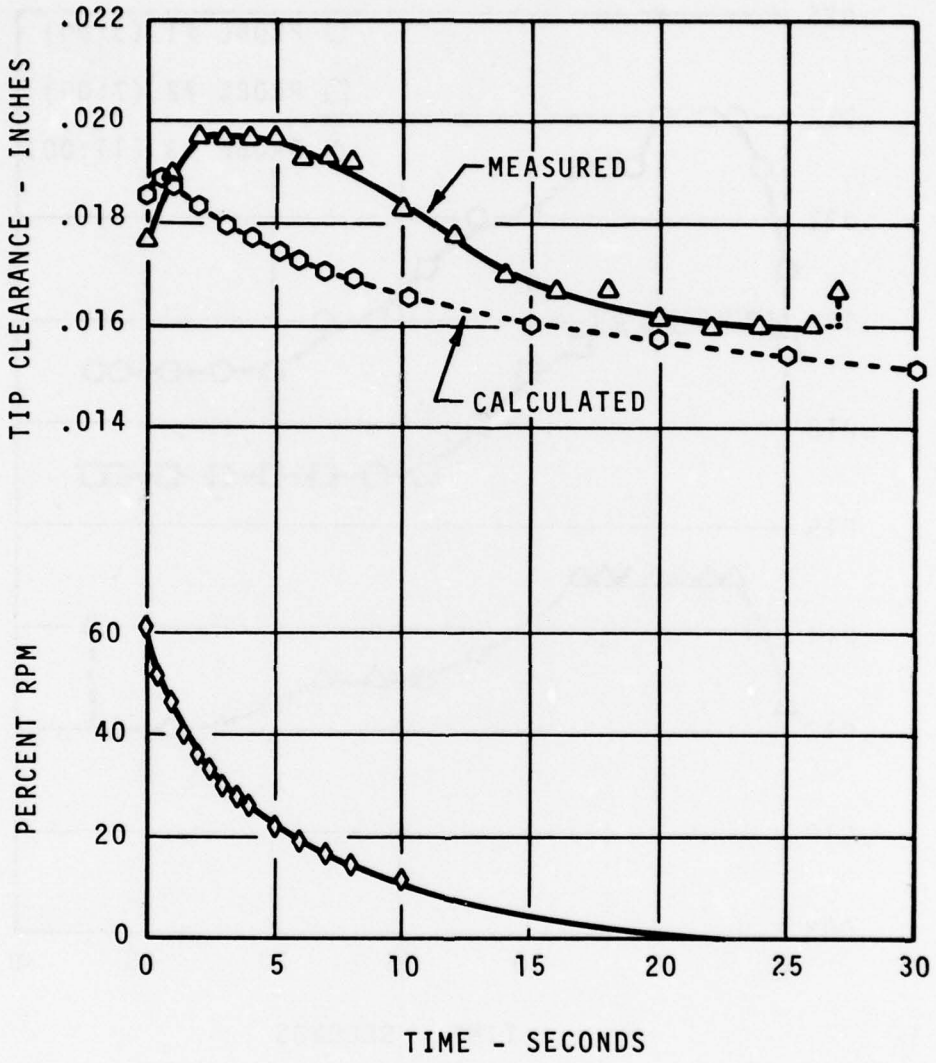

Figure 57. Transient Tip-Clearance Response - Shutdown (0-30 Seconds).

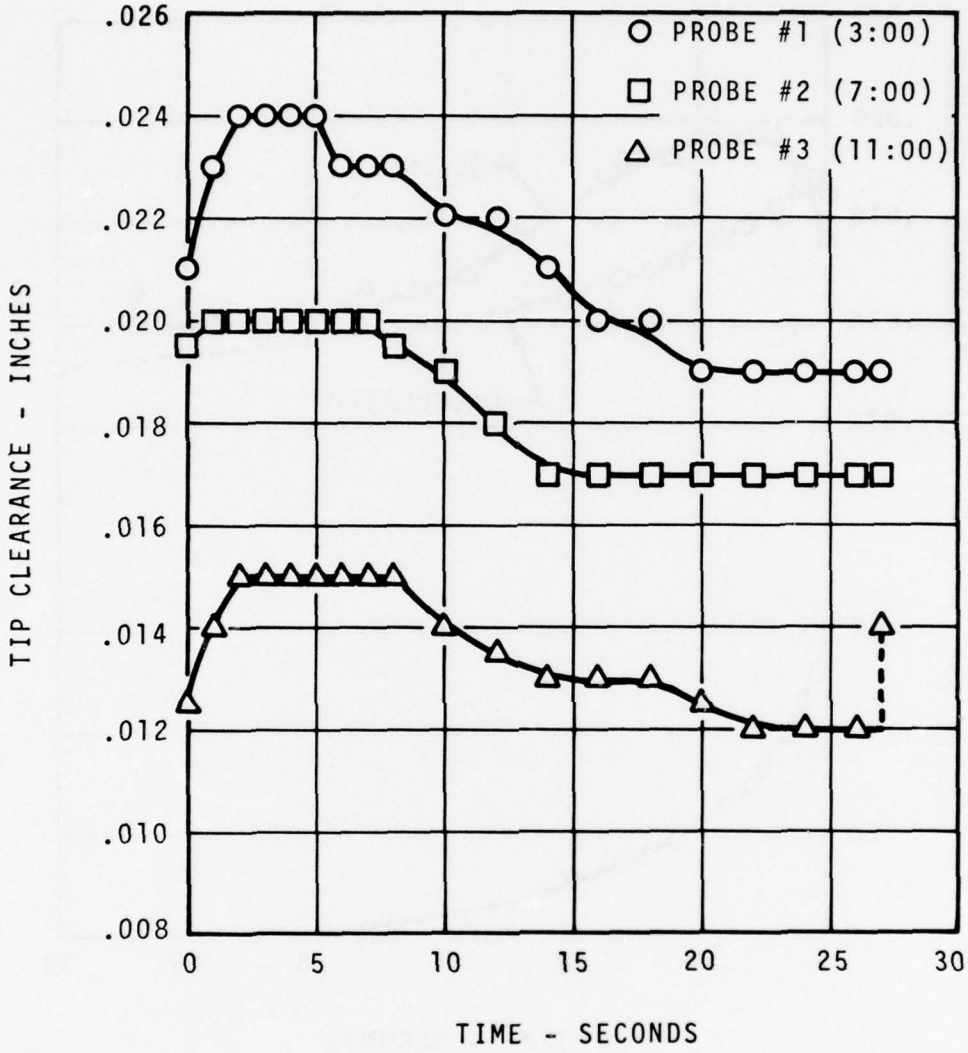

Figure 58. Measured Tip Clearance - Shutdown.

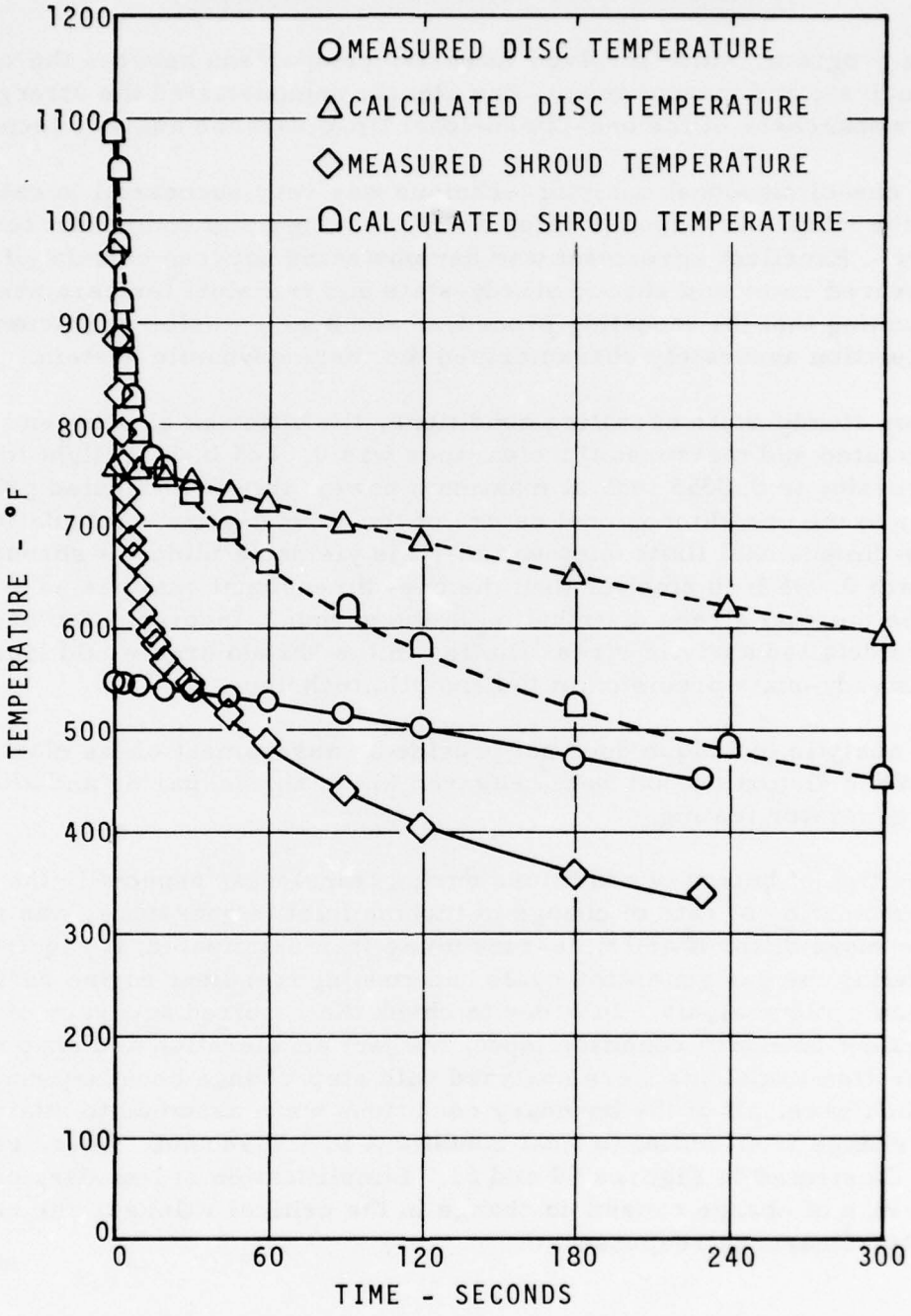

Figure 59. Component Temperature Response - Shutdown.

ASSESSMENT OF ANALYTIC TECHNIQUE

This program, which involved extensive comparison between the results of analysis and measurement, has clearly demonstrated the strengths and weaknesses of the one-dimensional tip-clearance analytic technique.

The one-dimensional analytic technique was very successful in calculating the transient response rates of tip clearance and component temperature. Excellent agreement was demonstrated between calculated and measured rotor and shroud steady-state and transient temperatures, indicating that the modeling procedure and heat-transfer coefficient calculation accurately characterized the thermodynamic system.

Under steady-state operating conditions, the differential between calculated and measured tip clearance was 0.0023 inch at flight idle, increasing to 0.0055 inch at maximum power; this is attributed primarily to the one-dimensional nature of the shroud-growth calculation. Two-dimensional finite-element analysis yielded a midpoint shroud growth 0.006 inch smaller than the one-dimensional analysis as a result of the thermal stress distribution in the shroud. Incorporation of a more detailed analytic stress linkage in the shroud area would increase the steady-state precision of the analytic technique.

The analytic technique does not provide an assessment of the elastic or inelastic distortion that was measured in the shroud during and after gas generator testing.

Definition of boundary conditions during transients, especially the determination of rate of change of turbine inlet temperature, was found to be more difficult and time-consuming than anticipated; it required modeling the gas generator cycle and running transient engine performance cycle analysis. In order to check the required accuracy of transient boundary condition input, the jam acceleration and snap deceleration transients were analyzed with step-change boundary conditions. In each case, all of the boundary conditions were assumed to attain the full change from initial to final conditions in 1.0 second. These results are illustrated in Figures 60 and 61. Simplification of boundary condition rate of change caused no change in the critical values of the resulting tip-clearance response.

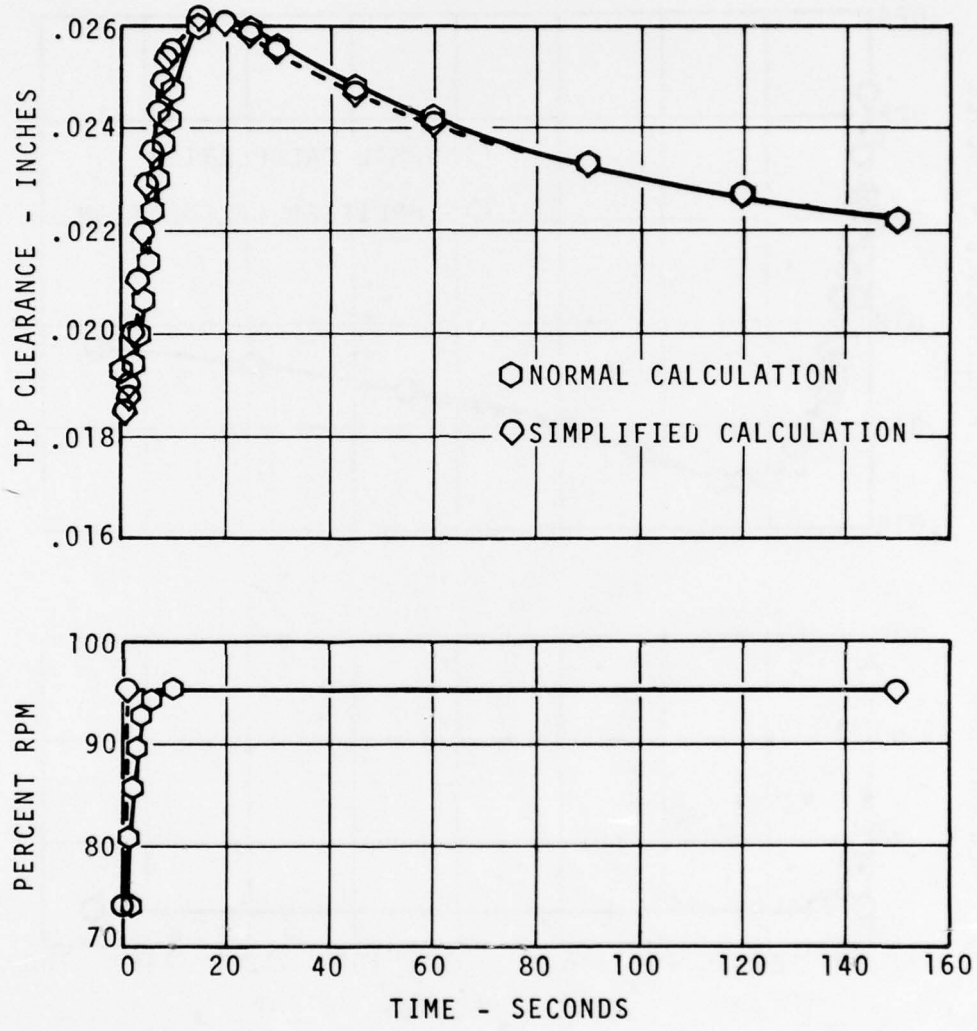

Figure 60. Transient Tip-Clearance Response Analysis With Simplified Boundary Conditions-Jam Acceleration.

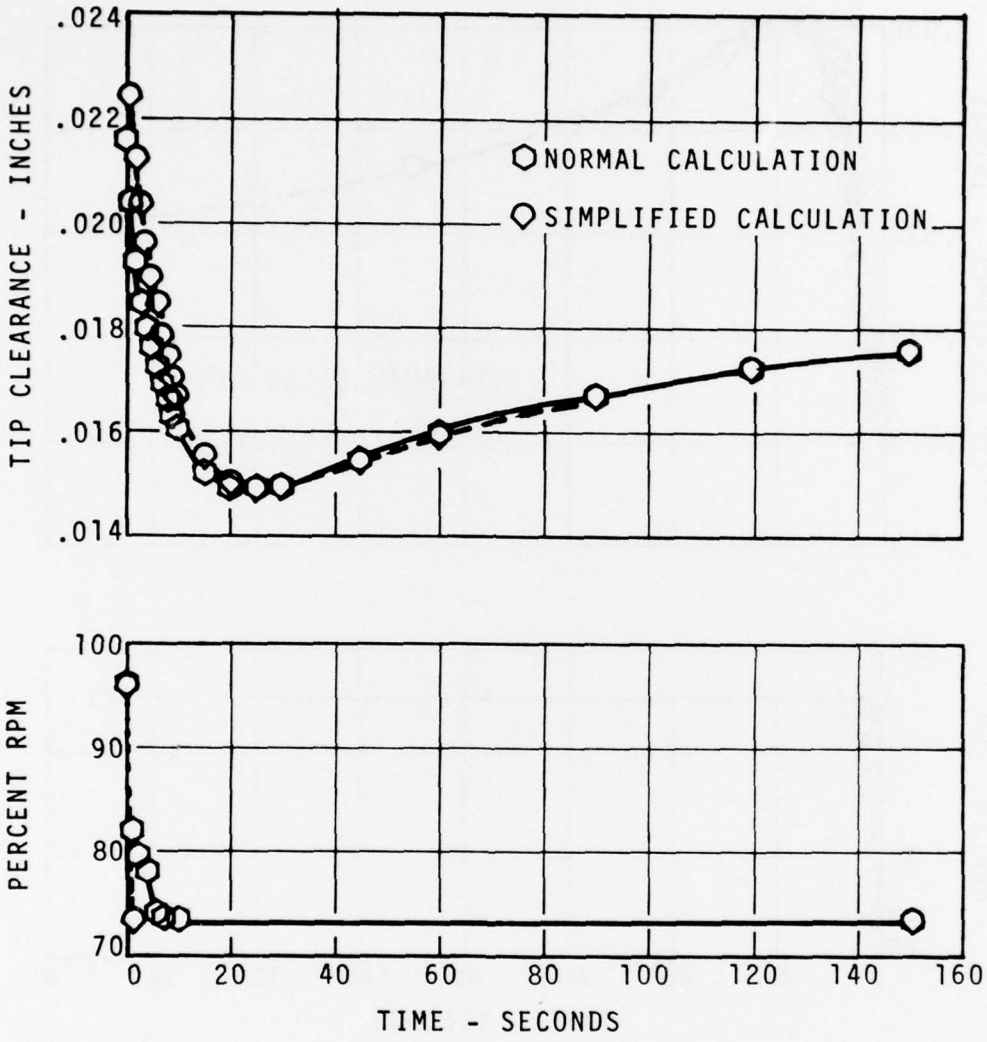

Figure 61. Transient Tip-Clearance Response Analysis With Simplified Boundary Conditions - Snap Deceleration.

CONCLUSIONS AND RECOMMENDATIONS

CONCLUSIONS

The accuracy of the analytic technique in determining transient tip-clearance response rate and component temperature level was demonstrated through comparison with measured values. Simplification of the rate of change of the transient boundary conditions caused no change in the critical values of calculated tip clearance.

Differentials between calculated and measured steady-state tip clearance were caused primarily by a two-dimensional thermal stress distribution in the shroud that was not accounted for in the analytic technique. Incorporation of a two-dimensional stress linkage in the shroud growth calculation would increase the accuracy of the analytic technique.

Shroud distortion in both the axial and circumferential planes was found to be very significant, generating clearance variations as large as the one-dimensional changes measured during severe transients.

Improvements in the operating tip clearance of turbine stages are possible through application of the one-dimensional tip-clearance calculation technique for designs providing closer matching of rotor and shroud response rates. Also, advanced designs must provide more positive control over shroud distortion in order to take full advantage of improved transient response characteristics.

The laser tip-clearance measurement system provided accurate and repeatable measurements under hot-section turbine operating conditions. Considerable effort, however, was required in the setup, calibration, and use of the system.

RECOMMENDATIONS

Modify the one-dimensional analytic technique to incorporate a more detailed stress linkage in the shroud growth calculation to improve the steady-state tip-clearance calculation accuracy.

Use the analytic technique as a tool to analyze the response of new shroud designs targeted in order to more closely match rotor transient growth characteristics through passive and active control techniques.

Design and develop, through analysis and test, techniques to control

shroud distortion to allow smaller average operational tip clearance.

Apply the one-dimensional analytic technique and the laser tip-clearance measurement system to other gas producer and power turbine stages to determine steady-state and transient tip clearance so as to provide a baseline for any necessary redesign.

Continue development of the measurement system to provide more positive optical setup and alignment and to allow direct readout of tip clearance.

APPENDIX A

FLUID NODE MODEL

The fluid node receives the flow from the preceding boundary condition or fluid node and may have several metal nodes adjacent to it. The description here is for a four-sided node.

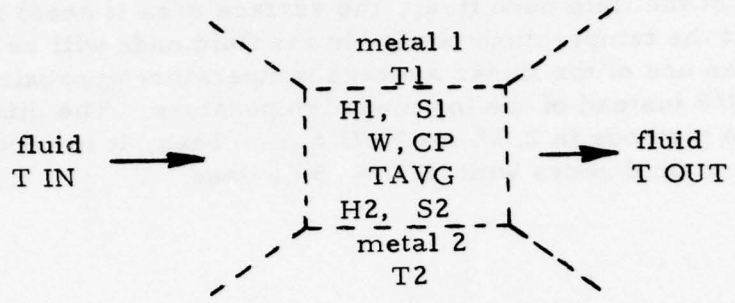

T1, T2... adjacent metal temperatures

T IN temperature of the incoming flow

W flow rate

S1, S2... adjacent surface area

H1, H2...heat transfer coefficients (HTC)

CP specific heat

T OUT temperature of the outgoing flow

T AVG average temperature

(TIN + TOUT)/2

$F1 = H1*S1 \qquad F2 = H2*S2 \qquad F3=...$

$\Sigma F = F1 + F2 + ...$

$\Sigma FT = F1*T1 + F2*T2 + ...$

$$TOUT = \frac{\frac{1}{W*CP} * \Sigma FT + \left[1 - \frac{1}{W*CP} * \frac{\Sigma F}{2}\right] * TIN}{1 + \frac{1}{W*CP} * \frac{\Sigma F}{2}}$$

$NTU = \frac{\Sigma F}{W*CP}$ Number of thermal units

NTU ≤ 2 for convergence stability

NTU is the ratio of the heat transfer rate from the adjacent metal nodes compared to the heat capacity rate of the fluid node. In the heat transfer model the size of the fluid node (i. e., the surface area it sees) must be selected so that the temperature change in the fluid node will be small. This permits the use of the linear average temperature approximation (T IN + T OUT)/2 instead of the log mean temperature. The difference between the two methods is 2. 1% for NTU = . 5. Thus, it is recommended that for accuracy fluid nodes with NTU $\leq$. 5 be used.

APPENDIX B

METAL NODE MODEL

A metal node can have several adjacent nodes which can be any combination of fluid, metal, and contact nodes. This method assumes small temperature changes so that thermal conductivity and specific heat values can be evaluated at the last calculated temperature.

The example uses two fluid and two metal nodes as adjacent nodes.

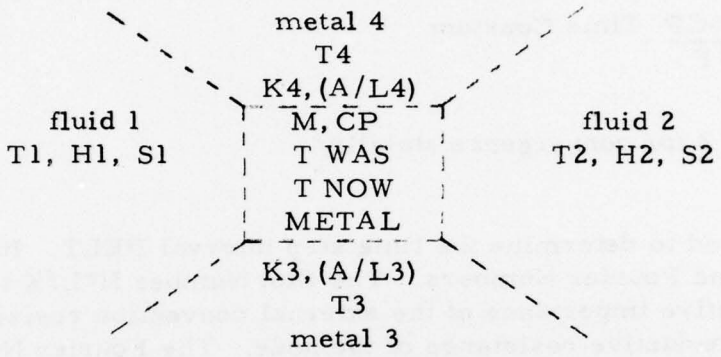

T1, T2, T3. . .	Surrounding temperature
T WAS	The temperature of the node at the last time step
T NOW	The new calculated temperature The T NOW temperature replaces T WAS for the next time step.
H1, H2 . . .	Heat Transfer Coefficient (HTC) values for the fluid nodes
S1, S2 . . .	Surface area of the node that faces the fluid nodes
K1, K2 . . .	Thermal conductivity
(A/L3), (A/L4) . .	Area-to-length ratio for the adjacent metal nodes
M	Mass of this node
CP	Specific heat
DELT	Delta time or time step

F1 = (H1 * S1) F2 = (H2 * S2)

$F3 = (K3 * (A/L3))$ $\quad F4 = (K4 * (A/L4))$

$F5 = \ldots$

$\Sigma F = F1 + F2 + F3 + \ldots.$

$\Sigma(FT) = (F1 * T1) + (F2 * T2) + (F3 * T3) \ldots$

$$T\,NOW = \frac{\frac{DELT}{M*CP} * \Sigma(FT) + \left(1 - \frac{DELT}{M*CP} * \Sigma\frac{F}{2}\right) * TWAS}{1 + \frac{DELT}{M*CP} * \Sigma\frac{F}{2}}$$

$TAU = \frac{M*CP}{\Sigma F}$ Time Constant

$\frac{DELT}{TAU} \leq 2$ for convergence stability

TAU is used to determine the time step interval DELT. It is related to the Biot and Fourier Numbers. The Biot Number H*L/K is a measure of the relative importance of the external convection resistance to the internal conductive resistance of the node. The Fourier Number $\frac{K*(A/L)*DELT}{M*CP}$ is a time-dependent measure of the relative thermal conductivity to capacity rates. For any node, the ΣF terms can be grouped as

$$\frac{DELT}{TAU} = DELT\left(\frac{\Sigma F}{M*CP}\right) = \frac{DELT}{M*CP}\left(\Sigma(H*S) + \Sigma K*(A/L)\right)$$

which can be recognized as the equivalent to

$$\frac{DELT}{TAU} = (\text{Fourier No. })\,(\text{Biot No. } + 1)$$

The time step DELT must be selected so that the nodal temperature change will be small. This permits the use of a linear average temperature approximation (TWAS + TNOW) / 2 during the time step. For mathematical reasons similar to those previously discussed for the fluid node, DELT/TAU for the metal node is recommended to be less than . 1 for accuracy.

APPENDIX C

HEAT TRANSFER COEFFICIENTS

The heat transfer coefficient (HTC) is calculated for the following conditions: (1) internal flow, (2) rotating disk, and (3) flat-plate flow. These formulas all use the following variables:

K - Thermal conductivity

CP - Specific heat

VIS - Dynamic viscosity

Pr - $\frac{VIS*CP}{K}$ - Prandtl Number

DEN - Density computed from the perfect gas law.

1. INTERNAL FLOW (HTC)

The formula used for internal flow is the Colburn equation:

$$HTC = j * \frac{W}{A} * CP * (Pr) ** - \frac{2}{3}$$

In general, j is a function of the flow regime (Re) and the flow development length (L/D). Tables from Kays and London[2] and experimental data are available in this form.

Reynolds number is based on hydraulic diameter

$$Re = \frac{D}{VIS} * \frac{W}{A}$$

---

2) W. M. Kays and A. L. London, "Compact Heat Exchangers", (New York: McGraw-Hill Book Company, Second Edition,1964).

Other parameters are defined below:

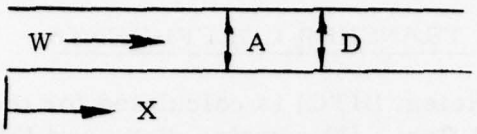

W - Flow rate

A - Cross sectional flow area

D - Hydraulic diameter

X - Length

2. ROTATING DISK (HTC)

The following equation for a small gap flow adjacent to a rotating disk is found in the G. E. Handbook Heat Transfer Data, Section G511 based on the method of Kapinos[3].

$$HTC = .042 * \frac{K}{R} * \frac{(Re)^{**}.8 * (Pr)^{**}.6 * PHI\ entry^{**}.2}{((R/R\ entry)^{**}2 - (R/R\ entry)^{**}-3.25)^{**}.2}$$

Reynolds Number is based on rotational speed

$$Re = \frac{2*\pi*RPM}{60} * (R)^{**}2 * \frac{DEN}{VIS}$$

Other parameters are defined below:

PHI - ratio of radial flow velocity to rotational speed

$$PHI = \frac{W * 60}{4 * DEN * RPM * S * (\pi * R)^{**}2}$$

PHI rim - PHI calculated at R = R rim

PHI entry = PHI calculated at R = R entry

RPM - Rotational speed

W - Flow Rate

R - Radius of the node of interest

R rim - Outer edge radius

R entry - Entry radius

S - Gap along side disk

3) "G. E. Heat Transfer Data Book", (Schenectady: G. E. Corp. Research and Development Center, 1970, and Revisions).

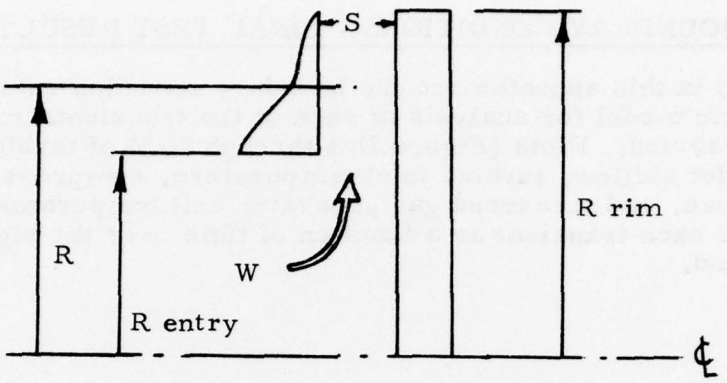

3. FLAT PLATE FLOW (HTC)

The formula for turbulent flow along a flat plate can be found in most heat transfer texts such as Kreith [4]

$$HTC = 0.0288 * \frac{K}{X} * (Re) ** 0.8 * (Pr) ** \frac{1}{3}$$

Reynolds number is based on flow length.

$$Re = \frac{X}{VIS} * \frac{W}{A}$$

See internal HTC for other parameter definition.

4) F. Kreith, "Principles of Heat Transfer", (Scranton: International Textbook Company; Seventh Printing,1963).

APPENDIX D

BOUNDARY CONDITIONS - FINAL TEST RESULTS

Presented in this appendix are the boundary condition values used in the analytic model for analysis of each of the transients run during the final test series. Plots (Figure D-1 through D-5) of turbine rotational speed, inlet airflow, turbine inlet temperature, compressor exit temperature, and measured gas generator exit temperature are presented for each transient as a function of time over the significant time period.

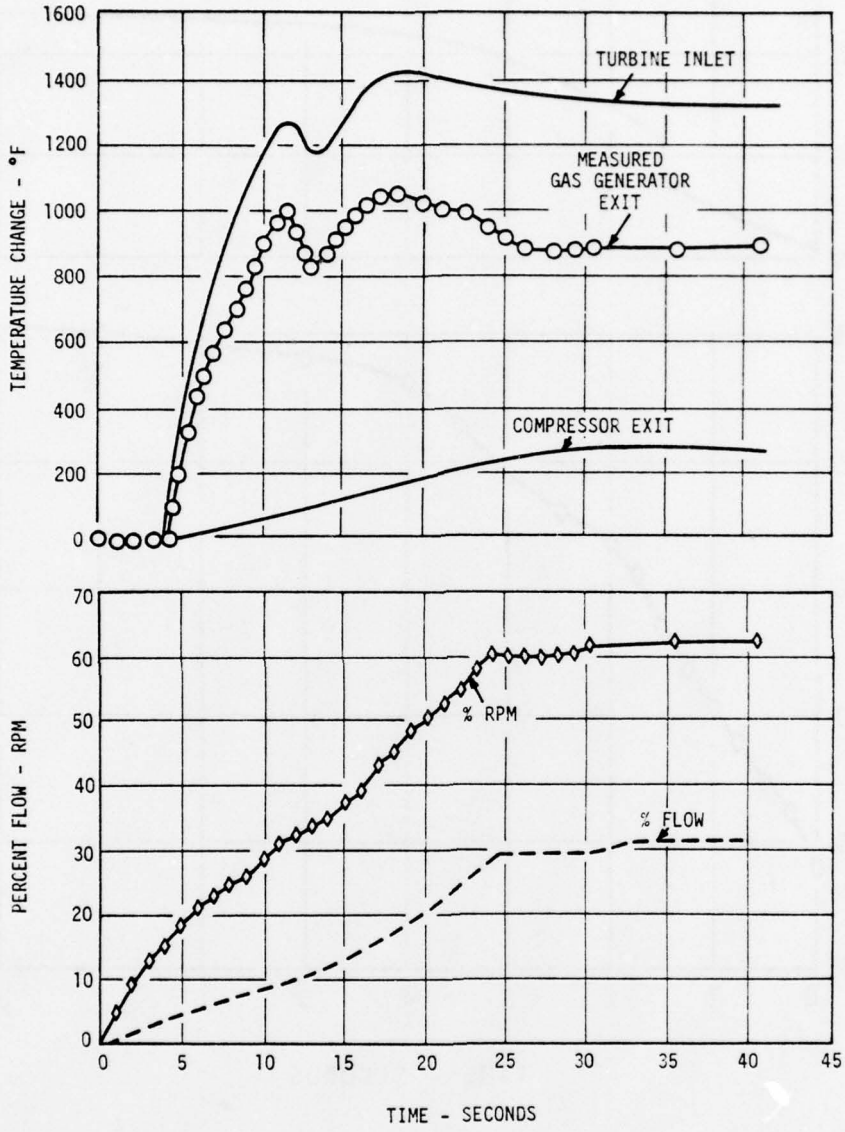

Figure D-1. Transient Boundary Conditions - Start.

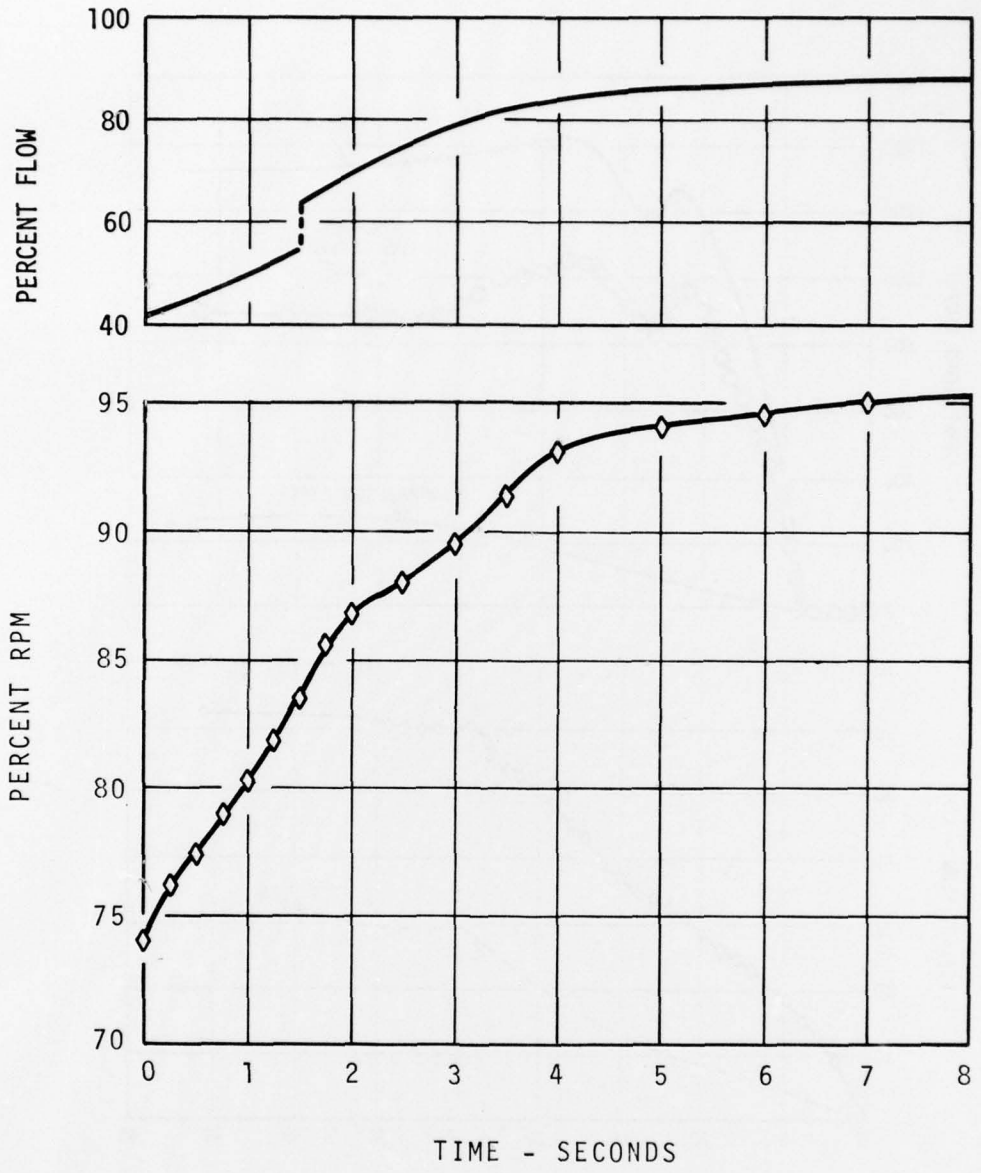

Figure D-2. Transient Boundary Conditions - Jam Acceleration (Sheet 1 of 2).

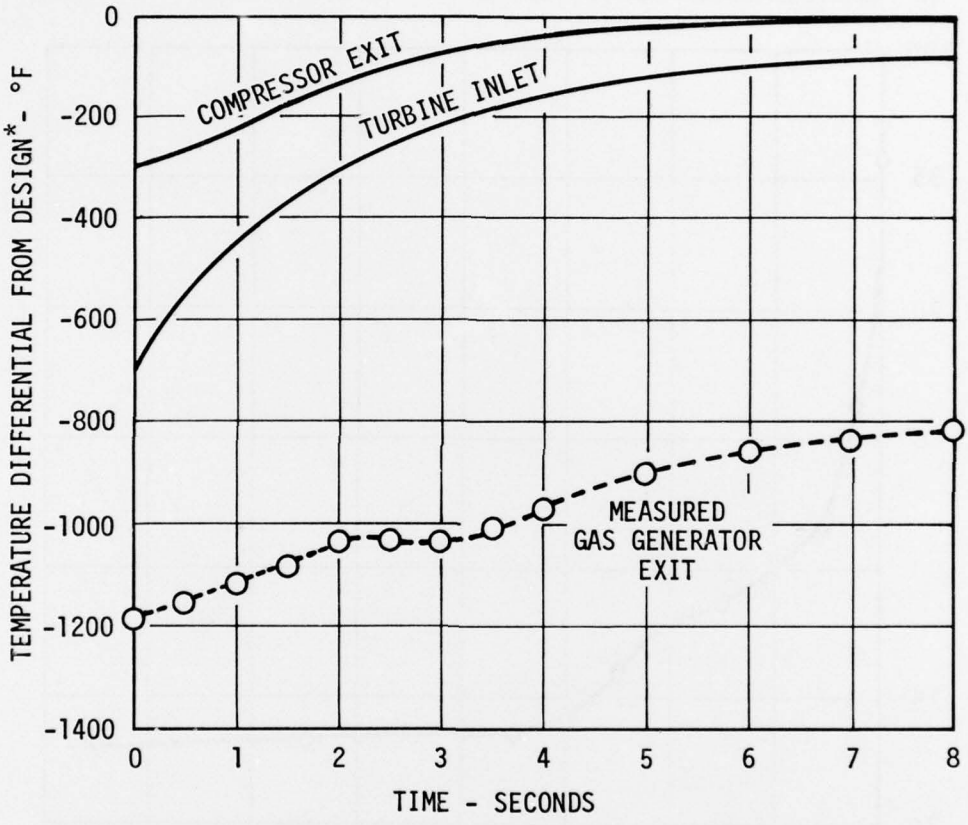

*Design compressor exit or turbine inlet temperature as applicable.

Figure D-2. Transient Boundary Conditions - Jam Acceleration (Sheet 2 of 2).

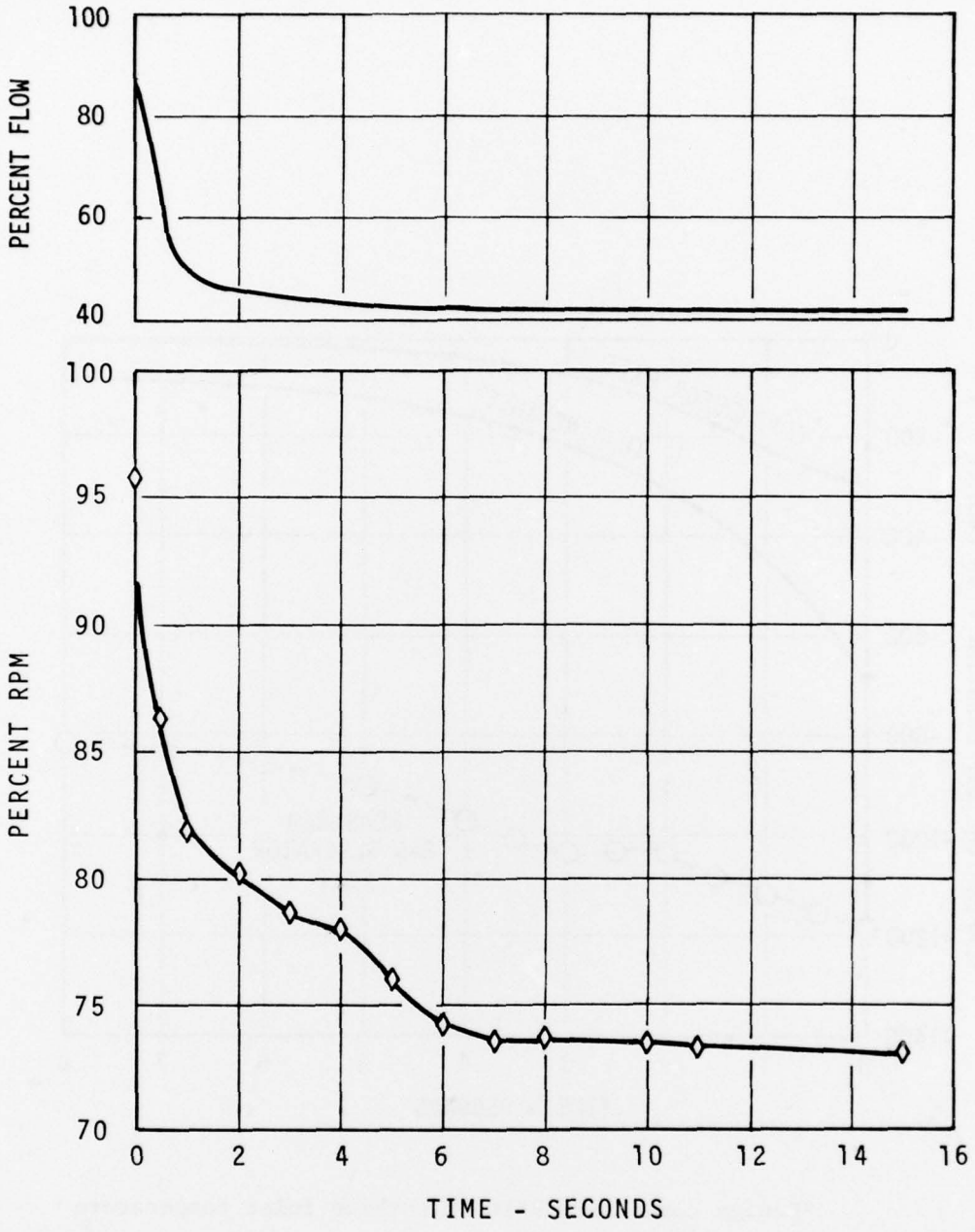

Figure D-3. Transient Boundary Conditions - Snap Deceleration (Sheet 1 of 2).

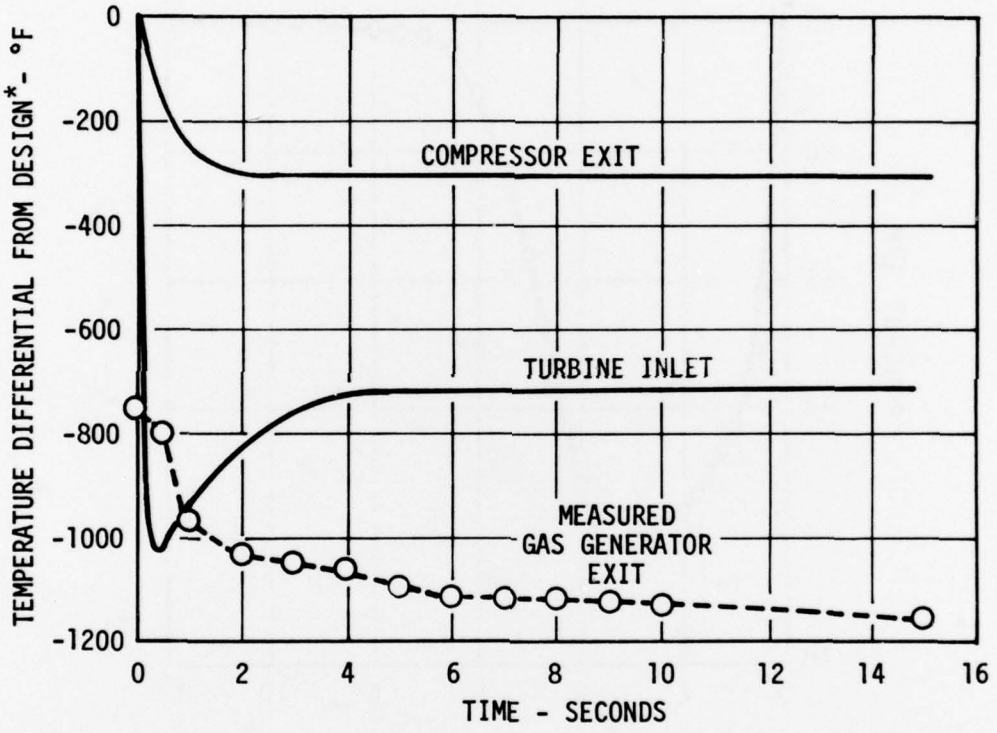

*Design compressor exit or turbine inlet temperature as applicable.

Figure D-3. Transient Boundary Conditions - Snap Deceleration (Sheet 2 of 2).

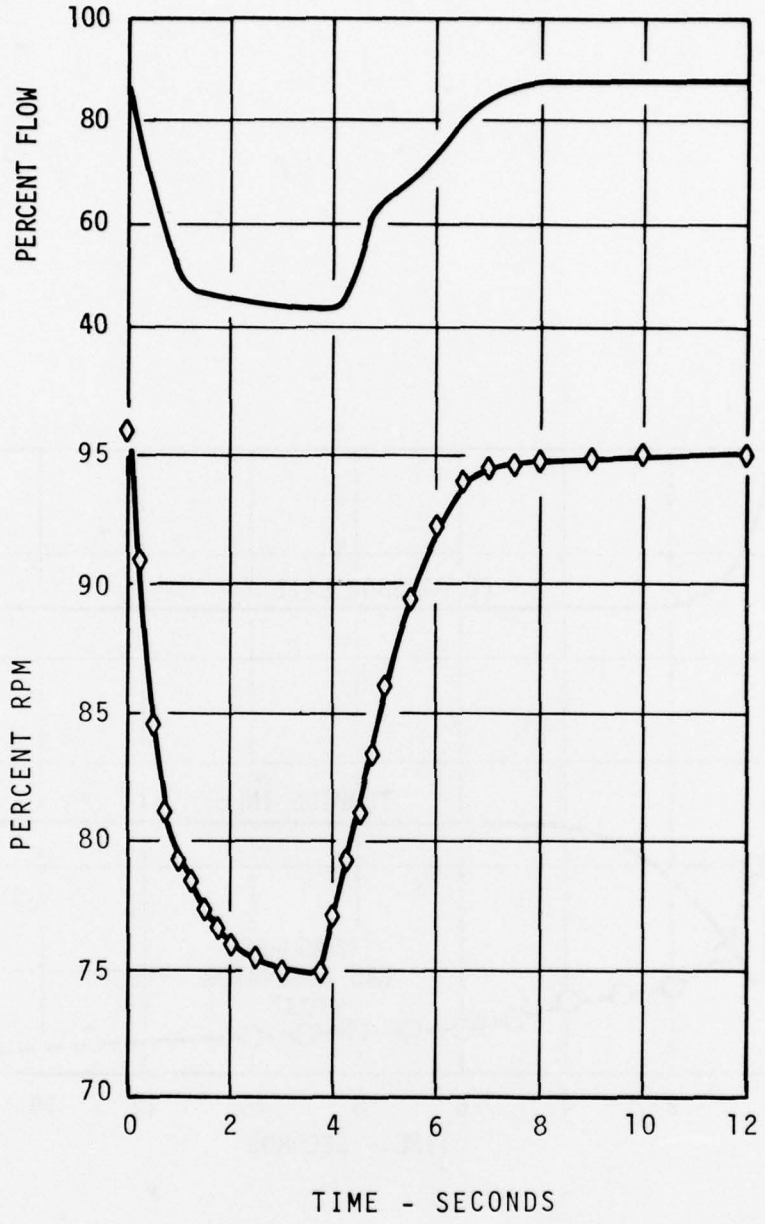

Figure D-4. Transient Boundary Conditions - Wave-off (Sheet 1 of 2).

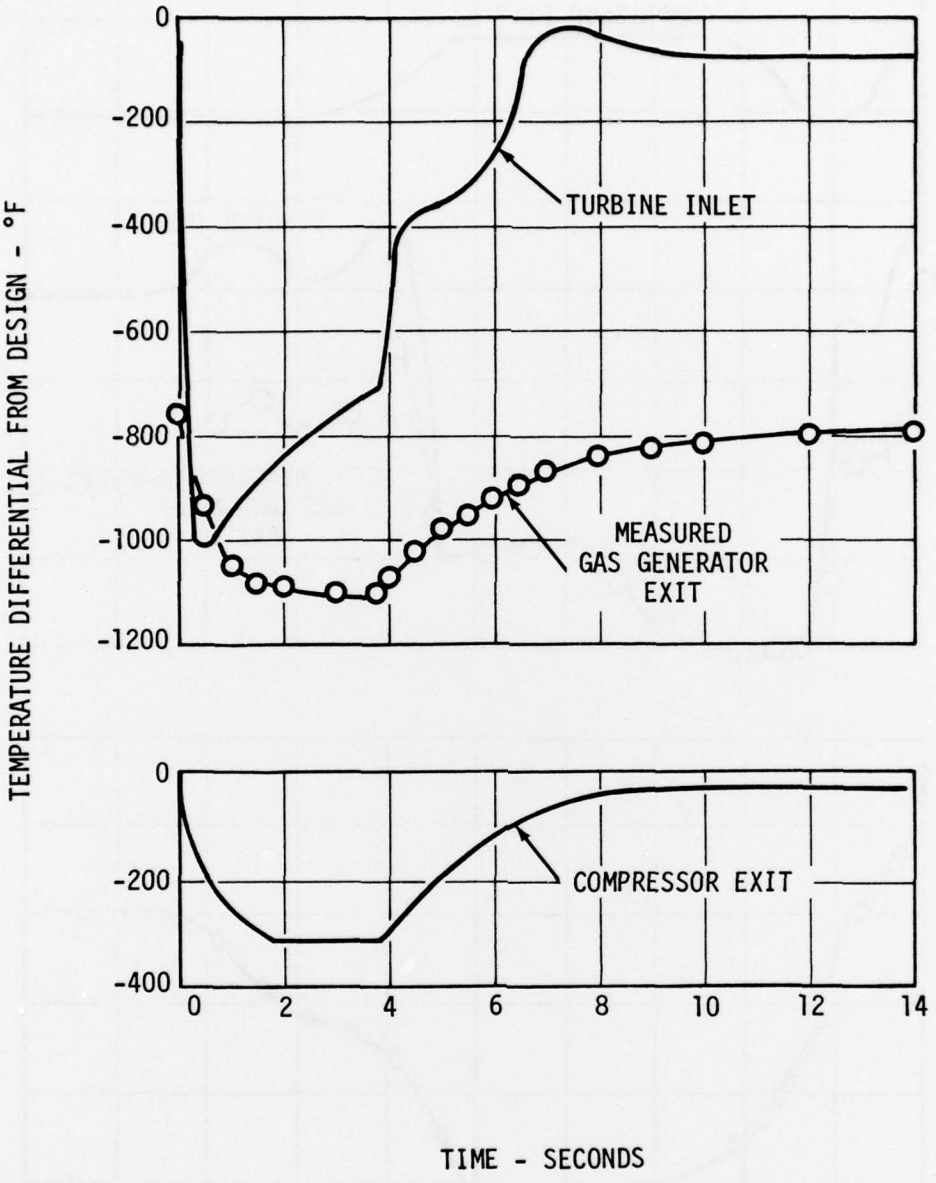

Figure D-4. Transient Boundary Conditions - Wave-off
(Sheet 2 of 2).

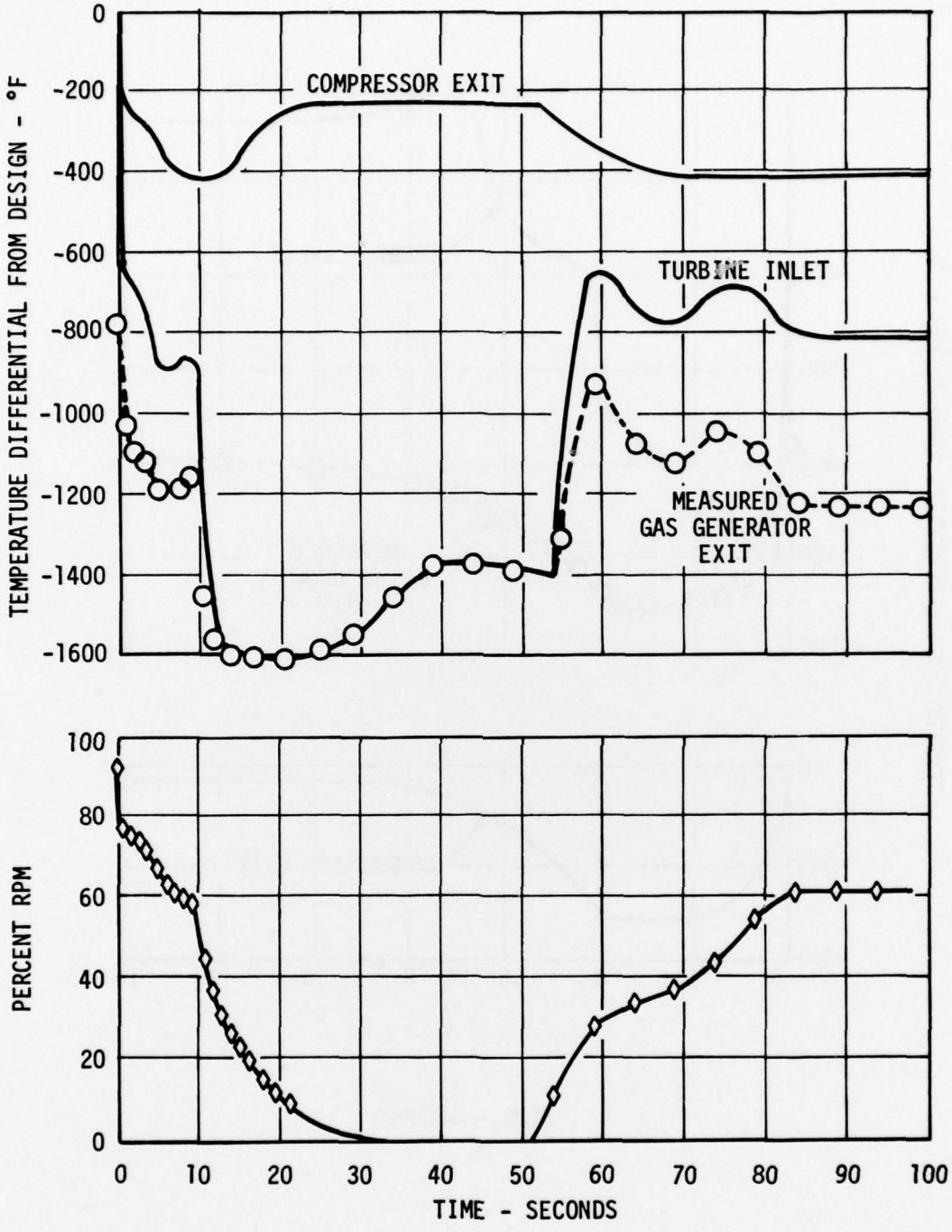

Figure D-5. Transient Boundary Conditions - Shutdown and Restart.

15052-77